MULTI-MODE CONTROL OF THE POWER ELECTRONIC INTERFACE OF THE

BATTERY STORAGE UNIT IN A DIESEL-HYBRID MINI-GRID

Maninder Singh

A Thesis

In the Department

Of

Electrical and Computer Engineering

Presented in Partial Fulfillment of the Requirements

For The Degree Of

Master of Applied Science (Electrical and Computer Engineering) at

Concordia University

Montreal, Quebec, Canada

Feb, 2014

CONCORDIA UNIVERSITY

SCHOOL OF GRADUATE STUDIES

This is to certify that the thesis prepared

By: **Maninder Singh**

Entitled: **Multi-Mode Control of the Power Electronic Interface of the Battery Storage Unit in a Diesel-Hybrid Mini-Grid.**

and submitted in partial fulfillment of the requirements for the degree of

Master of Applied Science (Electrical and Computer Engineering)

complies with the regulations of the University and meets the accepted standards with respect to originality and quality.

Signed by the final examining committee:

Dr. M. Z. Kabir _____   Chair

Dr. M. Chen _____   External Examiner

Dr. S. Williamson _____   Examiner

Dr. L.A.C. Lopes _____   Thesis Supervisor

Approved by Dr. William E. Lynch _____
                Chair of the Department

                Dr. Christopher Trueman _____
                Dean, Faculty of Engineering and Computer Science

Date   _____

ABSTRACT

Multi-Mode Control of the Power Electronic Interface of the Battery Storage Unit

in a Diesel-Hybrid Mini-Grid

Maninder Singh

A battery energy storage system (BESS) was conceived to reduce fuel consumption and maintenance costs of diesel-hybrid mini-grids [1]. It operates in 2 different modes. In the *genset support* mode, it balances the load and maintains a unity PF for genset, and it supplies/absorbs power to force the genset to operate with higher efficiency, less mechanical vibrations and less risk of carbon build-up. In the *grid forming* mode, it provides a balanced voltage to the highly unbalanced load, common in small autonomous power systems. In this Thesis, this theoretical study is taken to the next level by implementing it in the laboratory to assess its performance.

This system was so far tested theoretically by simulations, probably with ideal conditions. In this Thesis, after carefully studying the system, some modifications are brought into it, considering the real time challenges of test bench. The first modification is the implementation of a phase lock loop (PLL), considering the voltage unbalance issue, which is likely to occur at the point of common coupling (PCC) due to the highly unbalanced loads. The second modification is the implementation of the proposed per-phase synchronizer, which is required to change the mode of operation from one to another, instead of the formerly employed Intelligent Connection Agent (ICA), making the system simpler to implement. The final modification is in the MSTS block (Mode

Selection and Transition System) to bring intentional and unintentional change in the mode of operation, additional features.

After applying the above said modifications to the BESS system, it was tested in the laboratory to see if it meets the design specifications, where the control was implemented on a programmable inverter called Triphase® inverter system, and a power supply known as Ametek® (California Instruments) was working as a genset. The battery of the BESS was emulated, a contribution of Thesis, by a diode rectifier connected to Concordia's grid and a controllable bleeding resistor so that the emulated battery can supply and absorb active power to the AC grid.

Based on the experimental evidences, it is concluded that this BESS system is highly suitable for *genset support* mode, *grid forming* mode and while changing the mode from one to another.

ACKNOWLEDGEMENTS

Table of Contents

LIST OF FIGURES

LIST OF TABLES

NOMENCLATURE

BESS   Battery Energy Storage System

DG   Distributed Generation

FF   Feed Forward

FAE   Fictive Axis Emulation

FLL   Frequency Locked Loop

ICA   Intelligent Connection Agent

IGBT   Insulated-Gate Bipolar Transistor

LPF   Low Pass Filter

MSTS   Mode Selection and Transition System

PV   Photovoltaic

PI   Proportional Integral

PLL   Phase Locked Loop

PCC   Point of Common Coupling

PSC   Positive Sequence Components

PWM   Pulse Width Modulation

RES   Renewable Energy Source

S&H	Sample and Hold
SPWM	Sinusoidal Pulse Width Modulation
SOGI	Second Order Generalized Integrator
SOC	State-of-Charge
SCC	Symmetrical Components Calculator
SG	Synchronous Generator
THD	Total Harmonic Distortion
UPF	Unity Power Factor
VSI	Voltage Source Inverter

Chapter 1.

Introduction

1.1. Context and Issues

A local electrical network which is not connected to the main grid is known as mini-grid. In mini-grids, energy is usually produced by a diesel power plant, which is then distributed to the neighborhood customers (residential and commercial), through a local distribution system. Mini-grids in remote communities are usually subject to highly variable load profile, for instance the peak load demand is 5 to 10 times higher than the average load demand [2]. This requires the use of an oversized diesel engine generator-set (genset), considering only one geneset is employed, which will tend to operate in the low efficiency range for a considerable amount of time. A genset operating in the low efficiency region is subject to carbon build up in the diesel engine [3], which affects the maintenance cost and life time of it, high fuel consumption is obvious in the low efficiency range. Another issue in the mini-grids is the load unbalance, as diesel gensets supplying unbalanced loads experience overheating in the synchronous generator and vibrations [4]. This issue further affects the health of the genset. For efficient operation, the genset should operate near its full capacity and supply a balanced power.

Apart from high fuel consumption and maintenance cost, genset operating in the low efficiency region emits higher toxic air contaminants, including fine particles (aerosol) associated with negative health effects. When mini-grids use multiple types of energy resources, for example gensets and photovoltaic (PV), gensets and battery energy storage system (BESS), they are called hybrid mini-grids. According to [1], a battery energy storage system (BESS) is appointed with genset(s) to form a hybrid mini-grid, for

reducing fuel consumption and maintenance cost of its operation, also to protect the planet, the control system of which is experimentally assessed in this Thesis as a prime work.

1.2. Literature Review

Gensets has been the most preferred choice for electricity production worldwide, especially in the remote communities where national grid is not available (mini-grids). This is a mature technology with the well-known drawbacks of consumption of fossil fuels and greenhouse gas emissions. They are employed, as a single genset working alone or together in a group, to produce electricity for the mini-grid distribution systems. The latter option, a group of gensets, in which gensets of different capacity are selected, is considered an efficient method due to the highly varying load profile of the remote communities, otherwise a single large genset, probably an oversized one, has to operate inefficiently since the conventional gensets are not suitable to operate at low load condition (typically below 40 % of its capacity) [3]. For a group of gensets, with different capacities, to form a mini-grid, it requires a scheme/mechanism to decide the power-share of each genset, according to their rated power and their generation costs, to produce power efficiently. This scheme is known as optimal economic dispatch and has been reporter in literature in [5-9].

Another effective approach to address the high varying load profile is the demand side load control [10-13], to shave-off the peak load and to prevent low load condition. It includes either complete load shedding or reduction in the load from the load side. Heating and cooling systems and refrigeration units are common examples of controllable loads that could participate in the demand side management. Complete load

shedding causes loss of benefits to customers however reduction in load has shown a good response which makes this method implementable. Besides the highly varying load profile, another issue is the unbalance in the loads, which causes overheating and vibrations in the synchronous machine of the genset. To address this issue, [14-16] has been reported in literature, which does load balancing and protects the genset from overheating and vibrations.

Beside the above discussed problems, some challenges appear with the integration of the renewable energy sources (RESs), such as PV and wind mills, into the mini-grids to form a hybrid mini-grid. As RESs are intermittent power sources, they can cause power oscillation in the mini-grid, with impact on the frequency and sometimes on the voltage magnitude, either during the high penetration of RESs or during the low load condition, which are difficult to be compensated by the genset(s). In this scenario, excess energy from the RESs that would reduce the genset load or causes the power oscillation must be curtailed or dissipated in dump loads [17-21]. This method prevents low load operation of genset or power oscillation in mini-grid but does not allow one to utilize RESs fully. To reduce the power oscillation or the frequency deviation occurring in the mini-grid due to the high penetration of RESs, short term and long term storage has been reported in literature.

Short term storage is generally employed to improve dynamics of the mini-grid during a sudden load change. It acts like an added inertia to diesel-hybrid systems with RESs like PV and wind, that present no or less inertia as compared to diesel genset generators [22-26]. In this way, it can improve system dynamics reducing frequency nadirs and rate-of-change-of-frequency (ROCOF), as loads and RESs vary. The long term storage is

3

relatively expensive due to its larger size but provide a highly effective means to solve the majority of mini-grid issues [1, 27]. As per [1], the concerned BESS, it does load leveling to shave off the peak loads and prevents the low load condition, load balancing to protect the synchronous machine from overheating and vibrations, act as a reactive power compensator and has the ability to form a standalone grid on the highly unbalanced loads during the genset-less operation. This practice yields low maintenance cost and fuels consumption as the genset is always working at the high efficiency point and is not subject to abnormal load conditions, where it usually accumulates carbon inside the diesel engine, which reduces its life. This long term storage system is also known as battery energy storage system (BESS), the control system of which is experimentally assessed in this thesis as a major work.

1.3. Previous Work with Current Objectives

The main focus of this M. A. Sc. Thesis is to experimentally test the control system of a battery energy storage system (BESS), which was reported in [1] for reducing fuel consumption and maintenance cost of diesel-hybrid mini-grids. This BESS control system was proposed in [1] on the basis of simulation results only, and now in this thesis, it is taken to the next level by assessing it on an experimental test bench.

Prior to discuss the conceived design capabilities, a circuit diagram in Fig. 1.1, is presented which shows a genset with BESS, a single-phase RES and unbalanced load. This diagram is provided by [1], the concerned BESS control system, in which a three-phase BESS, based on a three-phase voltage source inverter (VSI) with an LC output filter, is connected in parallel to the genset at the point of common coupling (PCC). A three-wire distribution system connects the genset and the BESS to the loads and

4

residential rooftop type PV systems. The schematic diagram of the basic control loops of the BESS inverter is presented in Fig. 1.2, also provided by [1]. It employs a per-phase dq control strategy in which the β component of the inner current loop is emulated with fictive axis emulation (FAE) [28, 29], and the frequency adaptive second order generalized integrator (SOGI) is employed to generate the orthogonal components (αβ) required for getting dq components from single-phase quantities. Refer to [1] for further detail of per-phase dq control. It is important to mention that the PI controllers (in inner current and outer voltage loop) employed for this study have been designed, using the same approach as in [1] but for different LC parameters.
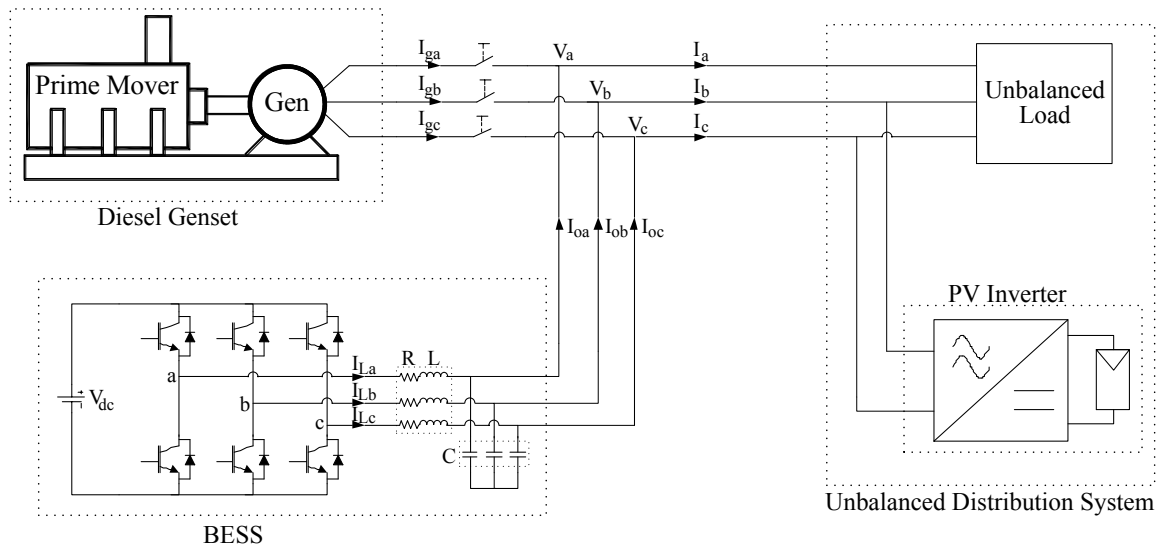
Fig. 1.1. Circuit diagram of a three-phase three-wire diesel-hybrid mini-grid with battery inverter, single-phase RES and unbalanced load.
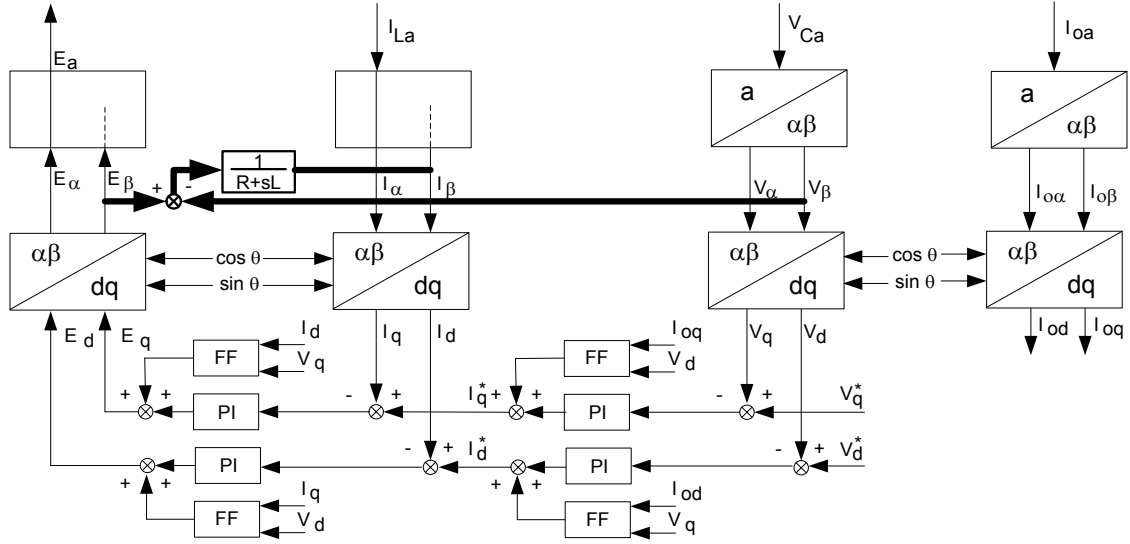
Fig. 1.2. Schematic diagram of the per-phase control of BESS inverter.

Now discussing the conceived design specifications based on simulation results [1]. It was claimed that this BESS control system will assist genset(s) to reduce fuel consumption and maintenance cost by keeping it operating within the high efficiency range (typically 40% to 90% of its capacity). Genset is operated at 90 % or lesser to ensure a power reserve (spinning reserve) for a sudden load increase and it is not operated below 40 % to prevent carbon built up in the engine, a drawback of the conventional gensets. BESS shall do so by absorbing/supplying active power whenever load profile drives genset outside the band of high efficiency. It should also supply negative sequence component of the load current into the genset grid for load balancing, so as to protect synchronous generator from overheating and vibrations. Finally, it should operate as a reactive power compensator, enabling genset to utilize its full capacity for active power injection. Besides, the BESS control system should form a balanced grid on the highly unbalanced loads, during the genset less operation, to maintain uninterrupted

6

power supply. The aforesaid design specifications or features of the concerned BESS control are experimentally tested and assessed in this Thesis.

1.4. Thesis Outline and Contributions

Chapter 2 of this thesis starts with a description of the constructed power circuit (in laboratory), which is employed to test the concerned BESS control system. It is then followed by the control design of battery emulation, its experimental verifications, designed to address the over-voltage issues that may occur at the DC side of the inverter, whenever it absorbs active power from the grid. Then the implemented phase lock loop (PLL) to acquire amplitude, phase and frequency of the grid is presented, addressing the voltage unbalance, a case likely to appear on the test bench. Then the proposed per-phase synchronizer is discussed which has the ability, verified in Chapter 3, to eliminate the need of formerly employed intelligent connection agent (ICA) for simplification reasons. Finally the entire BESS control system is presented, discussing every subsystem that incorporates it, one by one, including their real time Simulink implementations and test verifications. Simulink implementation is particularly included to serve practical knowledge and to show implementation details. In the end of Chapter 2, a summary is presented which scrutinizes the study and shows the outcomes.

Chapter 3 starts with a detailed description of the apparatus, which is employed to test the control system, such as the Ametek$^{®}$ power supply, which is working as a genset, the Triphase$^{®}$ inverter system working as a BESS, and the switchable loads creating severe unbalance in the load, whenever required, to test the control system.

Then it includes the experimental test results of the concerned BESS during its various operating modes. In the *genset support* mode, it is tested for supplying negative sequence current, maintaining a unity PF for genset, supplying and absorbing active power to keep genset operating in the high efficiency band. In the *grid forming* mode, it is tested for forming a balanced grid on the possibly highest unbalanced loads, to maintain an uninterrupted power supply during the genset-less operation. Then it includes the experimental verification of the proposed per-phase synchronizer for its ability to perform a smooth transition while changing the mode of operation from one to another.

Chapter 4 includes the final conclusions about the capability of the concerned BESS system in performing the assigned task. It also includes a summary of changes that are considered in the BESS design, while implementing it on the test bench, to make it easier to implement, to address the voltage unbalance issue and to enhance its features. Besides, it includes some suggestion for future work.

Therefore, to scrutinize the study, the main contributions of the research work are;

1) The experimental test of the concerned BESS control system was never conducted before, and now in this study it is been accomplished by implementing the entire control on a real time system considering the real time challenges.

2) The design and performance verification of a control loop for battery emulation is achieved in this study.

3) Design and performance verification of a new control block as "per-phase synchronizer," which eliminates the need of formerly employed Intelligent

Connection Agent (ICA) and makes the system simpler to implement without compromising the quality, has been achieved in this study.

4) Implementation of a PLL to acquire correct phase, frequency and amplitude of grid considering the voltage unbalance issues of the test bench has been suggested and implemented in this study.

5) Added features like intentional and unintentional change in the mode of operation of the BESS, to the already existing Mode Selection and Transition Module (MSTS) block.

Chapter 2.

Implementation of the Complete System

This Chapter includes the synthesis of the constructed power circuit, which is used to test the concerned battery energy storage system (BESS) control strategy. It includes a description of the various incorporated elements that forms the BESS system, and the assigned control strategies to operate behind them. Simulink implementation of the various control loops is provided throughout this Chapter, to make it easier for readers to understand concepts and to serve a practical exposure. Besides, it includes experimental evidences to demonstrate the effectiveness of the concerned control strategy during several modes of operation. Some new control loops, which include a controllable bleeding resistor and the per-phase synchronizer, have also been discussed in this Chapter, which are also confirmed with their experimental results.

2.1. Description of the Constructed Power Circuit (Laboratory)

A power circuit was constructed in the laboratory to test the adopted control strategy and it is shown in Fig. 2.1. This power circuit primarily contains five elements. First is the AMETEK® programmable power supply (model MX30-3Pi, California Instruments), working as a 2kW genset, supplying 208 V L-L, 60Hz and running in isochronous mode. The low THD, which is less than 1.0 %, allows it to work as a typical genset with a rotating synchronous generator and low voltage harmonics. It should be noted that the grid voltage in the power lab contains low order harmonics, making it inappropriate for this application, as the low order harmonic will pollute the D and Q components of the grid voltage, which are the basic foundation of the adopted control strategy.

Second is the Triphase® programmable inverter system (model PM10F30C), working as a BESS (battery energy storage system). Triphase® inverter system is a Belgium company product which is designed for research and development. It employs a linux operating system for real time applications and the entire control algorithm can be implemented using Simulink, Matlab©. The triphase system consists of a three phase diode rectifier and a three phase IGBT inverter, connected in series and it has an inbuilt LC filter in the AC side of the inverter, where L is 2.3 mH and C is 8.8 µF. Also, there are contactors K1 and K2 available, which can be set internally from within the control loops. Voltage and current sensors, as shown in the circuit diagram, are also parts of the Triphase system, and are employed for the voltage and the current control loops. Besides, a current sensor is also employed at the "load side" to measure the load current and to compute the negative sequence current and the load's real and reactive power. An IGBT switch is available in the dc bus, between the diode rectifier and the inverter, for controlling a "bleeding resistor." In this work, the bleeding resistor will be used for battery emulation, in the sense that the inverter can absorb active power while preventing the dc bus voltage from increasing.

Another element is the "Grid Concordia," available at 208 V L-L and 60 Hz. It is connected to the Triphase system through a step up transformer. The step-up transformer is to ensure sufficient DC bus voltage, after the rectifier, to be able to prevent the inverter of the BESS from going into the over modulation region when connected to an AC system of 208 V. The remaining two components are the unbalanced loads, to test the control strategy and the bleeding resistor, connected between the rectifier and the inverter, also used for battery emulation.
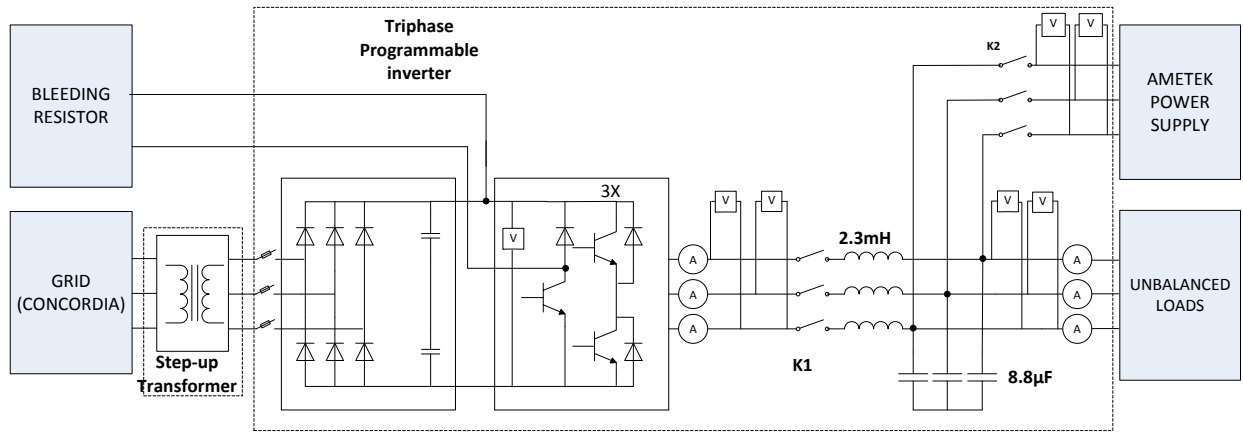
Fig. 2.1. Schematic diagram of the constructed power circuit

2.2. The Concept of the Battery Emulation

During experiments it was found that whenever the Triphase® inverter absorbs real power, the DC bus voltage tends to rise and it kept rising until system's protection gets active and aborts the execution of program. On further research it became clear that it happens since the diode rectifier forming the DC bus is unidirectional, and as a result the reverse power is inflating the DC bus voltage. On the other hand, if the DC bus was formed by a battery bank, the reverse power would have been absorbed by the battery itself, while keeping the DC bus voltage unchanged. Now, if one could burn this reverse power on this DC side it would correspond to the power stored in the battery. After careful observation and examination of the situation, a control loop was designed, which is regulating the DC bus voltage by dissipating the reverse power on a resistor called bleeding resistor.

This battery emulation control loop is not only limited to laboratory experiments where the DC bus is usually formed by a unidirectional rectifier but it's also applicable to the real scenario where it is formed by a real battery instead, and the state of the charge of the

battery bank has reached maximum. In this case, once the battery is fully charged, this control loop will activate the IGBT switch to allow the bleeding resistor to consume power absorbed by the BESS inverter, to prevent the battery from overcharging.

2.2.1. Control Loop Design for the Battery Emulation
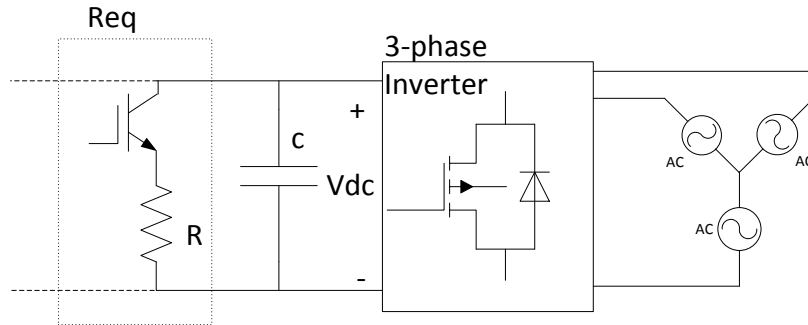
Fig. 2.2. Equivalent circuit diagram of bleeding resistor

The power absorbed by the resistor can be computed as;

$$P_R = \frac{vdc^2}{Req} = \frac{vdc^2}{R}d \tag{2.1}$$

Where, *vdc* is the DC bus voltage, *Req* is the equivalent resistance, *D* is the duty ratio of the IGBT switch and *R* is the resistance of the bleeding resistor.

The power being supplied to the capacitor, when the inverter operates as a rectifier, absorbing power from the AC grid, can be calculated from;

$$P_C = \frac{dEc}{dt} = 0.5C\frac{dvdc^2}{dt} \tag{2.2}$$

According to the power balance equation if the DC bus is to be kept constant;

$$P_R = -P_C \tag{2.3}$$

Linearizing equation (2.1) and (2.2) with a small signal perturbation; A lowercase letter is used to represent a variable, which includes its steady state DC value plus a small ac perturbation.

$$vdc = Vdc + \tilde{v}dc$$

$$d = D + \tilde{d}$$

Substituting the linearized equation (2.1) and (2.2) in the above power balance equation (2.3), one computes;

$$\frac{(Vdc + \tilde{v}dc)^2 * (D + \tilde{d})}{R} = -0.5 * C * s * (Vdc + \tilde{v}dc)^2$$

Thus, the influence of the variation of duty cycle of the IGBT switch on the DC voltage is;

$$\frac{\tilde{v}dc}{\tilde{d}} = -\frac{Vdc}{R * C * s + 2D} \tag{2.4}$$

The model of the plant is as shown in Fig 2.3. It should be noted that the voltage sensor is modeled by a simple (unity) gain.
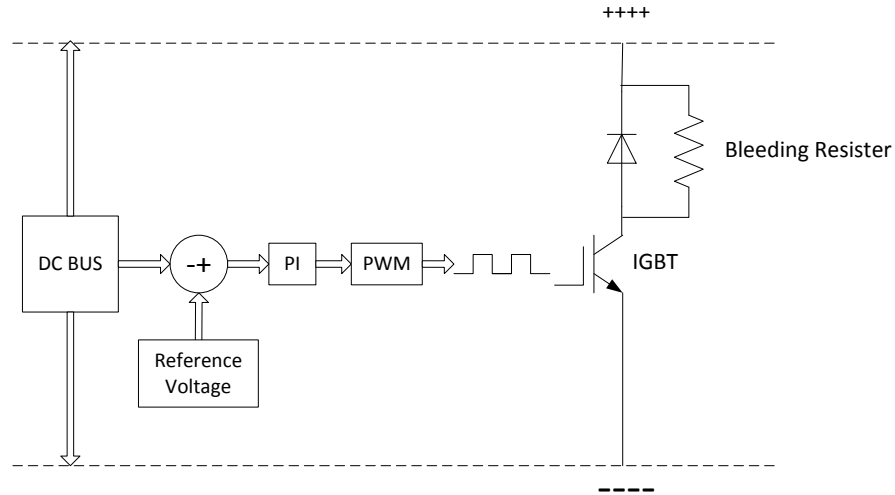
Fig. 2.3. Schematic diagram of the control loop of bleeding resistor

Now, considering the following circuit parameters, as used in the Triphase system;

The maximum DC bus voltage across the capacitor is chosen to be;

$$vdc = 500\ V$$

The total capacitance in the DC side of the Triphase system is;

$$C = 560\ \mu F$$

For a given bleeding resistor and a fixed DC bus voltage, it will dissipate maximum power, when duty ratio of the IGBT switch is 1. For higher power dissipation, the resistance of the bleeding resistor should either be reduced or the maximum DC bus voltage should be increased. In this design, the bleeding resistor is chosen to be 500 Ω to be able to dissipate a maximum power of 500 W, for the regulated DC bus voltage of 500 V. Thus,

$$R = 500\ \Omega$$

Since, the value of the duty cycle varies in between 0 and 1 and the intermediate value is

0.5. Therefore;

$$D = 0.5$$

Substituting the above parameters into the transfer function of the plant, equation (2.4);

The transfer function of the "Plant" becomes,

$$G(s) = -\frac{500}{0.28 * s + 1} \tag{2.5}$$

2.2.2. Designing a PI Controller for the Battery Emulation

The transfer function of a PI controller is;

$$GC(s) = Kp + \frac{Ki}{s} \tag{2.6}$$

The applied values of Kp and Ki are 0.1 and 1, and the corresponding response of the

controller can be seen in Fig. 2.5(b). The bode plot of the plant, loop transfer function

(LTF) and the designed controller can be seen in Fig. 2.4.
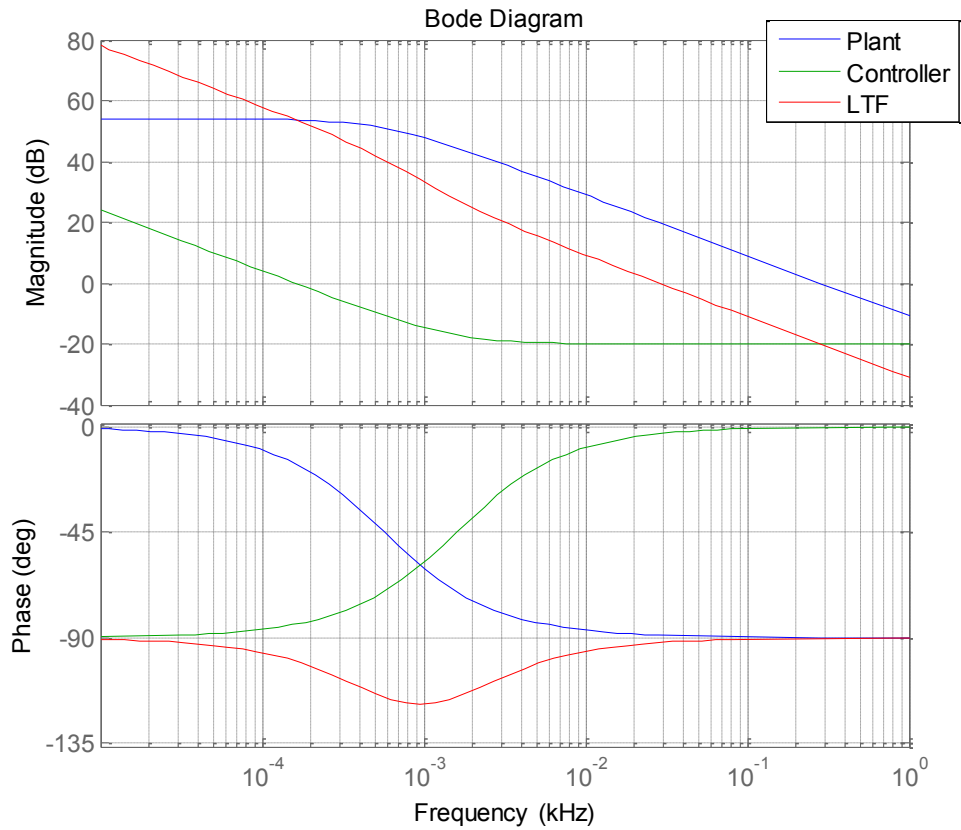
Fig. 2.4. Bode plot of the LTF of bleeding resistor.

2.2.3. Performance Verification of the Battery Emulation

In order to conduct the test, initially, the Triphase® inverter is connected to the Ametek® programmable power supply by closing the connectors K1 and K2 of Fig. 2.1, and is floating. Then the real power reference is made to -250 W, so that the Triphase inverter can absorb real power from the Ametek supply. The active power injected by the Triphase inverter into the grid, formed by the Ametek supply can be seen in Fig. 2.5(c). It is clear in Fig. 2.5 that the inverter starts to absorb active power at 19.18 sec, which is inflating the DC bus until it reaches the reference of 500 V at 19.39 sec. At 19.39 sec the PI gets activated, controller response is shown in Fig. 2.5(b), which further activates the

17

IGBT switch making the bleeding resistor to consume power and thereby regulating the DC bus. The regulated DC bus is shown in Fig. 2.5(a), at 19.6 sec at the reference value of 500 V by the designed control loop.

Based on the experimental results shown in Fig. 2.5, the designed control loop is capable of performing the assigned task, which is to maintain the DC bus voltage regulated during reverse power flow. Thus, BESS would operate with the inverter absorbing active power without any over voltages at the DC side.
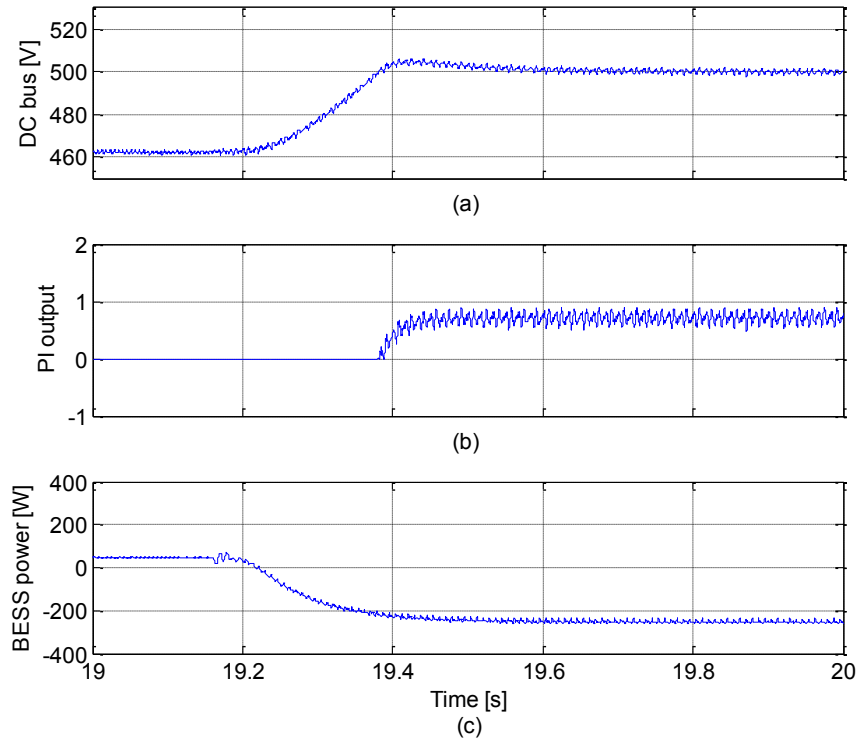
Fig. 2.5. Voltage regulation by bleeding resistor: a) DC bus voltage; b) controller response; c) power absorbed by the BESS inverter.

2.3. Introduction and Implementation of the Phase Lock Loop (PLL)

Acquiring the correct phase, amplitude and frequency of the utility is a fundamental aspect for the design of the control circuit of the grid-connected inverter system. There are two different scenarios in this experimental study: One is *grid support* mode in which a BESS inverter is tied to a grid and other is *grid forming* mode, a stand-alone (off grid) inverter system. In the *grid support* mode, for the system to work properly, the inverter has to be synchronized with the grid at the time of the connection and throughout the normal operation, so it requires correct and timely update of the grid voltage. If the inverter is not synchronized with the grid or other power source it is to be connected to, then large transient current may appear at the time of connection, which may damage the equipment. In this study, a special care is provided by designing critical transition steps, while going from *grid support* to the *grid forming* mode and during the resynchronization process. These design steps are presented and validated with experimental results in the later part of the Thesis.

In the literature, numerous synchronization techniques are available, one is open-loop method which includes detecting the zero crossing of the grid voltage and another is the closed-loop method. Closed-loop methods employ a PI to make sure that the information obtained is accurate. The conventional PLL is widely used in the single-phase application, whereas the synchronous rotating reference frame PLL (SRF-PLL) is widely used in the three-phase application. One common issue with the three-phase systems is the voltage unbalance. "The SRF-PLL can achieve excellent performance for ideal balanced conditions but the performance degrades dramatically with unbalanced voltage due to the second-order harmonics appearing in the PLL output" [30].

19

2.3.1. SOGI-based Single-Phase PLL [2]

In the experimental setup, the system is subject to various load unbalances, thus a single-phase PLL equipped with the SOGI-QSG (Second-order Generalized Integrator-based Quadrature-signal generator) is implemented [30], avoiding the occurrence of the second order-harmonics in the PLL output, and is shown in Fig. 2.6.
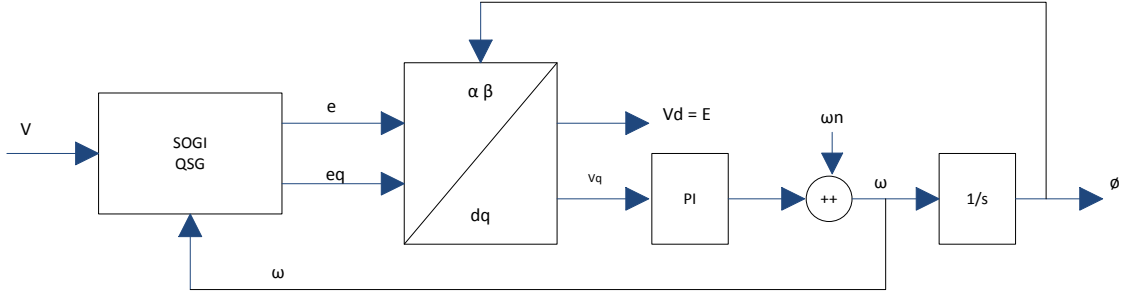
Fig. 2.6. Schematic diagram of single-phase PLL equipped with QSG

The SOGI-QSG is generating *e* and *eq* components, which are in-phase and quadrature-phase shifted w.r.t the fundamental component of the input V. The transfer function $G_d(s)$ from V to *e* is

$$G_d(s) = \frac{k\omega s}{s^2 + k\omega s + \omega^2} \tag{2.7}$$

Where ω is the resonant frequency of the SOGI-QSG; and the transfer function $G_q(s)$ from V to *eq* is;

$$G_q(s) = \frac{k\omega^2}{s^2 + k\omega s + \omega^2} \tag{2.8}$$

Both $G_d(s)$ and $G_q(s)$ are resonant filters for $0 \le K < 2$ and are able to select the component of V at the resonance frequency ω.

The components e and eq are treated as orthogonal sinusoidal components $V\alpha$ and $V\beta$, which are further transformed into DC components Vd and Vq using the Park transformation, as shown in Fig. 2.7. In order to acquire the phase, the amplitude and the frequency, a PI controller is used to drive Vq to zero. The output of the PI controller is added with the nominal frequency ωn to form the estimated frequency ω, which is then fed back to the SOGI-QSG so that it is able to select the components at the right frequency. The estimated frequency ω is integrated to obtain the estimated phase angle φ, which is also fed back to the Park transformation block to be able to compute the amplitude of the input V. When the phase is locked, $Vq = 0$, the estimated amplitude of the input V is calculated as $E=\sqrt{Vd^2 + Vq^2}$. As a result, the frequency, the phase and the amplitude of the input signal V are available.

2.3.2. Simulink Implementation of PLL

Fig. 2.7 shows the Simulink implementation of the SOGI-based single-phase PLL. The implemented PLL is to calculate the peak voltage, angular frequency and the phase angle of the phase 'a' of the genset. The applied PI parameters were $kp = 0.7$ and $ki = 68$, and the SOGI parameter was kept to 1.414.
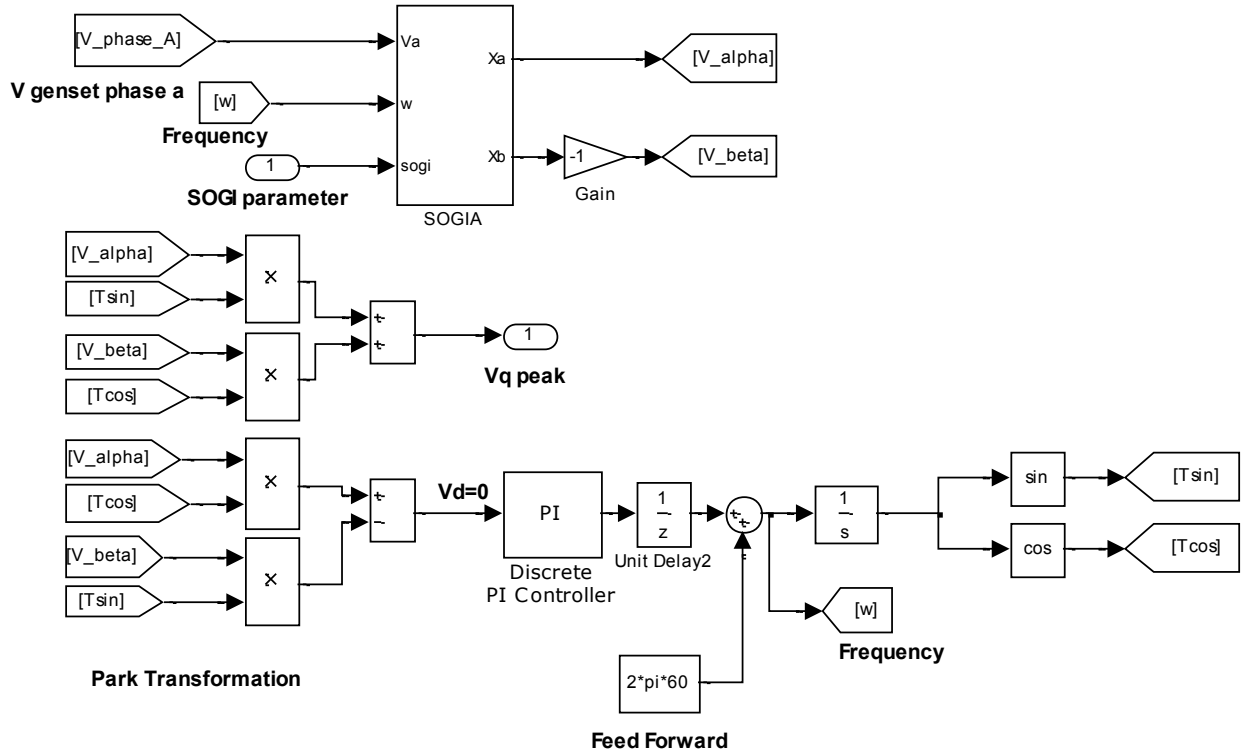
Fig. 2.7. Simulink implementation of the SOGI-PLL.

2.3.3. Experimental Results of the PLL

The experimental results of the implemented SOGI-PLL, calculating the amplitude, frequency and the phase angle of the phase 'a' of the genset is shown in Fig. 2.8. The genset (represented by Ametek supply) is programmed to 208 V L-L (120 V L-N), 60 Hz. The experimental results are as follows: 1) Fig. 2.8(a) is the calculated peak amplitude (~169.67 V) which is close to the programmed 169.71 V; 2) Fig. 2.8(b) is the computed frequency (~376.77 rad/s) which is close to the programmed 376.99 rad/s; 3) Fig. 2.8(c) is the acquired phase angle of the genset, which is smooth/linear and has no distortions. From the results presented in Fig.2.8, it is clear that the choice of the PLL to acquire correct amplitude, frequency and phase on the test bench is appropriate.

22
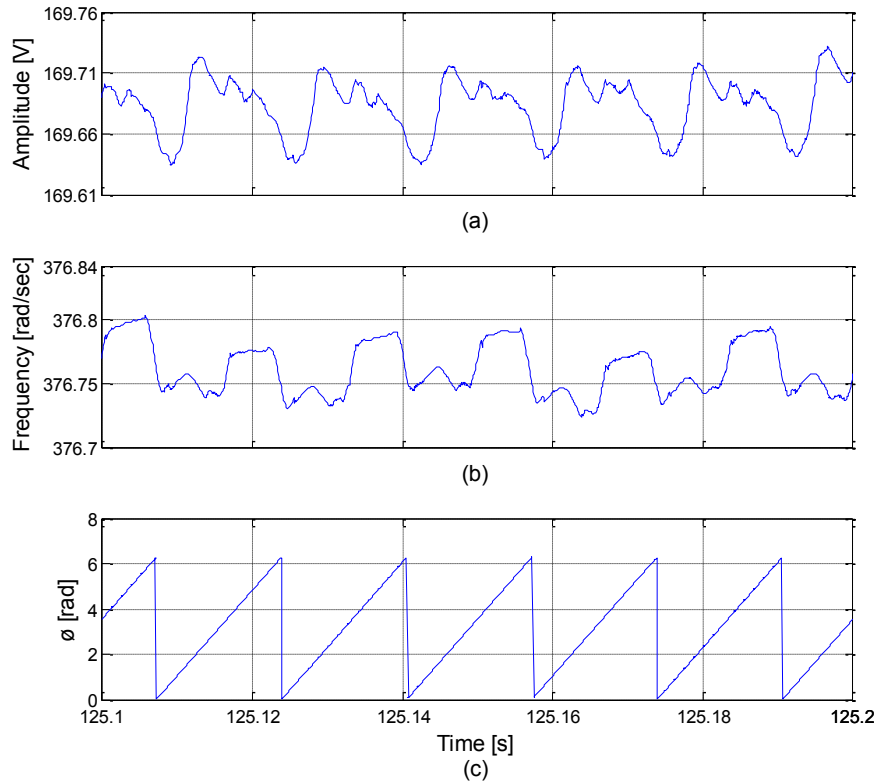
Fig. 2.8. Response of SOGI-PLL: a) amplitude; b) frequency and c) phase tracking of the phase 'a'.

2.4. Proposed Per-Phase Synchronizer

In the literature, in order to synchronize two separate AC sources to be able to connect them together in parallel without large transient currents; various sophisticated techniques are available like intelligent connecting agent (ICA) [31] etc. This study proposes the use of a simple Park transformation equation to achieve the desired synchronization results.

To synchronize a standalone *grid forming* BESS (considering it to be the first AC source) with the genset (the second AC source), the first step is to estimate the phase difference between them. Considering the both sources are at the same frequency, it is estimated by

23

applying the Park transformation equation on the standalone BESS w.r.t the angle of the genset. Afterwards, by eliminating the phase difference (error), using a PI, these two separate sources can be synchronized. It is important to mention that the three phases of the standalone BESS and the genset are synchronized individually following the same approach to overcome the effect of unbalanced voltages, if any. The Simulink implementation and the performance verification of the proposed per-phase synchronizer are presented in the next two sub-sections.

2.4.1. Simulink Implementation of the Proposed Per-Phase Synchronizer

Fig. 2.9 shows the per-phase block used for the synchronization process. The two constants, 169.71 and 2*pi*60 represents the reference peak voltage and frequency (in rad/s) of the BESS invertor to form the grid. Then they are converted into orthogonal sinusoidal components $V\alpha$ [Valpha] and $V\beta$ [Vbeta], through an integrator, sine and a cosine function block to obtain the corresponding dq components. The term [gcos] and [gsin] are the cosine and sine of the phase of the genset, extracted from the genset voltage sensor using the PLL, to which the BESS is to synchronize with, and [Vpcc_a] and [Vpcc_b] are the orthogonal components of the BESS grid at the point of common coupling (PCC). One of the equation of the Park transformation is implemented, whose output is led towards zero with a PI controller. The output of the controller is a frequency component, which is fed back into the reference frequency to complete the loop. To avoid algebraic loop error, a delay block is introduced within the control loop. The signal [resyn] is made 1 to start the synchronization process and it is kept to zero, otherwise.

24
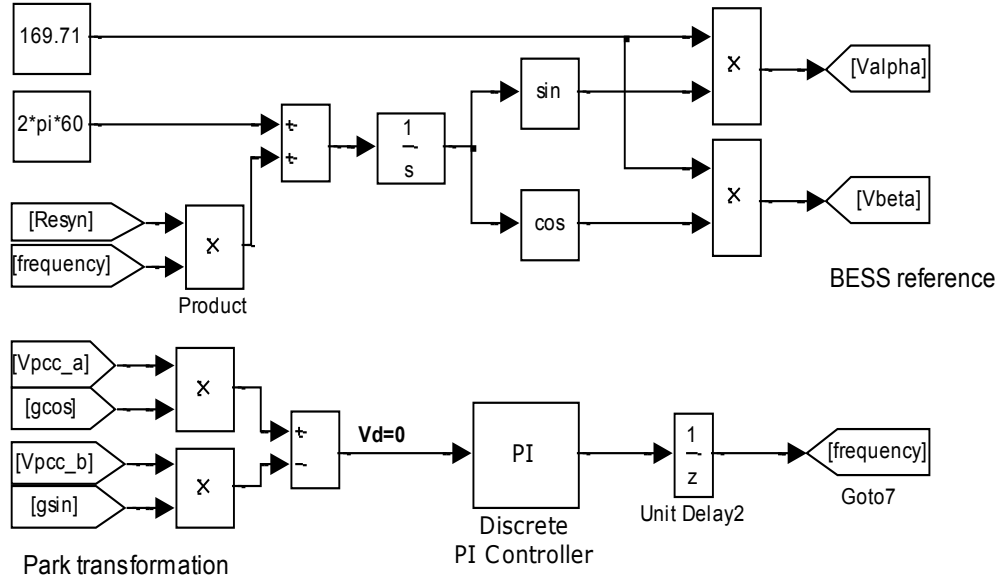
Fig. 2.9. Simulink implementation of the proposed per-phase synchronizer

2.4.2. Experimental Verification of the Proposed Per-Phase Synchronizer

In this test, it is expected for both the sources (considering a stand-alone BESS grid and a genset) to synchronize once the *'Resyn'* signal is changed from 0 to 1. Fig. 2.10 shows the experimental results verifying the effectiveness of the designed synchronization loop. To observe the synchronization process, Fig. 2.10 (a) is presented which shows the voltage waveform of phase 'a' of the genset and the BESS grid. The synchronization signal [Resyn], Fig. 2.10(c), is applied at 88.78 sec to start the synchronization process, and it can be seen that both of the sources have synchronized at 89.14 sec, after 21 line cycles, confirming the effectiveness of the design. Fig. 2.10 (b) is presented to show the output of the Park transformation driven to zero by the PI controller, proofing synchronization. The synchronization speed can be varied by changing the PI parameters. For this test, the PI parameters were kept to $kp = 2$ and $ki = 20$.
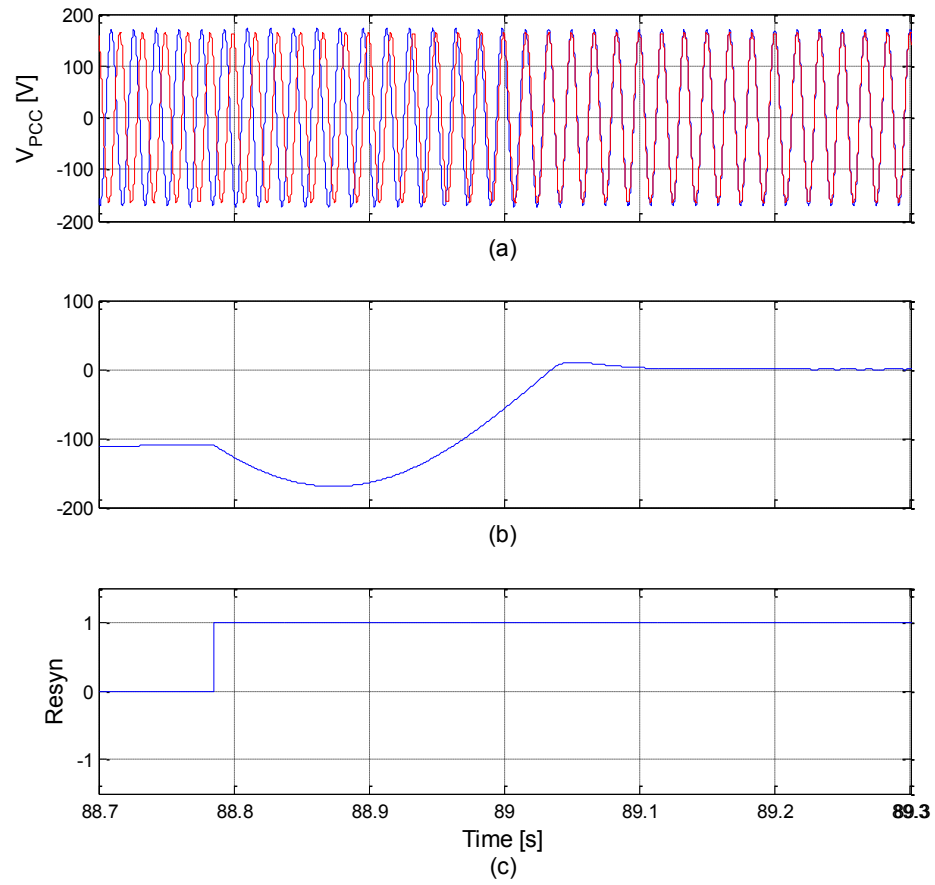
Fig. 2.10. Synchronization process: a) phase 'a' of the BESS and the genset; b) Park transformation of the BESS w.r.t genset; c) *'Resyn'* signal to start the process.

2.5. Control Circuit of the BESS

The entire control structure of the BESS can be seen in Fig. 2.11. It is provided by [1], and is employed here with some modifications. The first modification is the choice of the PLL, a single-phase QSG-PLL, shown in Fig. 2.6, is employed to tackle the voltage unbalance issue, which is usual to occur on the test bench, also explained in section "2.3 Introduction and Implementation of the Phase Lock Loop (PLL)". Secondly, proposed per-phase synchronizer, "2.4 Proposed Per-Phase Synchronizer", is employed instead of the formerly employed ICA (Intelligent connection agent) for simplification reasons. This proposed block is also presented in Fig. 2.12 and is employed to safely connect and disconnect the genset while changing the mode of operation. Finally, some modifications are introduced in the MSTS block to be able to execute the designed transition steps from *grid forming* to *genset support* and vice versa, which are further discusses in the section "3.8 Mode Selection and Transition (MSTS) Module".

On the top of Fig. 2.11, block *"Iref Generator in Genset Support Mode"* can be seen. It supplies a reference current to the inner current loop in the *genset support* mode, for load balancing, compensating the capacitor current, maintaining a unity power factor, and keeping the genset in a desired power range. All the reference generating sub-blocks within *"Iref Generator in Genset Support Mode"* block are discussed in detail, with their Simulink implementation and experimental verification in the later part of the Thesis.

In the middle of Fig. 2.11, the voltage controller and the current controller blocks can be seen, in which the voltage is the outer control loop and current is an inner control loop. During the *grid forming* mode both these loops work in cascaded connection, where the outer voltage loop generates a current reference for the inner current loop, which further

27

controls the inductor current. During the *genset support* mode, the reference of the inner current loop is generated by the block *"Iref generator in Genset support mode"*.

Individual PLLs for each phase are employed in this study, also known as per-phase QSG-PLL (Quad signal generation). The employed PLL is providing the frequency for the SOGIs to select the component at the right frequency, and the phase information of the genset for the Park and inverse Park transformations.

The MSTS block stands for the Mode Selection and Transition System. It selects and operates the BESS in the required mode of operation depending on the condition of the mini-grid distribution system. Also it generates several control signals like *'mode', 'gs2f', 'Resyn'* and *'rated'*, which performs the smooth transition between the *genset support* and the *grid forming* mode. MSTS is discussed in detail in the later part of the Thesis.
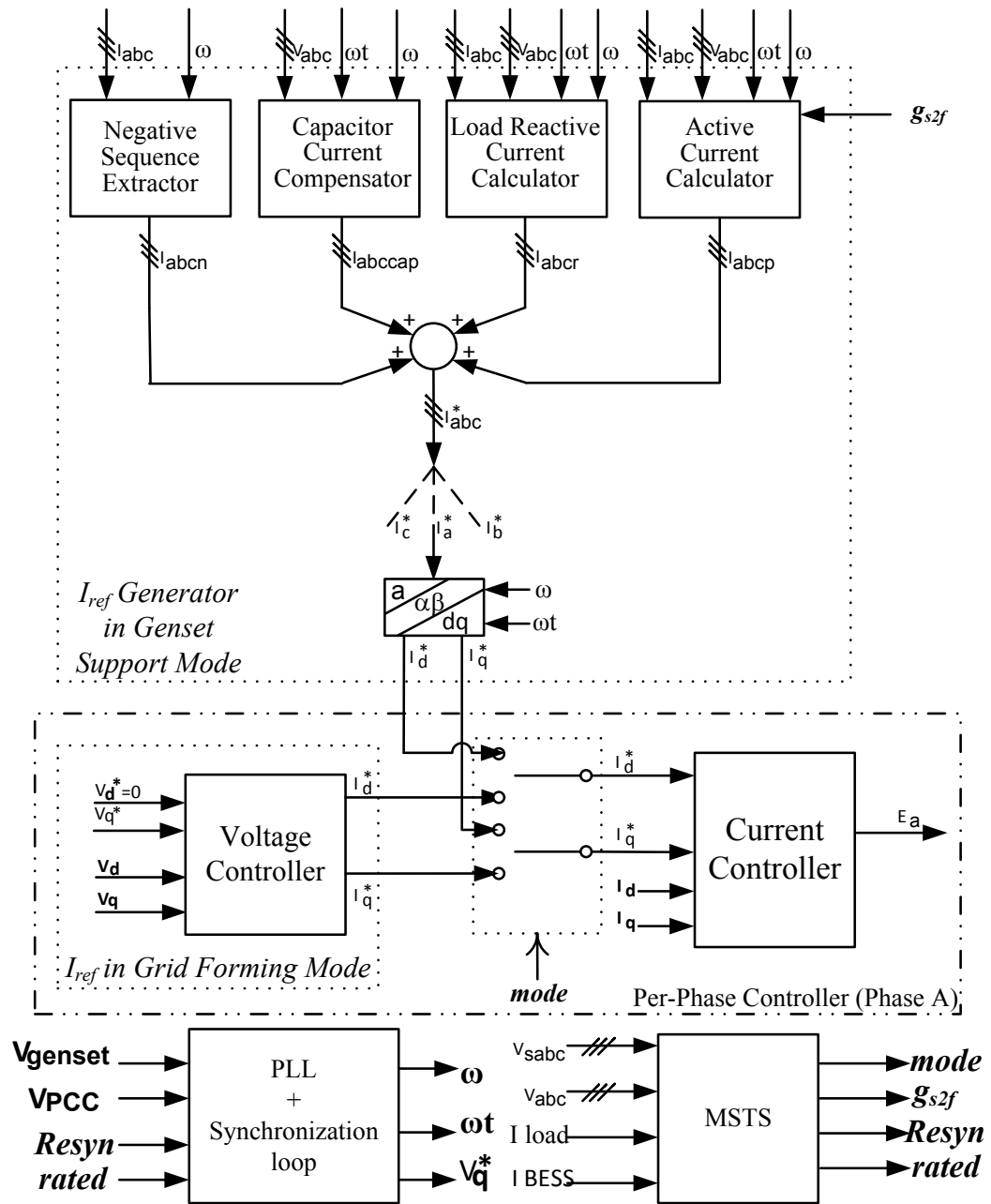
Fig. 2.11. Schematic diagram of the employed control circuit for the BESS
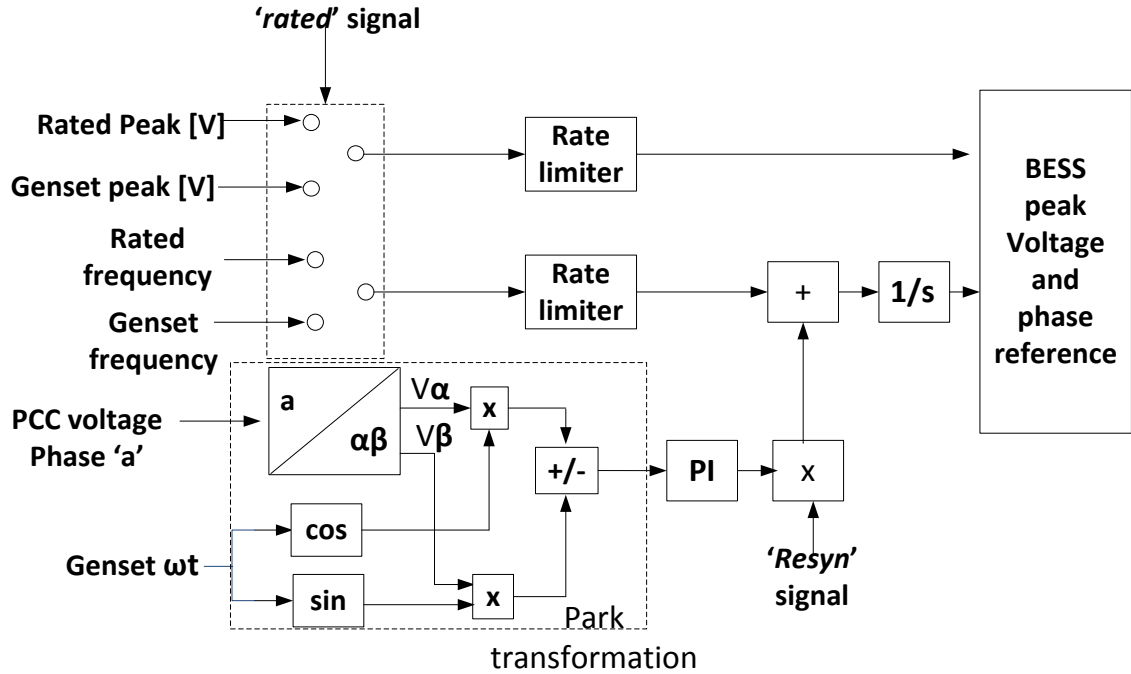
Fig. 2.12. Phase synchronization loop inside Fig 2.11

2.6. The Per-Phase Cascaded DQ Control Block

The per-phase dq control strategy provided by [1] is used to control the BESS operation. The block diagram of the per-phase dq control strategy for phase "a" of the BESS is shown in Fig.2.13. The use of the per-phase dq control makes it possible to control each leg of the inverter independently, which empowers the BESS inverter to be able to supply a negative sequence current during *grid support* mode and to form a grid on an unbalanced load during the *grid forming* mode, key features.

In the schematic diagram, Fig. 2.13, *Vd** and *Vq** are the voltage references for the external voltage loop and *Id** and *Iq** are the current references for the inner current loop. The voltage loop is active for the voltage regulation during the *grid forming* mode only, which then supplies a current reference to the internal current loop, and makes the

BESS work in the cascaded connection. *mode* Signal performs the connection of the current reference *Id** and *Iq**, to the output of the voltage loop when voltage loop is active during the *grid forming* mode and to the *"Iref Generator in grid support mode"* during the *grid support* mode. *"Iref Generator in grid support mode"* generates the current references externally for the inner current loop during the *genset support* mode and can be seen in Fig. 2.11.
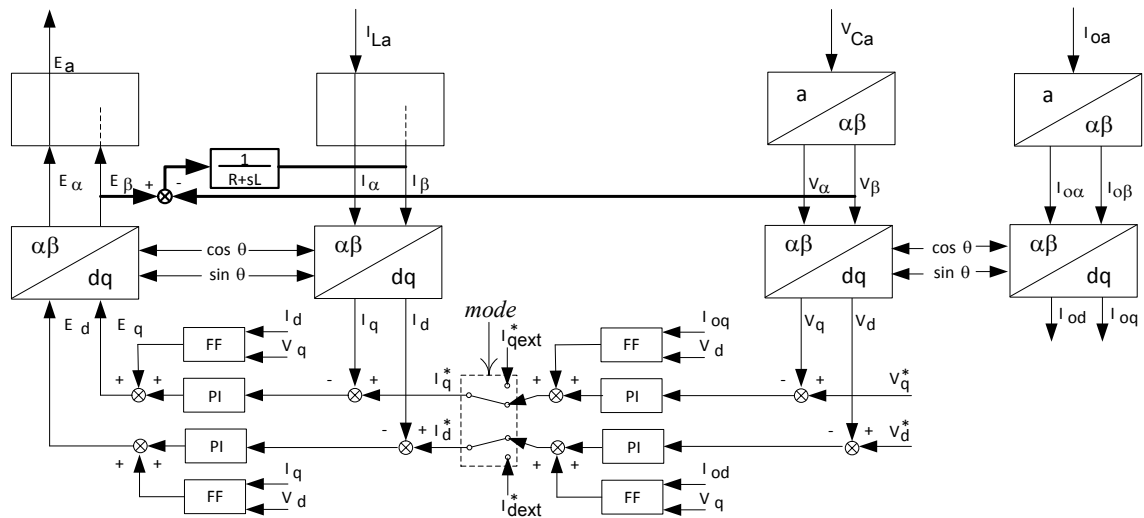
Fig. 2.13. Schematic diagram of the per-phase cascaded control block for the BESS.

The angular frequency (ω) used in the SOGIs for orthogonal signal generation is provided by their individual per-phase PLLs, Fig. 2.6. Besides, the *sinθ* and *cosθ* terms required for the Park and inverse Park transformations are also obtained from their same individual PLLs. The PI parameters for the outer voltage loop (*fx* = 40Hz) were kept to *Kp* = .002 and *Ki* = .045, and *Kp* = 9.013 and *Ki* = $1.3e^4$ (*fx* = 800Hz) for the inner current loop.

2.6.1. Simulink Implementation of the Per-Phase Cascaded DQ Control Block with β Emulation

The Simulink implementation of the cascaded voltage and current loop and the *β* emulation of the inductor current for the inner current loop can be seen in Fig. 2.14 and Fig. 2.15, respectively. Where, *Vd** and *Vq** are the reference voltages of the voltage loop during the *grid forming* mode and *Vd* and *Vq* are feedback components from the point of common coupling (PCC), where a reference is to be maintained. *Idref* and *Iqref* are the calculated reference currents by the voltage loop. In the inner current loop, Fig.2.14, it is clear that the *mode* signal has the authority to switch the reference current of the current loop between the output of voltage loop and the "*Iref generator in genset support mode*". *Ed* and *Eq* are the modulating signals which are further converted into abc frame and are fed back to the sinusoidal pulse-width modulator of the inverter to close the loop, conversion is not shown here.

Fig. 2.15 shows the *β* emulation of inductor current for the inner current loop, where *Vab, Vbb* and *Vcb* are the *β* components of the load voltage (PCC), of each phase and *Eab, Ebb* and *Ecb* are the *β* components of the modulating signal. *Iab, Ibb* and *Icb* are the emulated each phase *β* component of the inductor current. Here, an inductor of 2.3 mH and 0.2 Ω is considered as per Triphase specifications.
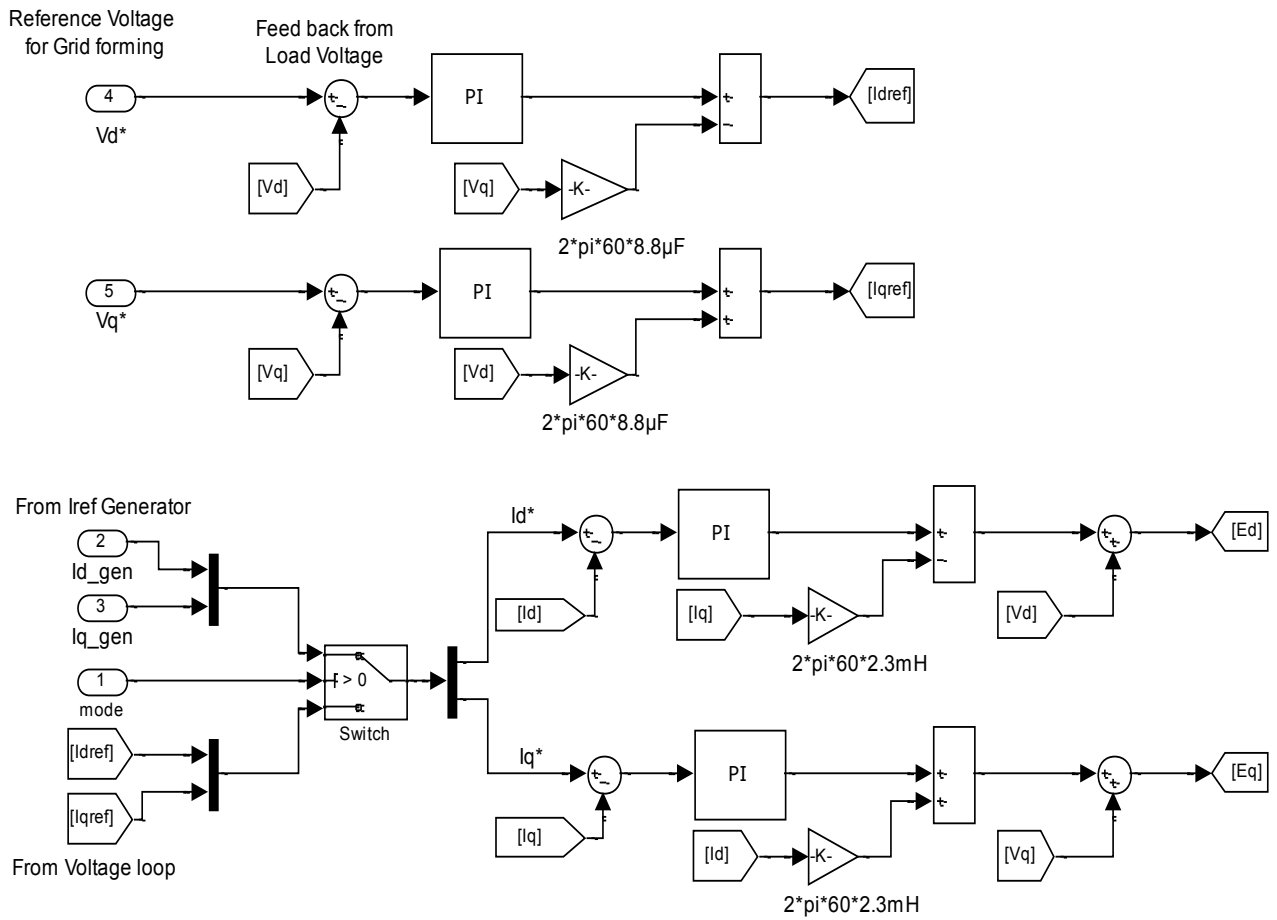
Fig. 2.14. Simulink implementation of the cascaded voltage and current loop.
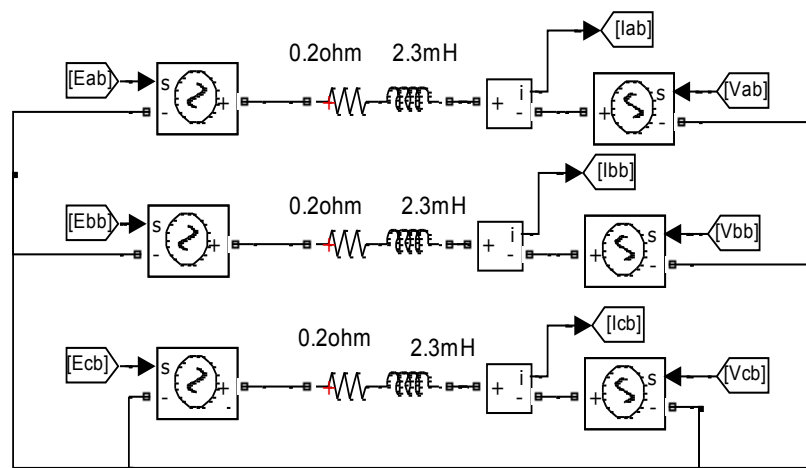
Fig. 2.15. Simulink implementation for the β emulation of the inductor current.

33

2.7. Reference Current Generation in *Genset Support* Mode

During the *genset support* mode, the reference current for the inner current loop is generated externally by the "I_{ref} *Generator in Genset Support Mode*" block as shown in Fig. 2.11. The reference current consists of four components and each component is presented, along with their Simulink implementation and validation, in the following sub-sections.

2.7.1. Negative Sequence Component Extraction from Load Current [1]

Before determining the symmetrical components of the unbalanced phasors, one needs to understand the concept of phase sequencing. Quite often, phase sequence is referred to as phase rotation, but this terminology is very misleading and is technically incorrect [32]. In fact, all phasors rotate counterclockwise always. While the direction of rotation never changes, the sequencing of the phasors may change.

Any sets of unbalance voltages or currents can be expressed as three symmetrical components of positive, negative and zero sequence; "The symmetrical components must satisfy the constraint that their vector sum equals the original set of the unbalanced phasors" [32]. In the absence of a neutral wire (return path), like in the case considered in this study, zero sequence current will not flow. The negative sequence current components can be extracted as follows. Clark and inverse-Clark transformation equations are used for transforming the variables between abc and αβ frame and are shown in equation (2.9) and (2.10).

$$\begin{bmatrix} X_\alpha \\ X_\beta \end{bmatrix} = \frac{2}{3} \begin{bmatrix} 1 & -\frac{1}{2} & -\frac{1}{2} \\ 0 & \frac{\sqrt{3}}{2} & -\frac{\sqrt{3}}{2} \end{bmatrix} \begin{bmatrix} X_a \\ X_b \\ X_c \end{bmatrix} \qquad (2.9)$$

$$\begin{bmatrix} X_a \\ X_b \\ X_c \end{bmatrix} = \begin{bmatrix} 1 & 0 \\ -\frac{1}{2} & \frac{\sqrt{3}}{2} \\ -\frac{1}{2} & -\frac{\sqrt{3}}{2} \end{bmatrix} \begin{bmatrix} X_\alpha \\ X_\beta \end{bmatrix} \qquad (2.10)$$

The positive and negative sequence αβ components of the three-phase unbalanced signals can be obtained with equation (2.11).

$$\begin{bmatrix} X_\alpha^+ \\ X_\beta^+ \\ X_\alpha^- \\ X_\beta^- \end{bmatrix} = \frac{1}{2} \begin{bmatrix} 1 & 0 & 0 & 1 \\ 0 & 1 & -1 & 0 \\ 1 & 0 & 0 & -1 \\ 0 & 1 & 1 & 0 \end{bmatrix} \begin{bmatrix} X_\alpha \\ X_\beta \\ jX_\alpha \\ jX_\beta \end{bmatrix} \qquad (2.11)$$

In order to extract the positive and the negative sequence components in αβ frame of the unbalanced abc load current, firstly the unbalanced abc load currents are converted into αβ frame with the Clark transformation equation (2.9), then each output of the equation (2.9) is passed through a SOGI, shown in Fig. 2.16, to generate their orthogonal components. The orthogonal component is represented by the j operator that corresponds to a 90° phase shift in equation (2.11). By applying the αβ components and their derived orthogonal components of unbalanced load currents in equation (2.11), one can compute the negative sequence component of the load current in αβ frame. This negative sequence in αβ frame is converted into abc frame with the inverse-Clark transformation equation (2.10), which is then supplied by the BESS for the load balancing.
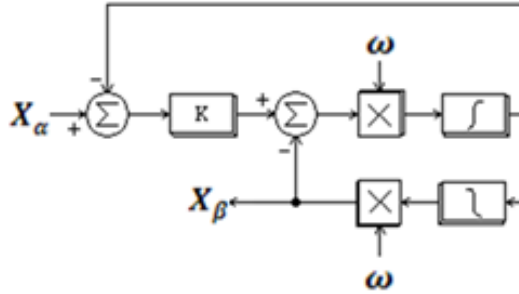
Fig. 2.16. Frequency adaptive second order generalized integrator (SOGI).

2.7.1.1. Simulink Implementation of the Negative Sequence Calculator

Fig. 2.17 shows the Simulink implementation of the negative sequence component calculator. Where, [Iabc] is the unbalanced load current and [I_neg_abc] is the computed negative sequence component. Besides, the implementation of equation (2.11), where the beta component of the unbalanced load current is calculated with a SOGI is also shown.
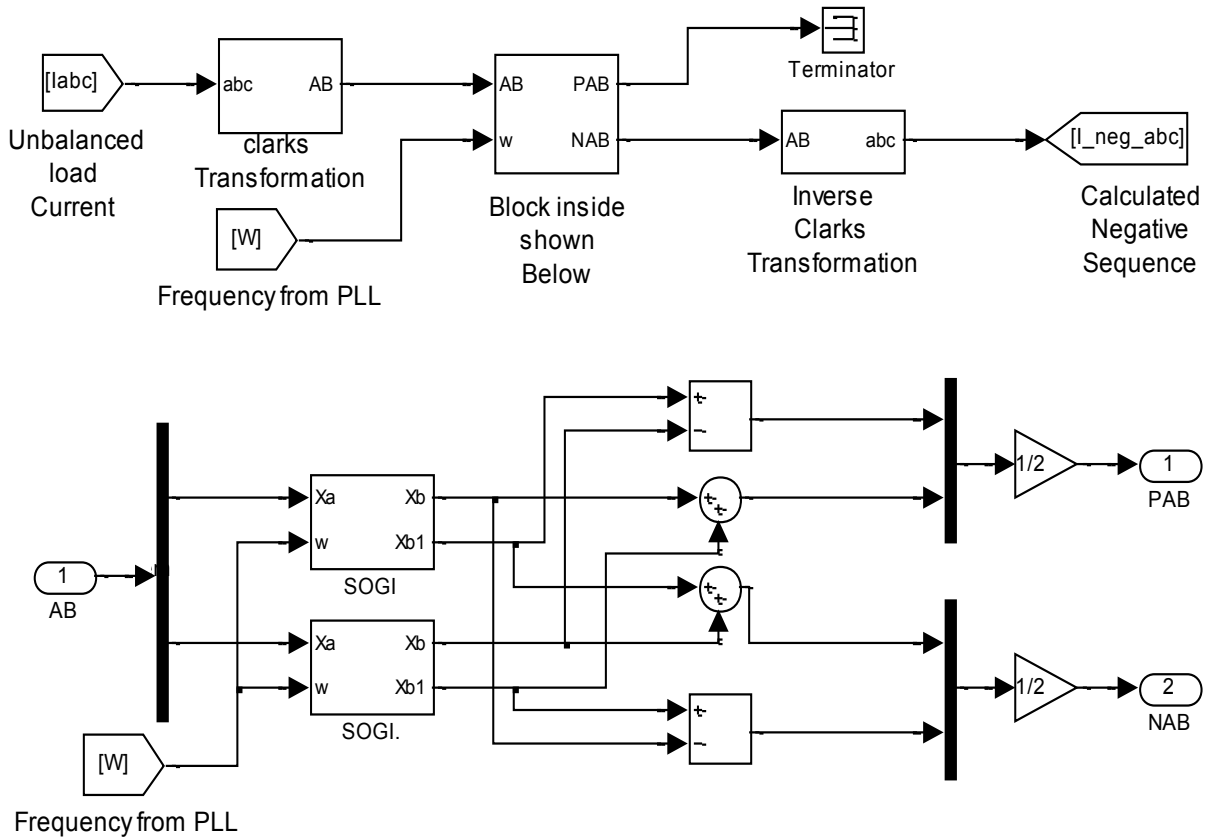
Fig. 2.17. Simulink implementation of negative sequence calculator.

2.7.1.2. Experimental Results of the Negative Sequence Calculator

To validate the implemented negative sequence calculator; "The symmetrical components must satisfy the constraint that their vector sum equals the original set of the unbalanced phasors" [32].

The computed symmetrical components, which are the negative sequence component as shown in Fig. 2.18(c), and the positive sequence component as shown in Fig. 2.18(d), are added together and shown in Fig. 2.18(e). It can be seen that their vector sum, shown in Fig. 2.18(e), equals the original set of unbalanced phasors, shown in Fig. 3.18(b). Thus, the presented experimental result demonstrates a good performance of the adopted strategy for the negative sequence current calculation. The unbalanced Y-connected load configuration considered to test the negative sequence calculator was $Za = Zb = 44\ \Omega\ and\ Zc = 22\ \Omega$. The computed negative sequence current component is injected by the BESS into the mini-grid for the load balancing, which is shown in Chapter 3.
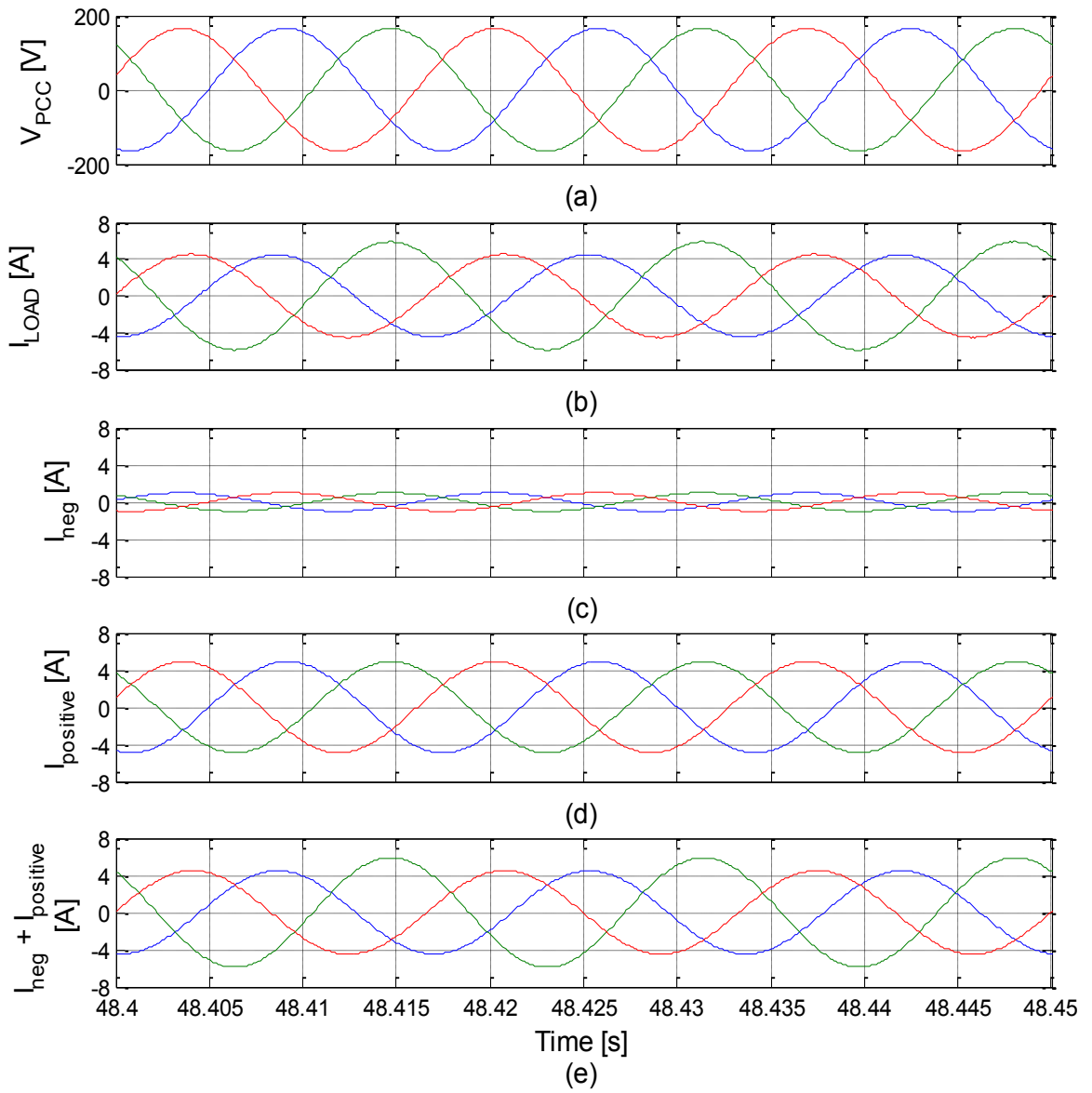
Fig. 2.18. BESS negative sequence current reference: a) voltage at PCC; b) load current; c) negative sequence current; d) positive sequence current and e) sum of negative and positive sequence current.

2.7.2. BESS Capacitor Current Compensation [1]

An LC filter is employed in the output of the BESS to reduce the switching frequency harmonics and it is mainly required during the *grid forming* mode. The BESS should supply the reactive currents of the capacitor C in the *grid support* mode to make the genset work at unity PF. Estimation of the reactive current flowing through each capacitor is done so that it can be supplied by the BESS. This is done by the following procedure. If v_α and v_β are the αβ voltage components for a phase, then the amplitude of each phase voltage is calculated as,

$$|V| = \sqrt{v_\alpha{}^2 + v_\beta{}^2} \tag{2.12}$$

Therefore, the amplitude of the required reactive current of the capacitor is given by,

$$|I| = \frac{|V|}{X_C} \tag{2.13}$$

Where, X_C is the capacitive reactance and it should be updated depending on the value of the angular frequency (ω). Similarly, the amplitude of the required reactive currents of other phases can be calculated. Using the phase angle from the PLL and the amplitude from equation (2.13), the required reactive current reference is generated for the three phases to compensate the capacitor current, which is shown in equation (2.14).

$$\left. \begin{aligned} i_{acap} &= |I| \sin\left(\omega t + \frac{\pi}{2} \right) \\ i_{bcap} &= |I| \sin\left(\omega t + \frac{\pi}{2} - \frac{2\pi}{3} \right) \\ i_{ccap} &= |I| \sin\left(\omega t + \frac{\pi}{2} + \frac{2\pi}{3} \right) \end{aligned} \right\} \tag{2.14}$$

2.7.2.1. Simulink Implementation of the Capacitor Current Calculator

Fig. 2.19 shows the Simulink implementation to compute the capacitor current reference. Where, '*V_pcc*' is the voltage at the point of common coupling (PCC) of the phase 'a' and 'Frequency from PLL' is the extracted frequency of the phase 'a' using a per-phase PLL. '*Ica*' is the estimated current flowing through phase 'a' which is then supplied by the BESS for the capacitor current compensation. A similar implementation is done for the phase 'b' and 'c' to compute their respective currents.
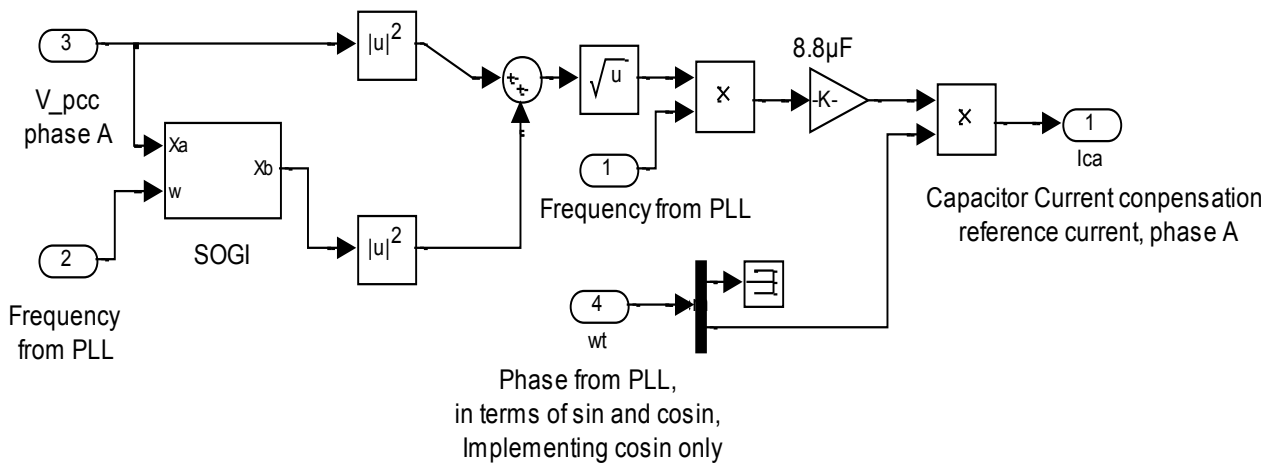
Fig. 2.19. Simulink implementation of the capacitor current calculator.

2.7.2.2. Experimental Results of the Capacitor Current Calculator

Fig. 2.20 shows the control signals from the experimental setup, showing the voltage at the point of common coupling and the computed capacitor current. It is evident from Fig. 2.20 that the calculated current leads the voltage by 90^0, which shows its capacitive nature.

The theoretical peak value of the capacitor current, for a capacitor of 8.8 µF, when subject to 120 V and 60 Hz, is found to be 0.56 A, and the computed value from the test bench (0.55 A) are comparable, which validates the implemented capacitor current calculator. It is to be noted that the computed capacitor current from the test bench, shown in Fig. 2.20(b), is the fundamental component only, however the actual current flowing through the capacitor will depend on the equivalent series resistance (ESR) of the capacitor and voltage harmonics, which are not considered here for simplification.
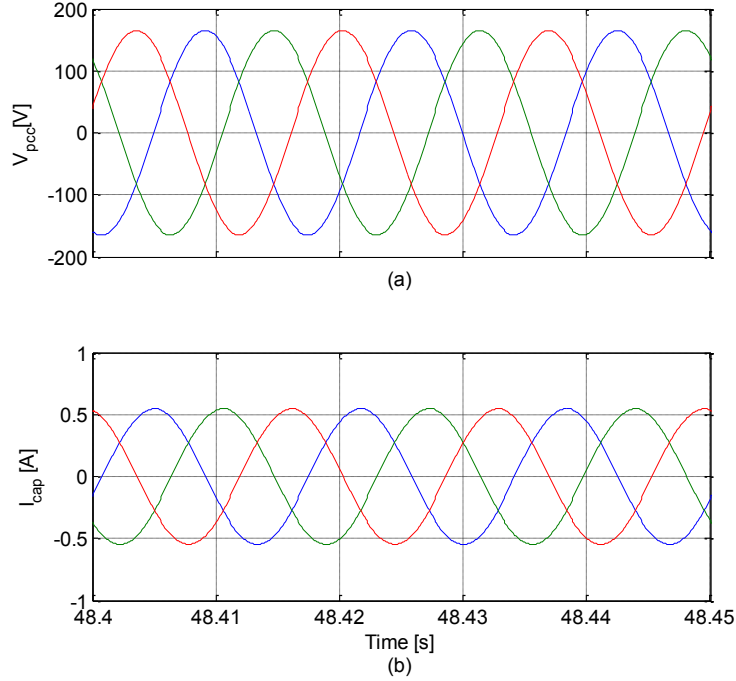
Fig. 2.20. BESS capacitor current reference: a) voltage at PCC; b) computed capacitor current.

2.7.3. Load Reactive Power Compensation [1]

To utilize the full capacity of genset for supplying active power, BESS must satisfy the load reactive power demand. The total positive sequence reactive power of the load can be calculated as,

$$Q^+ = 1.5\left(v_\beta^+ i_\alpha^+ - v_\alpha^+ i_\beta^+\right) \tag{2.15}$$

To be able to use equation (2.15), initially equations (2.9) and (2.11) are applied on the PCC voltage and the load currents to extract their positive sequence $\alpha\beta$ components ($v_{\alpha\beta}^+$ and $i_{\alpha\beta}^+$). Then they are applied to equation (2.15) to obtain the positive load reactive power Q^+.

The power calculated from equation (2.15) is further applied in equation (2.16) to calculate the corresponding peak value of the reactive current reference.

$$I_{ar} = -\frac{Q^+}{3}\frac{2}{V^+} \tag{2.16}$$

Where, I_{ar} is the computed peak of the reactive current reference, V^+ is the peak value of the positive sequence voltage component of PCC, and Q^+ is the computed reactive power from equation (2.15). The negative sign is to make the BESS supply the reactive power. The instantaneous reactive current references in the abc are generated by the product of the peak of the reactive current reference, computed in equation (2.16), with the cosine of the phase angle generated by the per-phase PLLs.

2.7.3.1. Simulink Implementation of the BESS Reactive Current Reference Calculator

Fig. 2.21 shows the Simulink implementation for load reactive power compensation, where the unbalanced load currents [Iabc] and the PCC voltages [Vabc] are first converted into αβ positive symmetrical components, by using equations (2.9) and (2.11). Then, the three-phase reactive power and peak voltage calculations are done by using equations (2.15) and (2.12). Finally, the reference currents are generated by the product of the computed peak of the reactive current, represented by [Q] in Fig. 2.21, with the cosine of the angle of each phase provided by per-phase PLLs.
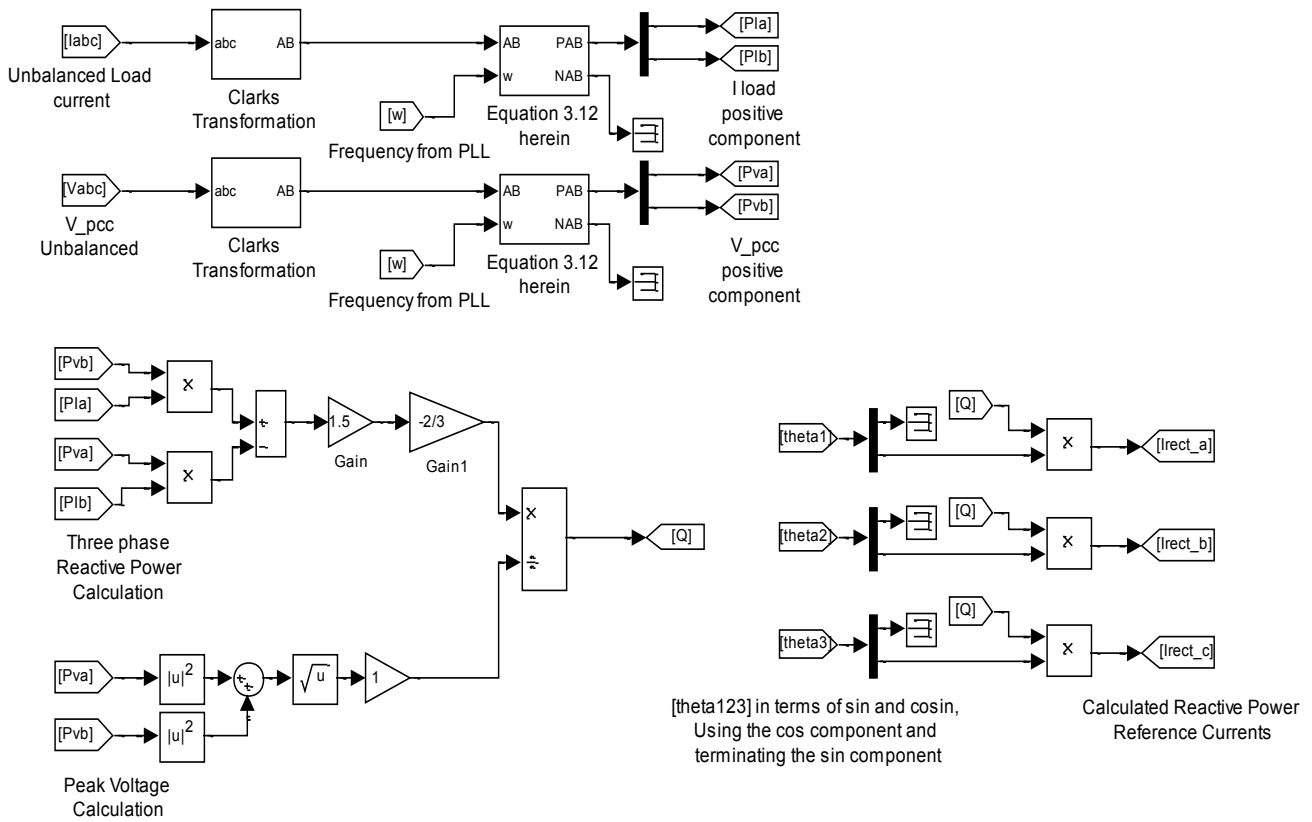
Fig. 2.21. Simulink implementation for load reactive power compensator.

2.7.3.2. Experimental Results of the BESS Reactive Current References Calculator

To test the reactive power current reference calculator, a Y-connected reactive load of $Za = Zb = Zc = 11 + j12\ \Omega$ is connected at the PCC. The real and reactive power consumed by this load is shown in Fig. 2.22. And Fig. 2.23 is presented to shows the voltage at the point of common coupling, load current drawn by the connected load and the computed reactive current references by the calculator. The justification of the presented test results is as follows.
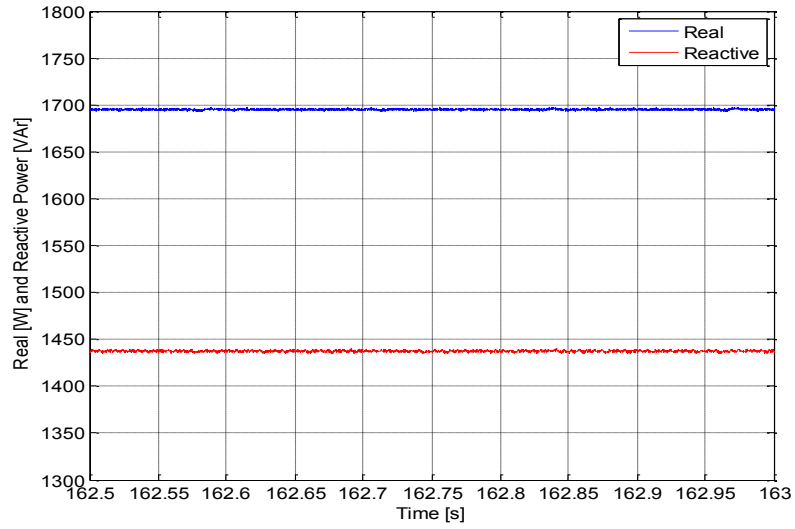
Fig. 2.22. Real and reactive power consumed by the load

For the genset to work at unity power factor, the reactive power consumed by load, 1438 VAr in Fig. 2.22, must be supplied by the BESS. For that, the BESS should inject a 90^0 lagging current whose theoretical amplitude should be,

$$Q_{3\emptyset} = -1438 \, VAr$$

$$Q_{1\emptyset} = -479.33 \, VAr$$

$$Voltage = 120 * \sqrt{2} \, V \, (peak) \quad \text{(programmed in California Instruments)}$$

Therefore,

$$I_{ref} = \frac{Q_{3\emptyset}}{Voltage} = 3.99 \, A = 5.64 \, A \, (peak) \tag{2.17}$$

The matching of the theoretical value of the current reference of equation (2.17), to the experimentally computed reactive current references of Fig. 2.23(c), demonstrates that

the adopted strategy for computing the reactive current references has a good performance. The computed reactive current references are then supplied by the BESS for the load reactive power compensation. This section only deals with the computational analysis of the reference reactive currents w.r.t the load reactive power. However, the execution of this computed references by the BESS, to make the genset work at unity PF is demonstrated in Chapter 3.
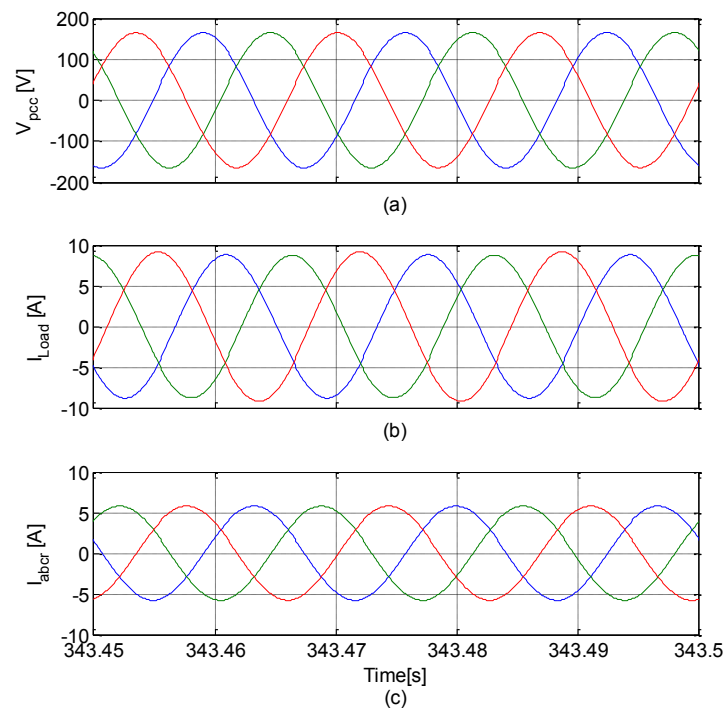
Fig. 2.23. BESS reactive current reference: a) voltage at PCC; b) load currents; c) computed reactive current references.

2.7.4. 'BESS' Active Component Current Calculation to Operate the Genset within the Desired Range [1]

The BESS active reference current is expected to keep the diesel genset operating in the high efficiency range and to have a safe margin of the capacity of the genset as spinning

reserve for sudden load disturbances, which means oil (fuel), is converted into electric energy with high efficiency (high kWh/liters) and the required size of the genset is condensed as the BESS supplies supplement power during the peak load conditions. To achieve these features, the BESS supplies supplement power during the peak load conditions, while consuming it to charge the battery bank during the low load conditions, where the genset usually presents lower efficiency.

This logic can be implemented using the information of the mini-grid load power demand. BESS should supply or absorb positive sequence power in order to ensure the operation of the genset within the desired power range. The total positive sequence power of the load can be calculated as in [1] by,

$$P^+ = 1.5\left(v_\alpha^+ i_\alpha^+ + v_\beta^+ i_\beta^+\right) \tag{2.18}$$

Equations (2.9) and (2.11) are applied on the PCC voltage and the load currents to obtain the positive sequence αβ components ($v_{\alpha\beta}^+$ and $i_{\alpha\beta}^+$) required for using equation (2.18) to determine the load positive sequence power.

The power calculated from equation (2.18) is passed through a comparator block, as shown in Fig. 2.24, to generate an active current reference for the BESS. The characteristics of the logic describing the relationship between the BESS positive sequence power (P_{BESS}^+) and the load positive sequence power (P^+) is given by,

$$P_{BESS}^+ = \begin{cases} P_{min} - P^+ & ; P^+ < P_{min} \\ 0 & ; P_{min} \leq P^+ \leq P_{max} \\ P^+ - P_{max} & ; P^+ > P_{max} \end{cases} \tag{2.19}$$

Therefore the peak value of the positive sequence active component of the reference current of the BESS is given as in [1] by,

$$I_{ap} = \frac{P_{BESS}^+}{3} \frac{2}{V^+}$$

(2.20)

Where, V^+ is the peak value of the positive sequence (phase) voltage components of PCC. And P_{BESS}^+ is the power to be supplied by the BESS computed from equation (2.19). The instantaneous reference active currents $[i_{pow\_abc}]$ of the BESS are generated by the product of I_{ap} [Ipow_abc] and the sine of the phase angle from the PLLs.
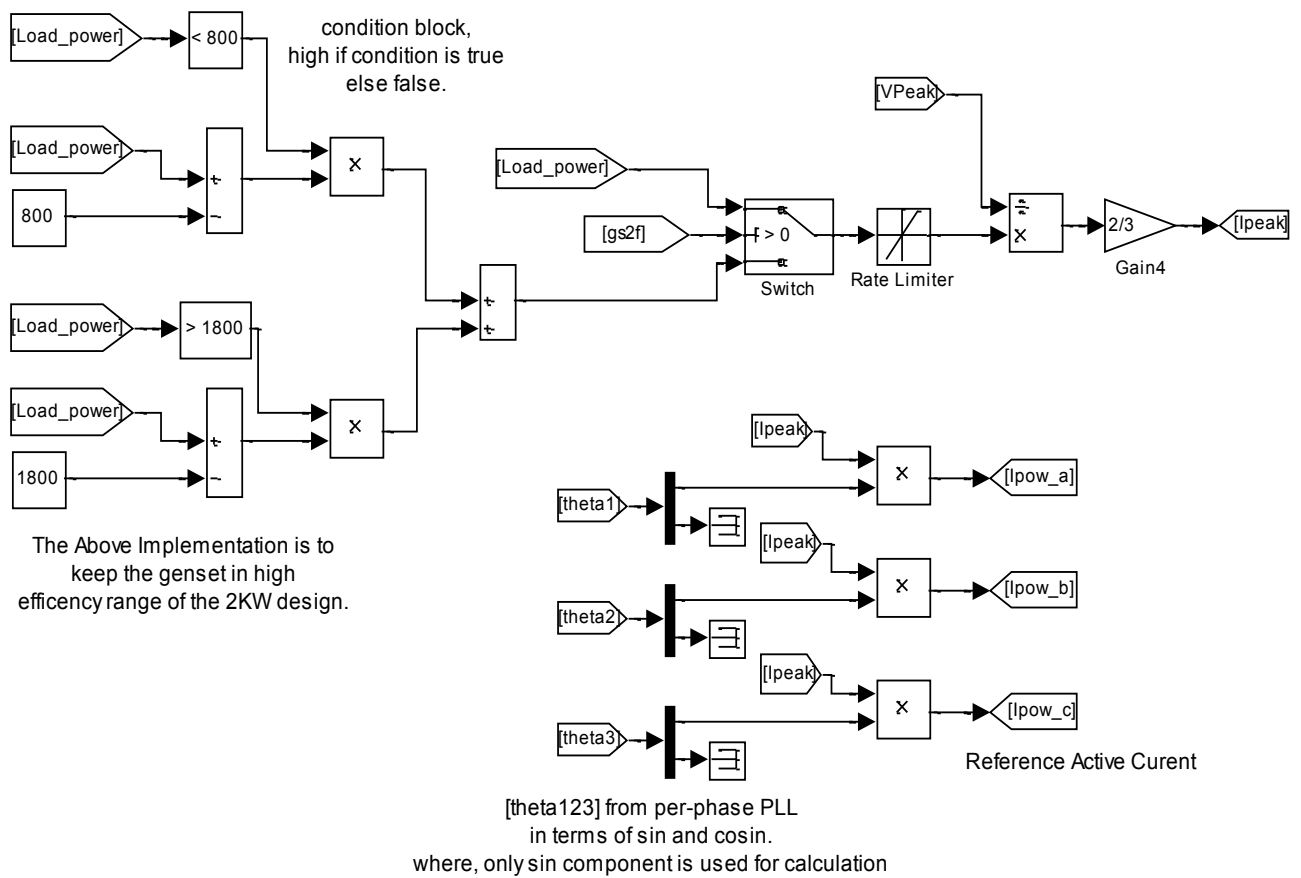
Fig. 2.24. The active power reference current calculator

2.7.4.1 Simulink Implementation of the Active Current Reference Calculator

Fig. 2.24 shows the Simulink implementation of the control logic that keeps the genset operating in high efficiency range, which is considered to be in between 800 W and 1.8 kW for a 2 kW genset. Whenever the positive sequence load power goes below 800 W or goes higher than 1.8 kW, the condition block sets to high. The difference power which is calculated by subtracting the instantaneous mini-grid power from a constant of 800 W and 1.8 kW for low and high power cases respectively. It is sent further as the power reference to calculate the active reference current. After that, equation (2.21) is implemented which divides the reference power with the calculate voltage peak [Vpeak], not shown here, to calculate the peak current. Finally, the peak current [Ipeak] is multiplied with the sine of the angle provided by the PLLs to generate the reference active power currents.

2.7.4.2 Experimental Results of the Active Current Reference Calculator

To test the active current reference calculator, any load below 800 W is considered to create a low load condition and higher that 1.8 kW, a high load condition, for a genset of 2 kW. It is expected by this calculator to estimate the reference currents for the BESS so as to keep the genset operating in the desired power range. To create a low load demand, a resistor of 88 Ω was subject to 208 V L-L and 60 Hz. And for the high load demand, the considered Y-connected load was $Za = 44 \, \Omega \, \& \, Zb = Zc = 11 \, \Omega$, also subject to 208 V L-L and 60 Hz. These loads were considered appropriate since the load power is a function of load voltage, load resistance and frequency. The positive active power consumed by the connected loads are shown in Fig. 2.25, where Fig. 2.25(a) shows the

49

power consumed during the low load demand and Fig. 2.25(b) shows the power consumed during the high load demand.
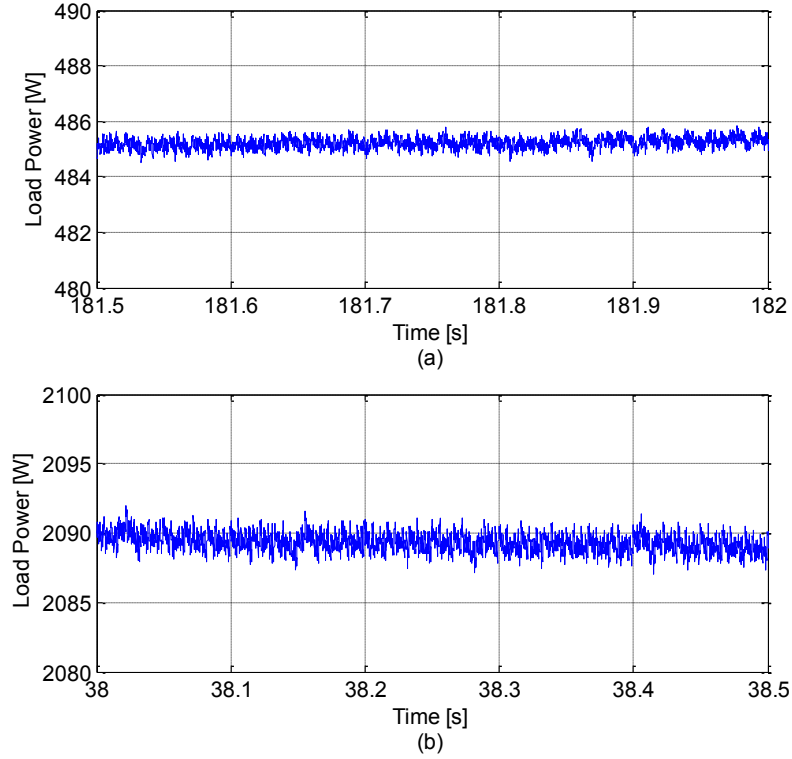
Fig. 2.25. Load power demand: a) low load demand; b) high power demand.

To keep the genset operating between 800 W and 1800 W, the BESS must absorb 315 W and supply 290 W into the grid. The peak value of the load voltage from the point of common coupling is $Vpeak = 120 * \sqrt{2} = 169.71\ V$, programmed in the California Instruments (Ametek supply) working as genset. Theoretically, to absorb 315 W, the reference currents of the BESS should be,

$$P_{3\emptyset} = -315\ W$$

$$I_{ref1} = \frac{315}{3} * \frac{2}{169.71} = -1.24\ A \qquad (2.21)$$

Negative sign indicate that the current should be out of phase with voltage.

And for BESS to supply 290 W the reference current should be,

$$P_{3\emptyset} = 290\ W$$

$$I_{ref2} = \frac{290}{3} * \frac{2}{169.71} = 1.14\ A \tag{2.22}$$

The theoretical values computed in equation (2.21) and (2.22) matches to the presented experimentally calculated active current references of Fig. 2.26(b) and Fig. 2.27(b), which shows the correct implementation of the active current reference calculator.
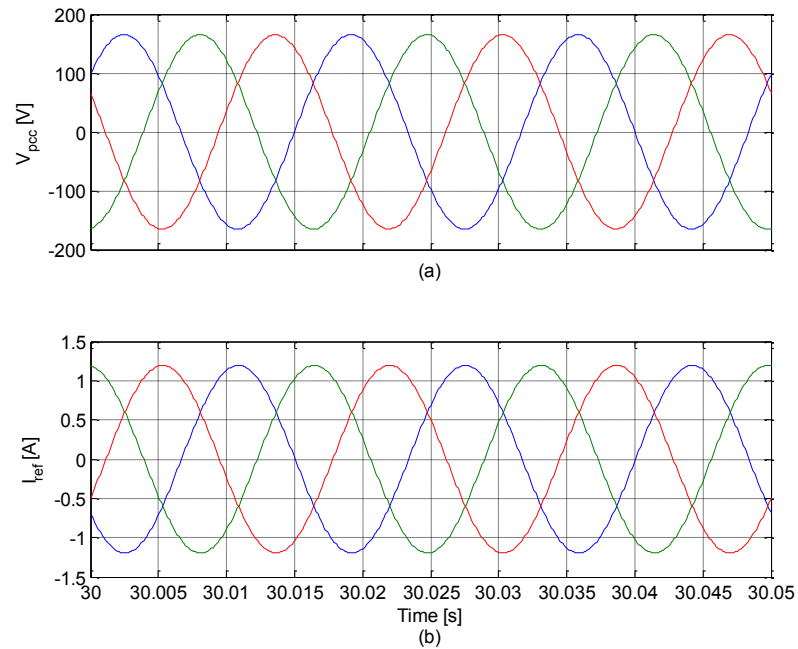
Fig. 2.26. Active current reference during low load: a) voltage at PCC; b) computed active current reference for BESS to absorb power.
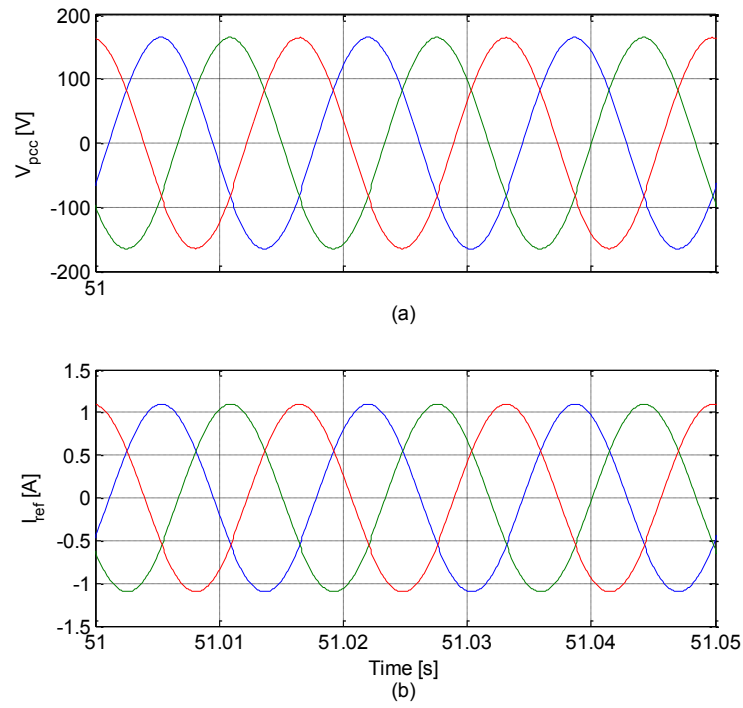
Fig. 2.27. Active current reference during high load: a) voltage at PCC; b) computed active current reference for BESS to supplying power.

2.8. Mode Selection and Transition System (MSTS) Module

Considering the various load situations that might occur in the mini-grid distribution system. Mode selection and transition system module (MSTS) is designed to select and operate the BESS in a required mode to be able to cope with the situations.

There could be two possible ways to change the mode of operation of the BESS. One is unintentional and another is intentional. The first (unintentional) one, is required when the BESS is working in *genset support* mode, which means supplying negative sequence current, load reactive power and capacitor current, and during that the load demand drops below the lower limit of the high efficiency range of the genset. At this time, initially, BESS will absorb power to return and keep the genset in the high efficiency range until the state of charge (SOC) of the battery reaches maximum. Once the SOC reaches maximum, or it is the case when the battery was already at maximum charge when the load dropped, there are two further possibilities; the first one, if the load power is less than the rated capacity of the BESS and the second, when the load power is higher than the rated capacity of the BESS. For the first case, the mode of operation of the BESS will change unintentionally from the *genset support* to the *grid forming* mode, with the BESS forming stand-alone grid. In the second case, BESS will keep working in *genset support* mode while absorbing power, to keep the genset operating in the high efficiency range; power is further dissipated on the bleeding resistor now.

The second possible change in the mode could occur intentionally. The power station operator could simply shift the mode from *genset support* mode to the *grid forming* mode to perform maintenance operation of the genset. Once the maintenance is complete, the system can return back to *genset support* mode by the operator. This transition can also

occur when the operator knows that the BESS can meet the actual and forecasted load demand, by itself or assisted by a renewable energy source (RES).

It is to be noted that the MSTS module will not allow changing mode intentionally, when the load power exceeds the rated capacity of the BESS. To do so, the MSTS block is provided with the load information continuously.

The Mode Selection & Transition System (MSTS) Module will change the mode of operation of the BESS unintentionally, depending on the status/condition of the system as stated earlier and intentionally on the users request to perform genset maintenance operation. To ensure that the mini-grid distribution system does not experience any voltage disturbance at the PCC during a *mode* transfer, the MSTS also performs the controlled smooth transition between the two operating modes. For this purposes, it generates the following four control signals. Only general description of signals is provided here. For detail procedure and state of signals, please follow the next sections.

- 'g_{s2f}' signal: It performs the smooth loading and unloading operation of the genset.
- '*mode*' signal: This signal directly controls the genset breaker and switches the reference signal sent to the inner current loop between the output of the voltage loop and the *"Iref generator in the genset support mode"*.
- '*rated*' and 'Resyn' signals: Both these signals are employed to synchronize the BESS grid forming reference with the genset voltage sensor parameters, required to change the mode of operation.

2.8.1. 'g$_{s2f}$' Signal for Loading and Unloading the Genset

'gs2f' signal is generated by the MSTS block, intentionally or unintentionally as discussed earlier, for the loading and unloading operation of the genset. Genset is unloaded prior the mode transfer from *genset support* to *grid forming*, to prevent sags (disturbance) in the PCC voltages at the moment genset breaker goes off, and then it is loaded once it returns back to the *genset support* mode. To ensure a smooth loading and unloading process, a rate limiter block is also employed within the design. In Fig. 2.28, when 'gs2f' changes to 1, all the load power demand [Load_power] is sent to be the BESS active power reference [Reference_p] through a rate limiter block. In other words, with 'gs2f' = 1, unloading of genset starts by the BESS injecting the active load power into the grid, smoothly, through a rate limiter block. And when 'gs2f' signal changes to 0, the BESS reduces the load active power supply, smoothly, loading the genset. Once genset is loaded, the BESS supplies the supplementary power only, if required. The supplementary power calculation logic is also presented in the same Fig. 2.28, and it is discussed in detail under section "2.7.4 'BESS' Active Component Current Calculation to Operate the Genset within the Desired Range [1]". The loading and unloading time can be varied by choosing an appropriate positive and negative slew rate of the rate limiter block.
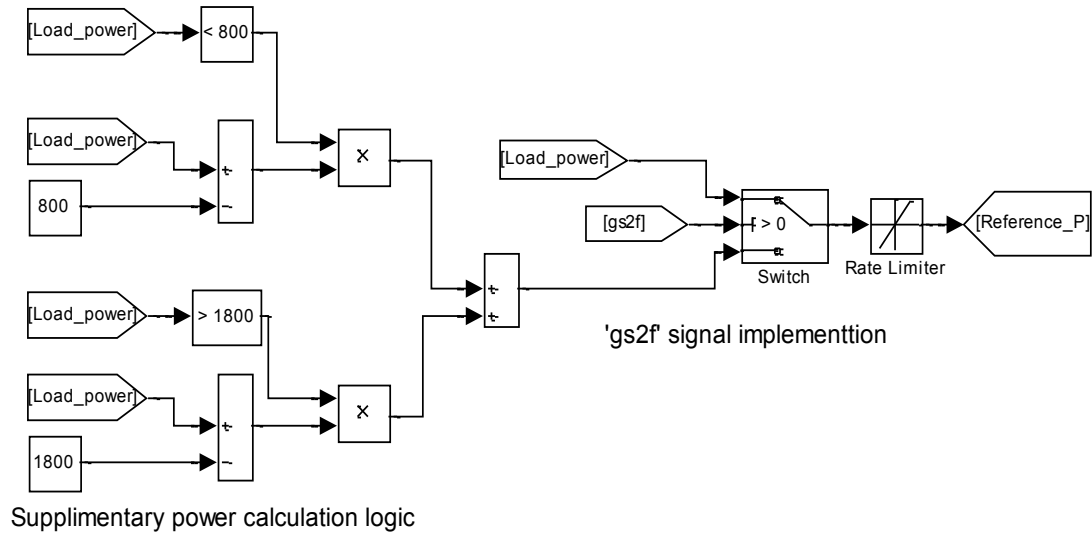
Fig. 2.28. Simulink implementation showing '*gs2f*' signal.

2.8.2. *'mode'* Signal to Change the Mode of Operation of BESS

The MSTS module changes the state of '*mode*' signal once the unloading process of the genset is completed and the system is ready to change the mode to *grid forming* or when the synchronization process is completed and system is ready to change the mode to *genset support.* To ensure a safe transition, the MSTS module is provided with the load and BESS SOC update.

The '*mode*' signal directly controls the genset breaker and it indicates the operating mode of the BESS. The BESS operates in *genset support* mode, when '*mode*' = 1, and it operates in *grid forming* mode, when '*mode*' = 0. When '*mode*' signal changes from 1 to 0, the genset breaker opens and the BESS forms a grid on the mini-grid distribution system to supply uninterrupted power. And when '*mode*' signal changes from 0 to 1, the genset breaker closes and the grid is now formed by the genset, with the BESS supporting it.

The '*mode*' signal also selects the control loop for the per-phase controllers, i.e., when '*mode*' = 1, the inner current loop takes the reference current from the *"Iref Generator in Genset Support Mode"* block, in the *genset support* mode and when '*mode*' = 0, it takes the reference current from the output of the voltage control loop, in the *grid forming* mode. The Simulink implementation showing the '*mode*' signal, performing aforesaid task, can be seen in Fig. 2.14, where it controls the references of the inner current loop.

2.8.3. *'Resyn'* and *'rated'* Signals for Synchronization

These signals are generated by the MSTS block to smoothly change the mode of operation from one to another. Both these signals are generated in a specific order to handle the task (smooth operation) properly. Their working order, to change the mode of operation from one to another, is presented in the following two sections.

2.8.4. Steps from *Genset Support to Grid Forming* Mode

The first step is to unload the genset, once it is unloaded, the very first voltage amplitude, frequency and phase angle applied across the mini-grid distribution system at the moment the genset breaker goes off, must be exactly the same as it was during the breaker "on" position. This will ensure that the mini-grid distribution system does not experience any voltage disturbances. The proposed method is implemented in Fig. 2.29 and is able to achieve a smooth transition while changing the mode of operation. Its experimental verification is presented in Chapter 3. Table 2.1 includes the description of the input and output ports of Fig. 2.29. It is to be noted that the first reference, which consist of peak voltage, frequency and phase angle, applied by the BESS grid, the moment genset breaker goes off, should be coming from the genset voltage sensor as discussed earlier. And to achieve it, the '*rated*' signal and '*Resyn*' signal are employed, which will

synchronize the BESS grid forming references to the genset voltage sensor parameters. For synchronization details, refer to section "2.4 Proposed Per-Phase Synchronizer".

After successfully *grid forming* by BESS with the genset voltage sensor parameters as references, it is obligatory to go to the rated mini-grid distribution parameters in order to eliminate the role of the genset voltage sensor from the BESS grid forming references. Otherwise, the BESS will keep tracking the output voltage of the genset and will not allow it to shut down. It is achieved in the following steps;

Firstly, the '*Resyn'* signal is changed from 1 to 0 to break the synchronization loop between the BESS grid reference and the genset voltage sensor. Secondly, the '*rated'* signal is changed from 1 to 0, which drives the BESS grid, from the peak voltage and frequency of the genset voltage sensor, towards the rated mini-grid parameters provided in constant blocks, as $120 * \sqrt{2}$ and $2 * pi * 60$ shown in Fig. 2.29, smoothly. The smooth operation is achieved by the rate limiter block. Henceforth, BESS is operating in the *grid forming* mode and the genset is allowed to shut down. Table 2.2 is presented to show the state of signals, *'mode', 'rated', 'Resyn'* and *'gs2f'* during the transition.
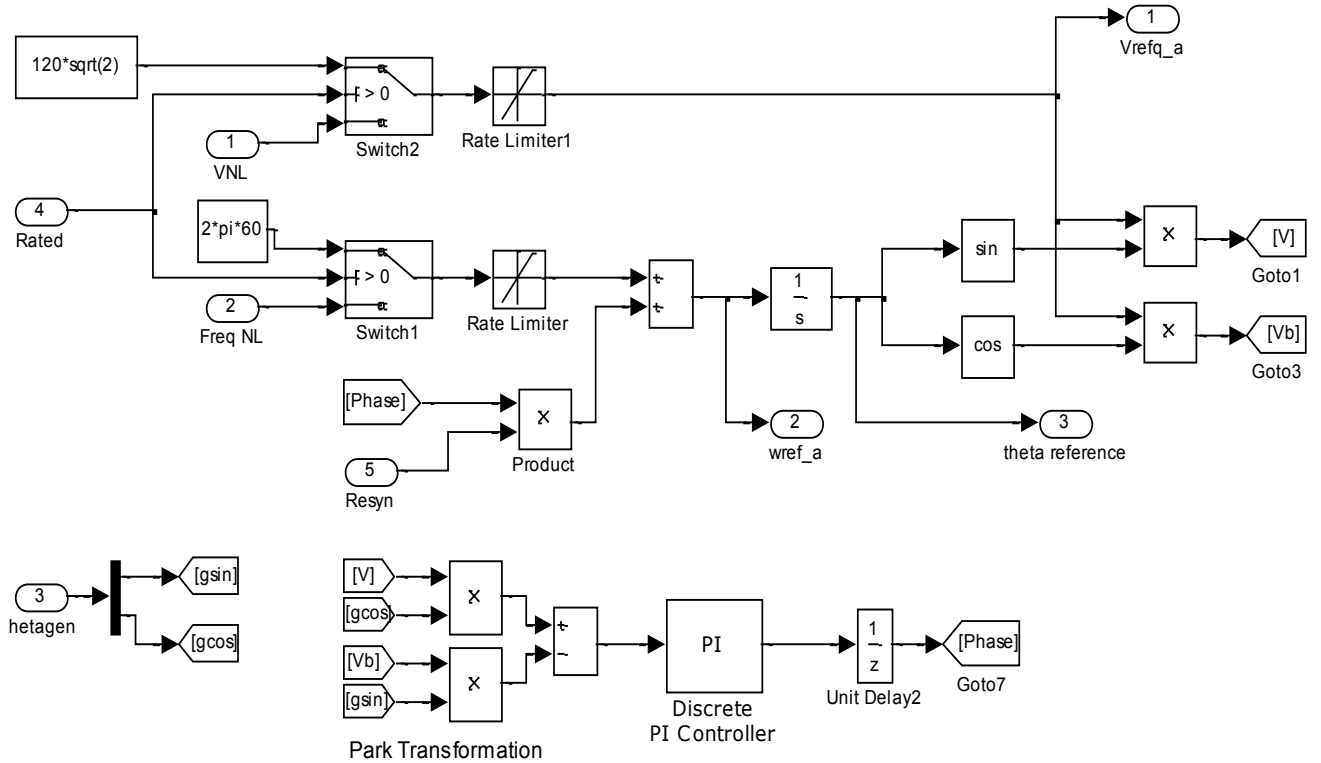
Fig. 2.29. Proposed block for smooth mode transition employing the *'rated'* and *'Resyn'* signals.

Table 2.1. Description of input and output signals of Fig. 2.29

Port No.	Input port	Output port
1	Genset peak voltage	BESS peak voltage reference
2	Genset frequency	BESS frequency reference
3	Genset phase angle	BESS phase reference
4	'rated' signal	Not applied
5	'Resyn' signal	Not applied

Table 2.2 State of the signals by MSTS module when BESS goes form the *genset support* to *grid forming* mode.

BESS in *genset support* mode	Unloading genset	Grid formed by BESS (Tracking genset voltage sensor)	BESS grid forming (stand-alone)
'mode' = 1	*'mode'* = 1	*'mode'* = 0	*'mode'* = 0
'gs2f' = 0	*'gs2f'* = 1	*'gs2f'* = 1	*'gs2f'* = 1
'Resyn' = 1	*'Resyn'* = 1	*'Resyn'* = 1	*'Resyn'* = 0
'rated' = 1	*'rated'* = 1	*'rated'* = 1	*'rated'* = 0

2.8.5. Steps from *Grid Forming to Genset Support* Mode

The first step is to synchronize the BESS grid to the genset output voltage parameters. It is important to mention that the output of genset is not being controlled through the BESS, so the BESS should drive itself to match the genset parameters to be able to change the mode. The *'Resyn'* and *'rated'* signals are employed to drive the BESS from *grid forming* to *genset support* mode and the MSTS generates them in the following order.

Firstly, the *'rated'* signal is changed from 0 to 1, which drives the BESS grid from the rated mini-grid distribution parameters to the genset voltage sensor parameters. To enable a smooth drive, a rate limiter block is included. Secondly, the *'Resyn'* signal is changed from 0 to 1, which activates the synchronization loop and eliminates any phase difference between the two sources. Once the BESS grid has synchronized with the genset; *'mode'* signal changes to 1 to close the genset breaker and to allow the genset to form the grid. Then the load power is smoothly transferred from the BESS to the genset, and the system returns to the normal *genset support* mode of operation. Table 2.3 is presented describing the state of signals *'mode', 'rated', 'Resyn'* and *'gs2f'* during the transition.

Table 2.3 State of the signals from MSTS module when BESS goes form the *grid forming* mode to the *genset support* mode

BESS in *grid forming* mode	BESS grid synchronized with genset	Genset forming the grid	Genset is loaded and BESS is in *genset support* mode
'mode' = 0	'mode' = 0	'mode' = 1	'mode' = 1
'gs2f' = 1	'gs2f' = 1	'gs2f' = 1	'gs2f' = 0
'Resyn' = 0	'Resyn' = 1	'Resyn' = 1	'Resyn' = 1
'rated' = 0	'rated' = 1	'rated' = 1	'rated' = 1

2.9. Summary of Chapter 2

This Chapter discusses the implementation details of the concerned BESS, such as the schematic of the constructed power circuit (in laboratory) to test the control system, the cascaded current and voltage control loops description and how they operate for various modes of operations and while changing the mode of operation. A block known as mode selection and transition system (MSTS) was discussed which selects and operates the BESS depending on the load situation of the mini-grid distribution. Every section of control which was discussed in this Chapter includes its real time Simulink implementation, and it has been done to serve a practical exposure.

In terms of contributions, "2.2 The Concept of the Battery Emulation" and "2.4 Proposed Per-Phase Synchronizer" were the major outcomes of this chapter. Besides, the choice of the per-phase Second-Order Generalized Integrator based Quadrature Signal Generator PLL (SOGI-QSG PLL) to make system capable of enduring real time challenges (voltage unbalance) of test bench has also been included.

Chapter 3.

Experimental Verification of the Complete System

3.1. Introduction

This chapter includes a description of the experimental setup and experimental verification of the concerned BESS control system. It includes the BESS working in *genset support* mode, *grid forming* mode and the transient when it changes the mode from one to another. The experimental setup consists of: 1) AMETEK® programmable power supply, which is working as a genset and is shown in Fig. 3.1; 2) the Triphase® programmable inverter which is working as a BESS; and 3) switchable loads. The following sections are discussing them in detail.

Fig. 3.1. AMETEK® programmable
power supply

3.2. AMETEK® Power Supply working as Genset

AMETEK® programmable power supply is also known as California Instruments and is presented in Fig. 3.1. One can see a key-pad mounted in front of it, which helps to program it, for a desired output voltage and frequency. The low THD, which is less than 1.0 %, allows it to work as a typical genset with a rotating synchronous generator and low voltage harmonics. It should be noted that the grid voltage in the power lab contains low order harmonics, making it inappropriate for this application, as the low order harmonic will pollute the D and Q components of the grid voltage, which are the basic foundation of the adopted control strategy. California Instruments herein is working in isochronous mode, forming a 208 V L-L and 60 Hz grid.

3.3. Triphase® Inverter System working as BESS

Fig. 3.2 shows the Triphase® programmable inverter, which is working as a BESS and is connected to the PCC through a LC filter. The LC filter is a part of the Triphase inverter system and can be seen in the schematic diagram of the Triphase inverter, Fig. 3.3. Please refer to next section for the detail information of the schematic diagram. The entire control algorithm is initially implemented in Simulink, Matlab, using an engineering PC, also shown in Fig. 3.2. Then it is uploaded into a real-time Linux based operating system known as the target PC, also shown in Fig. 3.2, which finally runs and executes the implemented control strategy on the Triphase inverter system. A sampling time of 100 µs is being used to run this application.
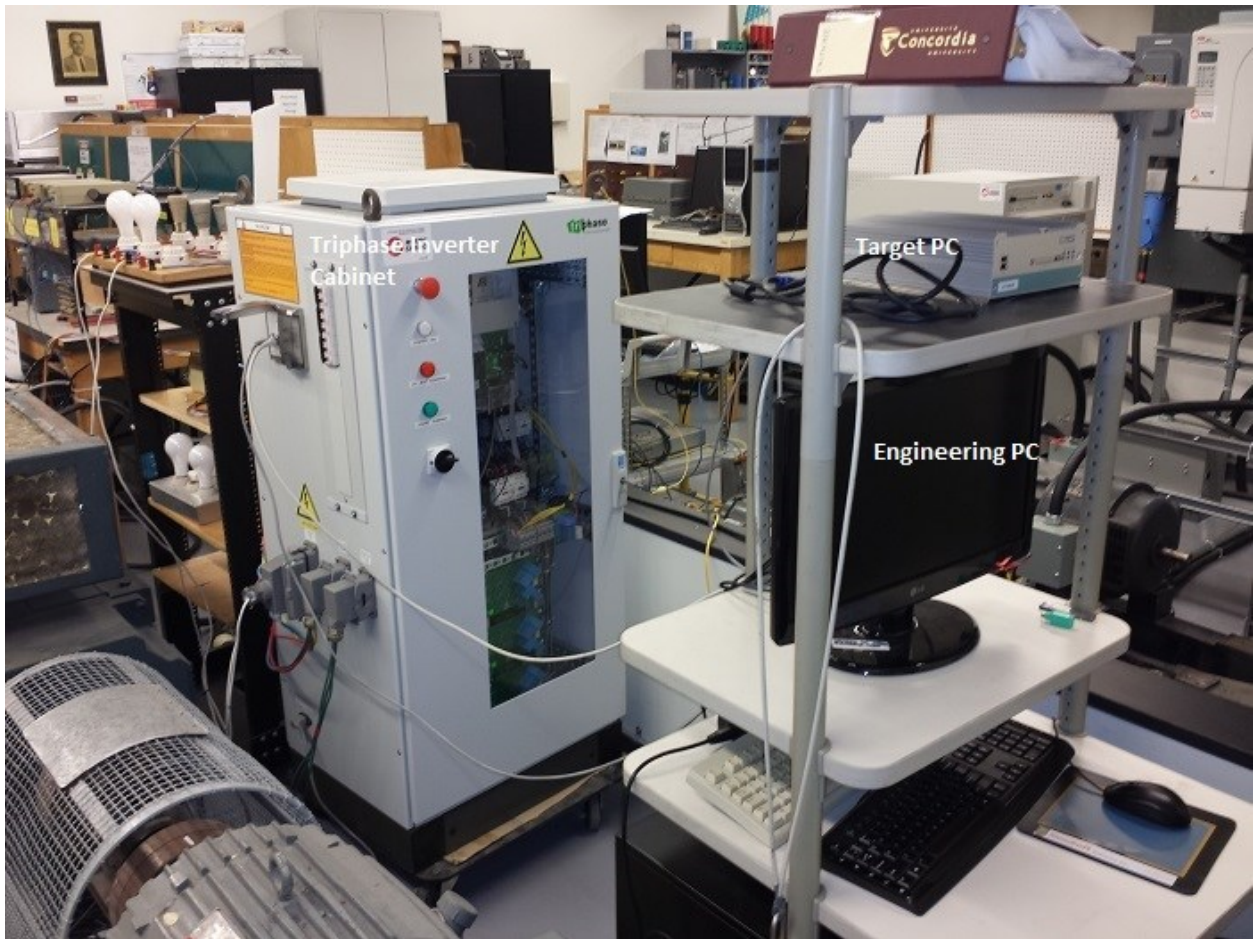
Fig. 3.2 Triphase cabinet, engineering PC and the target PC

3.3.1. Modified Schematic Diagram of the Triphase® Inverter

The schematic diagram of the Triphase system is shown in Fig. 3.3, this document is provided by the Triphase Company itself, and then modified to make it suitable for the BESS application. The modification done is the installation of new wires and by removing some previous connections. The installed new wires are shown in Fig. 3.3, (in red), whereas the dashed blue line shows the previous connection. It is to be noted that this modification has provided a separate access, port P1 in the schematic diagram, to the rectifier of the Triphase system, which is now connected to the output of the step up

transformer whose primary is connected to the grid Concordia, 208 V L-L. It is done to ensure a sufficient DC bus voltage to prevent the BESS inverter from going into the over-modulation region, when connected to a 208 V L-L genset. This three port configuration of the Triphase system is suitable for the BESS application. Where, port P1 is connected to grid Concordia as discussed above, port P2 is connected to the Ametek supply working as a genset and port P3 is connected to the loads.

Fig. 3.3. Schematic diagram of the Triphase® System.

3.4. Three-Phase Switchable Load

The three-phase load is as shown in Fig. 3.4. It can be switched to create a desired unbalance, through the switches available, where each switch represents a 44 Ω resistor in parallel. The load is chosen to be switchable to be able to test the BESS control strategy under various load configurations, comparable to the real scenario.
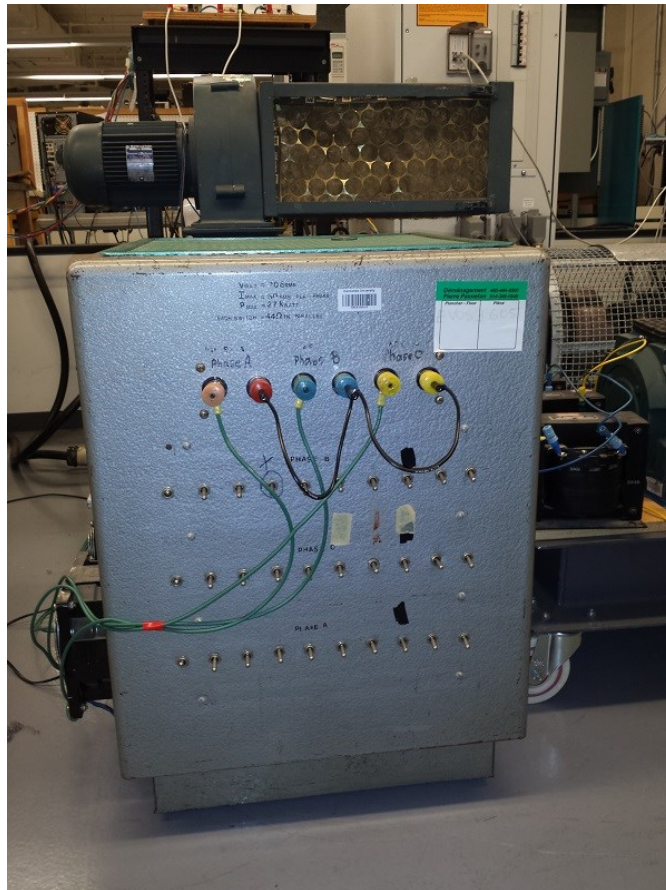
Fig. 3.4. Three-phase switchable load

3.5. Experimental Results of the BESS working in *Genset Support* Mode.

In *genset support* mode*,* the BESS supplies negative sequence current for load balancing, if necessary, load reactive power plus the capacitor current to maintain the genset operating at unity PF and the supplement power, whenever required, to keep the genset operating in the high efficiency region. In this study the high efficiency region is considered in between 800 W and 1.8 kW of the selected 2 kW genset. It is assumed that the rated capacity of the BESS is appropriate to supply the loads by itself.

Please refer to Fig. 3.3 (or Fig.2.1) for the location of voltage and current sensors available in the circuit, through which power could be measured. It is to be noted that the Triphase® inverter (Model PM10F30C) has a limited number of inbuilt voltage and current sensors, and no extra channels are available at the Ethernet controlled power electronics (ECPE) interface board, to be able to install new sensors and to feed their measurements into the system. Now, in order to measure the output power of the BESS, the voltage signal is generated by the voltage sensor available at PCC while the BESS output current is obtained by subtracting the inverter current, available at the inverter current sensor, from the estimated capacitor current. Refer to section "2.7.2 BESS Capacitor Current Compensation" for the capacitor current estimation. It is to be noted that the effect of the equivalent series resistance (ESR) is not considered while estimating the capacitor current, and the implemented capacitor current calculator estimates the fundamental component only, it was done for simplification purposes, which might reflect a small difference, an inconsiderable one, in the calculated BESS output power and the actual one. This difference is disregarded in this study.

3.5.1. BESS Response during a Sudden Load Variation and for a Reactive Load

Fig. 3.5(a) and Fig. 3.5(b) show real and reactive power curves of the BESS and the load, during a sudden load variation. To create a sudden load variation, the Y-connected load configuration, is initially connected as $Za = 44\ \Omega$, $Zb = 22\ \Omega$ and $Zc = 22\ \Omega$, and then finally Zc is changed to 11 Ω. It can be seen in Fig. 3.5(a) that, before and after the load variation, the load demand has remained within the high efficiency region of the genset, which is in between 800 W and 1.8 kW, and as it should be, the BESS power has remained unchanged. This shows correct operation of the implemented BESS control strategy against a sudden load variation.

Fig. 3.5(c) and Fig. 3.5(d) shows real and reactive power curves of the BESS and the load, when load is reactive. Knowing that the real and reactive power is a function of voltage and load impedance. For a reactive load, the Y-connected load is considered to be $Za = Zb = Zc = 11 + 12\ \Omega$. It is clear in the Fig. 3.5(d) that the reactive power supplied by the BESS, (in red), is close to the load reactive power demand, (in blue). Thus, the implemented BESS control strategy is capable of supplying load reactive power, to make it possible for the genset to utilize its full capacity for supplying real power only. Real power supplied by the BESS, Fig. 3.5(c) is close to zero, since the genset is working within the high efficiency range of its capacity.
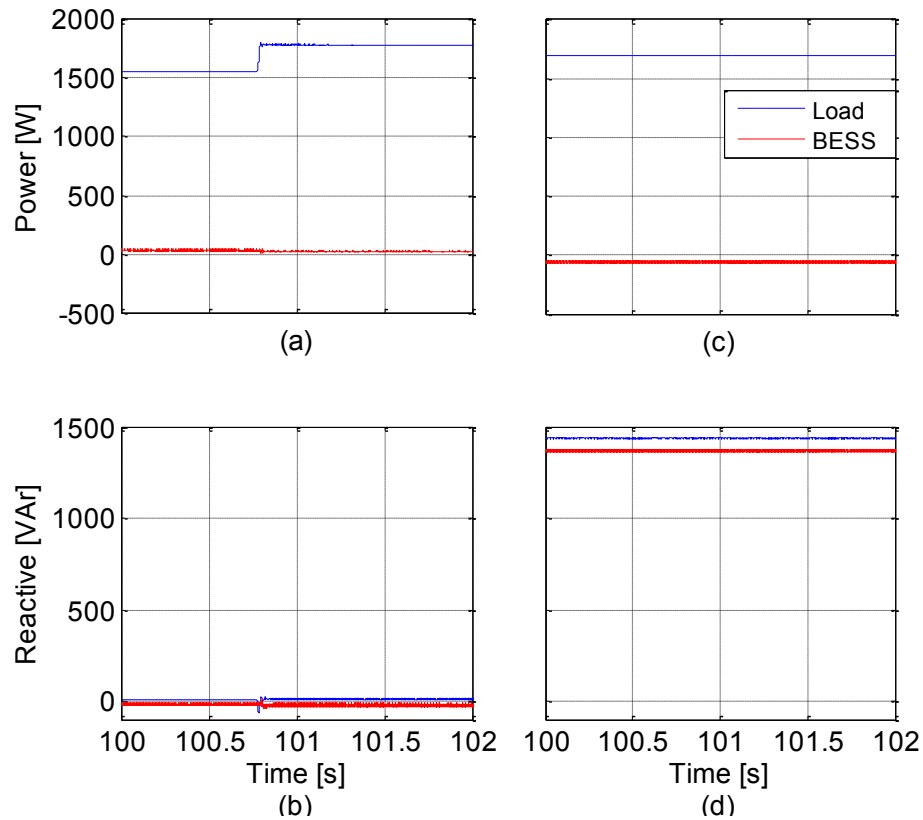
Fig. 3.5. BESS in *genset support mode*: a) and b) real and reactive power of the
load and the BESS, during a load variation; c) and d) during a reactive load.

3.5.2. BESS Response during Peak Load Demand and Low Load Demand

In this case, the BESS is working in *genset support* mode and during that, a load variation
drives the genset into its low efficiency region, which is outside the recommended high
efficiency band of 800 W and 1.8 kW of the 2 kW design. The experimental study is
further divided into two scenarios, peak load condition and low load condition, presented
as follows.

Fig. 3.6(a) and Fig. 3.6(b) show real and reactive power curves of the BESS and the load,
during the peak load condition. To create a sudden peak load condition, the Y- connected

load configuration is initially connected as, $Za = 44\ \Omega$, $Zb = 22\ \Omega$ and $Zc = 11\ \Omega$ and then finally Zb is changed to 11 Ω. This change in the load drives the genset above the recommended range of the high efficiency region, also known as the peak load condition. Elevation in the red curve (BESS power), Fig. 3.6(a), shows that the BESS now supplies the supplement power so that genset can operate in the high efficiency range. Thus, the BESS is capable of supplying active power during the peak load conditions. The BESS reactive power curve is shown in Fig. 3.6(b), which is close to zero since load is resistive only, and is simply disregarded.

Fig. 3.6(c) and (d) shows real and reactive power curves of the BESS and the load, during a sudden low load condition. To create a sudden low load condition, the Y- connected load configuration is initially connected as $Za = Zb = Zc = 44\ \Omega$, and then finally the phase 'c' of the load is made open circuit. This change in the load configuration goes equivalent to an 88 Ω resistor connected in line to line, and it drives the genset below the recommended range of the high efficiency region, also known as the low load condition. It is clear in the Fig. 3.6(c) that the BESS now absorbs active power to bring the operation of the genset back into the high efficiency range. The power absorbed is dissipated on the bleeding resistor, follow section "2.2 The Concept of the Battery Emulation" for more details on the bleeding resistor control. Thus, it is concluded that the implemented BESS control strategy is capable of absorbing real power during the low load conditions so that the genset can operate in the high efficiency region. The BESS reactive power curve, Fig. 3.6(d), which is close to zero due to the resistive nature of the load, is considered negligible.
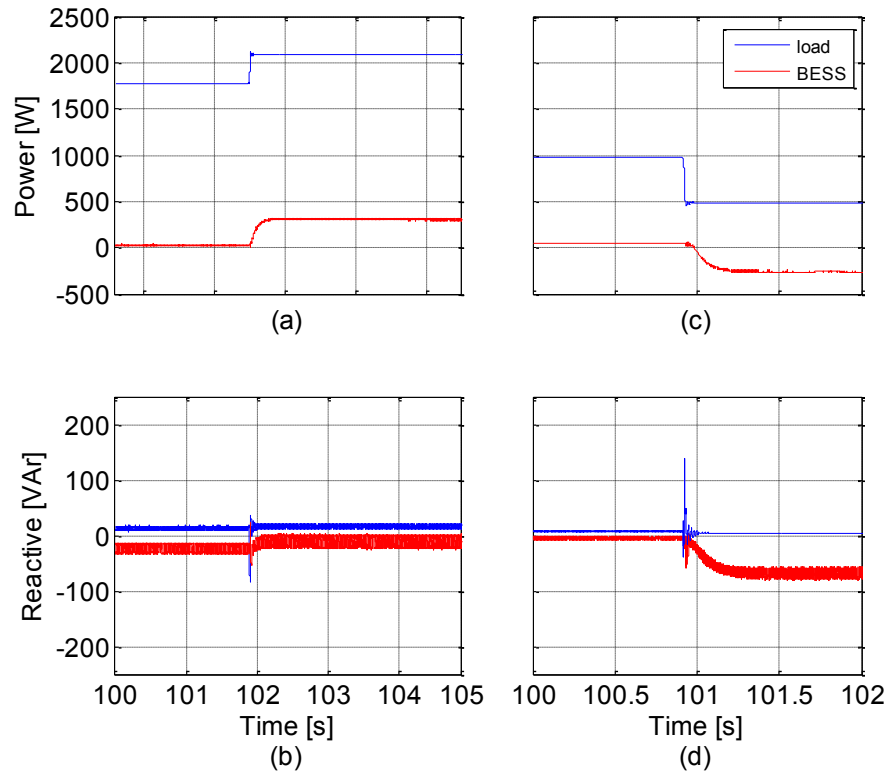
Fig. 3.6. BESS in *genset support mode*: a) and b) real and reactive power of the BESS and the load, during peak condition; c) and d) during low load condition.

3.5.3. BESS Supplying Negative Sequence Current

Fig. 3.7 shows BESS working in *grid support mode* and is injecting the negative sequence component of the load current into the genset grid. It is doing so, to balance the load, and to protect the synchronous generator from overheating and vibrations. To perform this test, the unbalanced Y-connected load configuration is considered to be $Za = 44\ \Omega,\ Zb = 22\ \Omega,\ Zc = 11\ \Omega$. Fig.3.7(c) shows the filter current which is unbalanced, as expected, since it is composed of the negative sequence component and the capacitor current. To verify the impact of the BESS, Fig. 3.8 and Fig. 3.9 are presented, which are taken from the Ametek environment, showing the genset currents

72

with and without the BESS. It is clear in Fig.3.9 that the genset currents are well balanced by the support of BESS, when compared to Fig. 3.8, where BESS is disabled and currents are unbalanced. Thus, the implemented BESS control strategy is capable of injecting the negative sequence component of the load current into the genset grid, to make the load appear balanced for the genset.
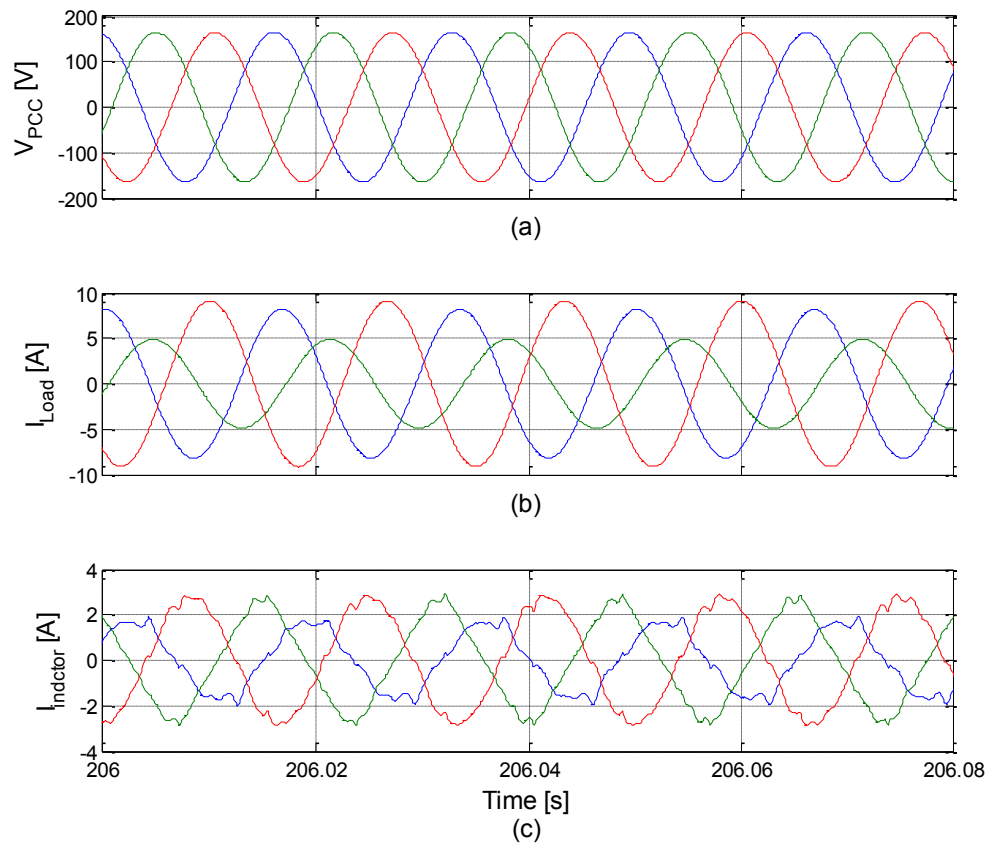
Fig. 3.7. Negative sequence current supplied by BESS inverter: a) PCC voltage; b) unbalanced load current; c) inverter current of BESS.
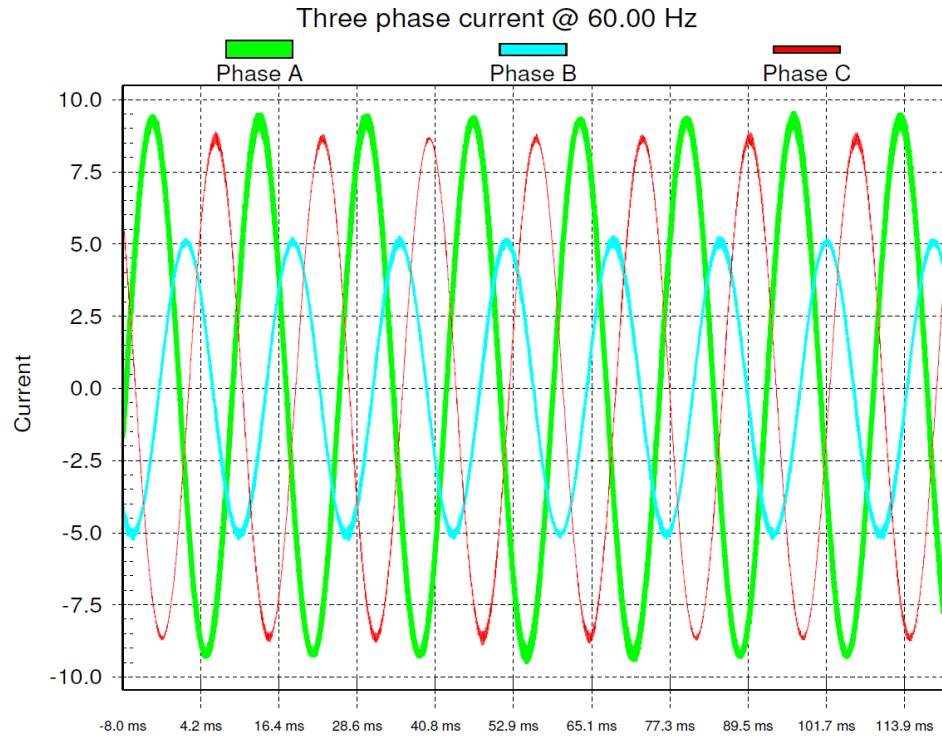
Fig. 3.8. Unbalanced genset currents without BESS support.
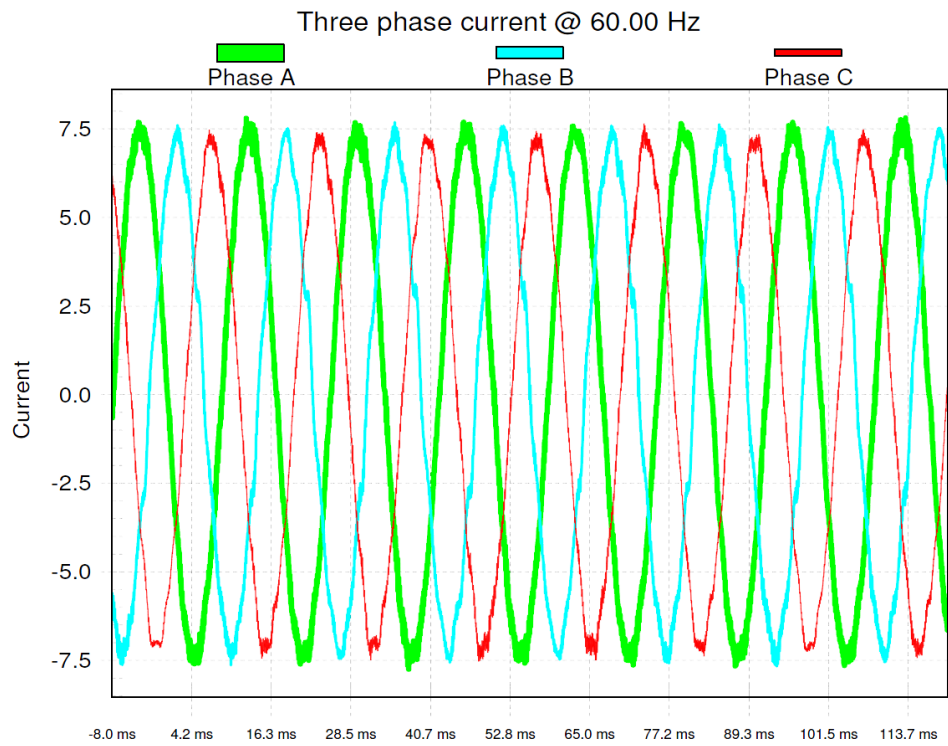
Fig. 3.9. Balanced genset currents with BESS support

74

3.5.4. BESS Supplying Reactive Current Reference

Fig 3.10 shows BESS working in *grid support* mode and is supplying reactive current reference to maintain a unity PF for the genset. For this test, a reactive load was required so the Y-connected load configuration is taken to be $Za = Zb = Zc = 11 + j12$ Ω. Fig. 3.10(c) is the filter current supplied by the inverter of the BESS, which is filtered in there and then fed into the grid to maintain a unity PF for the genset. To supply reactive power, the required reactive nature of the currents, which is 90° lagging w.r.t voltages, can be clearly seen in Fig. 3.10(c). To verify the impact of the BESS, Fig. 3.11 shows genset currents w.r.t PCC voltages without the BESS support and Fig. 3.12 shows the genset currents with the BESS support. It is clear in Fig. 3.12 that the genset currents are in phase with the PCC voltages when the BESS is supporting the genset by itself supplying the load reactive power. Thus, the BESS is capable of making a unity PF for the genset. Some distortion can be observed in the genset currents when it is supported by the BESS; refer to Fig. 3.12 (in red) to observe the distortion. Results were considered acceptable since the LC filter and the switching frequency of the apparatus (the Triphase® system) were fixed, which leaves no flexibility for further reduction in harmonics.
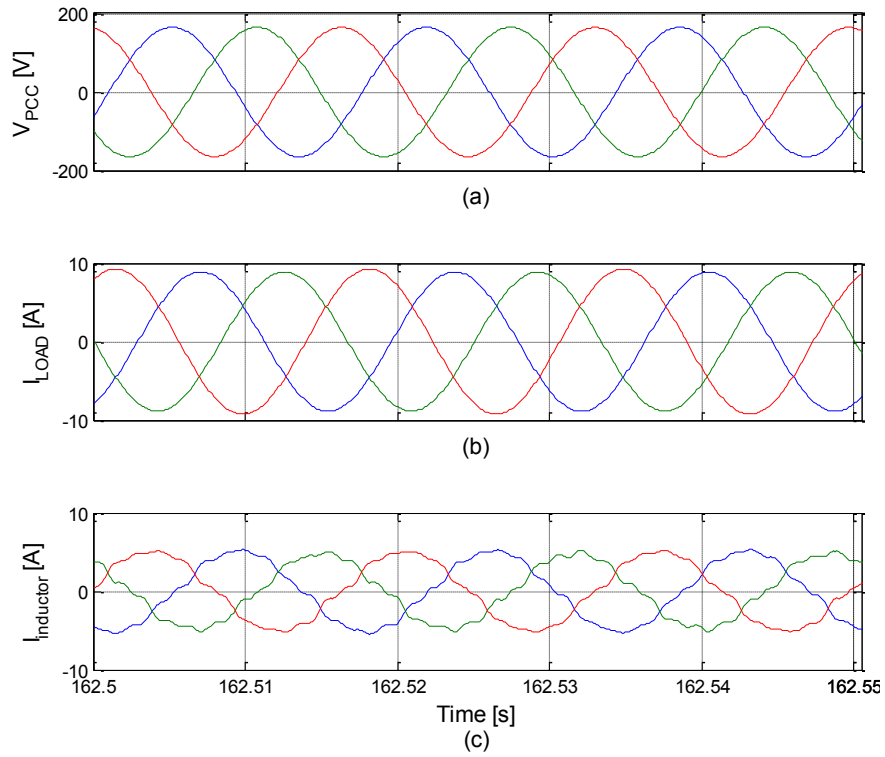
Fig. 3.10. Reactive current supplied by BESS inverter: a) PCC voltage; b) load current; c) inverter current of BESS.
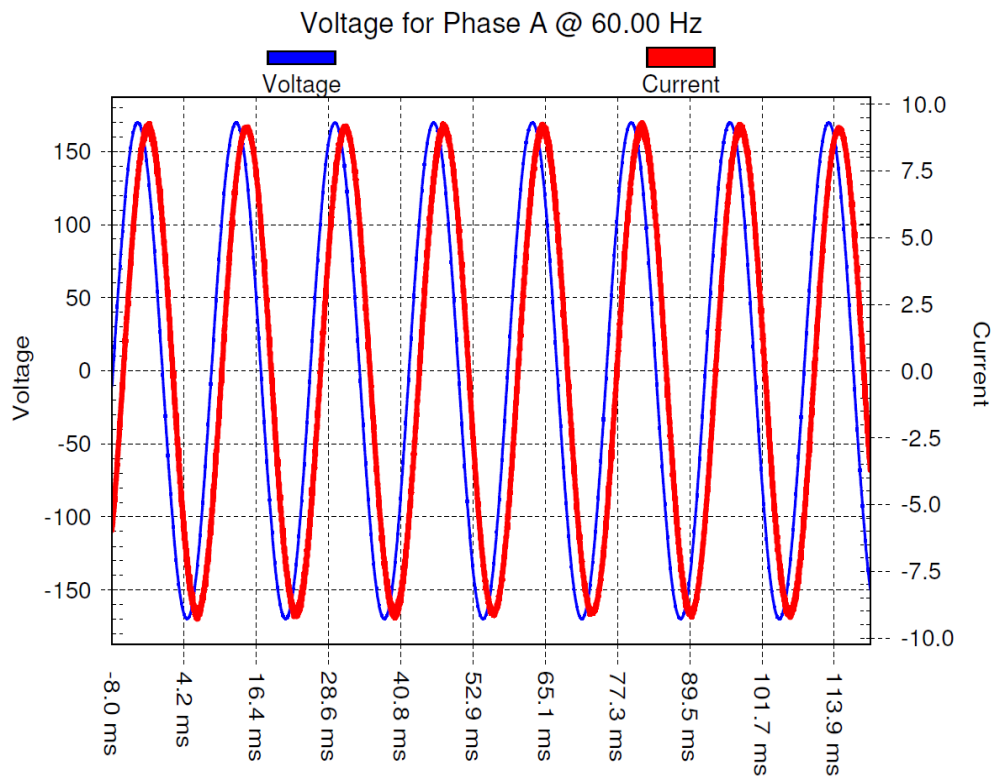
Fig. 3.11. Genset current and the PCC voltage of phase 'a' without BESS support.
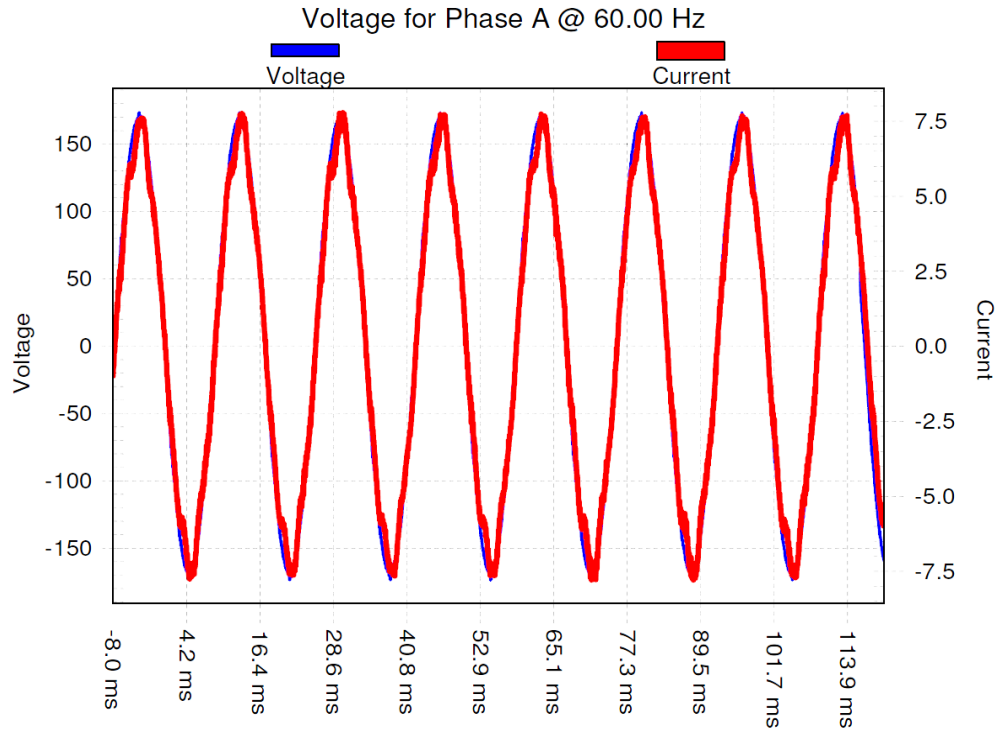
Fig. 3.12. Genset current and PCC voltage of phase 'a' with BESS support.

3.6. BESS *Genset Support* to *Grid Forming* Transition

As discussed in "2.8.4 Steps from *Genset Support* to *Grid forming* mode", the MSTS block generates several control signals to perform the controlled smooth transition between the two operating modes. There are three major steps in this transition, first is to unload the genset smoothly. It starts when '*gs2f*' signal changes to 1, the BESS smooth power transfer curve is shown in Fig. 3.13(a), where the genset is unloaded in 1.65 sec. Once the genset is unloaded, the second step is to open the genset breaker and to form a BESS stand-alone grid while the system is tracking the genset voltage sensor for the frequency, phase and the amplitude as references. It was done so to ensure a smooth transition process. And then the final step is to drive the BESS grid from the genset voltage sensor parameters, to the rated mini-grid distribution parameters to eliminate the

role of the genset voltage sensor from the control loops prior allowing the genset to shut down. Fig. 3.13(b) shows reactive power curve of the BESS and the load, which are close to zero due to the resistive nature of the load, and is simply disregarded in the study.

Fig. 3.14 shows experimental results when the mode of operation of the BESS is changed from the *genset support* to the *grid forming* by opening the genset breaker, and the BESS applies the genset voltage parameters as references. In Fig. 3.14(c), when the *mode* signal changes to 0, the genset breaker goes off and the voltage control loop of the BESS gets activated, which regulates the PCC voltage by applying the genset voltage parameters. It is to be noted that the state of the *mode* signal changes at 542.84 sec and a change in PCC voltage has appeared at 542.88 sec, this delay corresponds to the opening time of the genset breaker. This transition is achieved with a Y-connected load of 44 Ω in each branch.

Once forming BESS grid by applying the genset voltage sensor parameters as references, the MSTS block generates *'rated'* and *'Resyn'* signals, which drives that grid to the rated mini-grid distribution parameters, shown in Fig. 3.15. When the '*Resyn'* signal goes to 0, it breaks the synchronization loop between the BESS standalone grid and the genset output voltage. After that, the *'rated'* signal goes to 0, which drives the BESS grid from genset voltage sensor parameters to the rated mini-grid distribution parameters and eliminates the role of the genset voltage sensor from the control loops. No change is observed in the PCC voltage, Fig. 3.15(b), during the transfer of references from the genset parameters to rated mini-grid distribution parameters. It was an expected result since the genset was operating in isochronous mode and its parameters were close to the rated mini-grid parameters. From the results shown in Fig. 3.13, 3.14 and 3.15, the MSTS

block has successfully formed a BESS standalone grid with the designed critical steps and the proposed logic, ensuring a smooth transition process. Thus, the implemented control strategy works well for the *genset support* to *grid forming* transition.
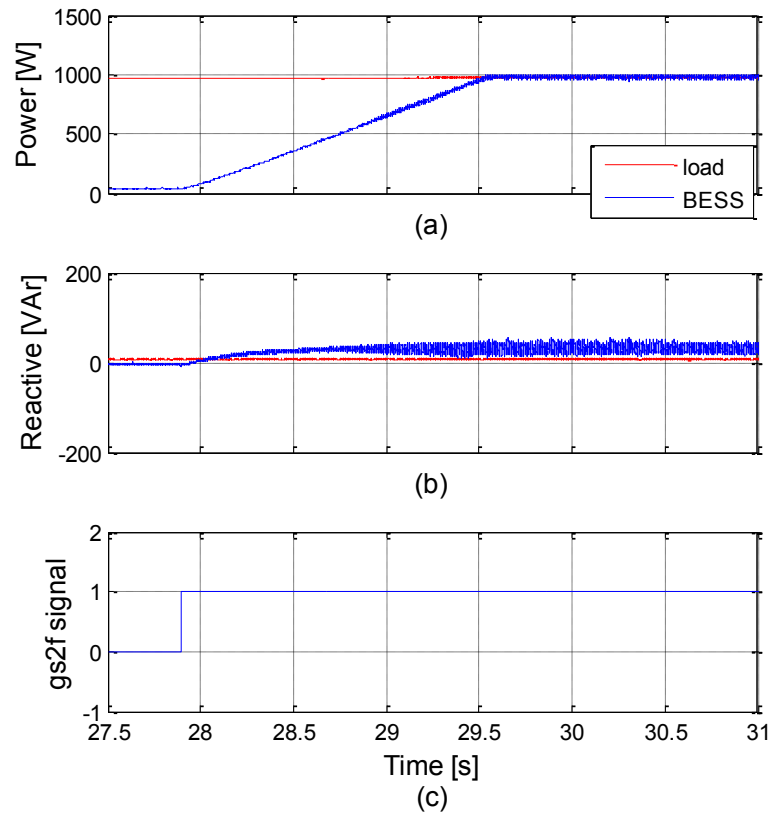
Fig. 3.13. Smooth unloading of genset: a) real power curve of the load and the BESS; b) reactive power curve of the load and the BESS; c) *'gs2f'* signal
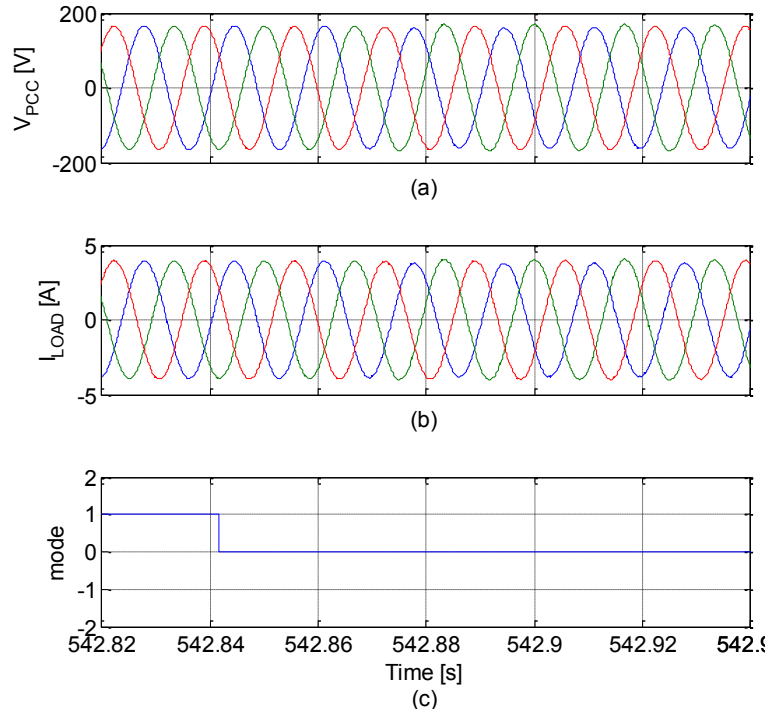
Fig. 3.14. BESS *genset support* to *grid forming* transient step 1: a) voltage at PCC; b) load current; c) '*mode*' signal.
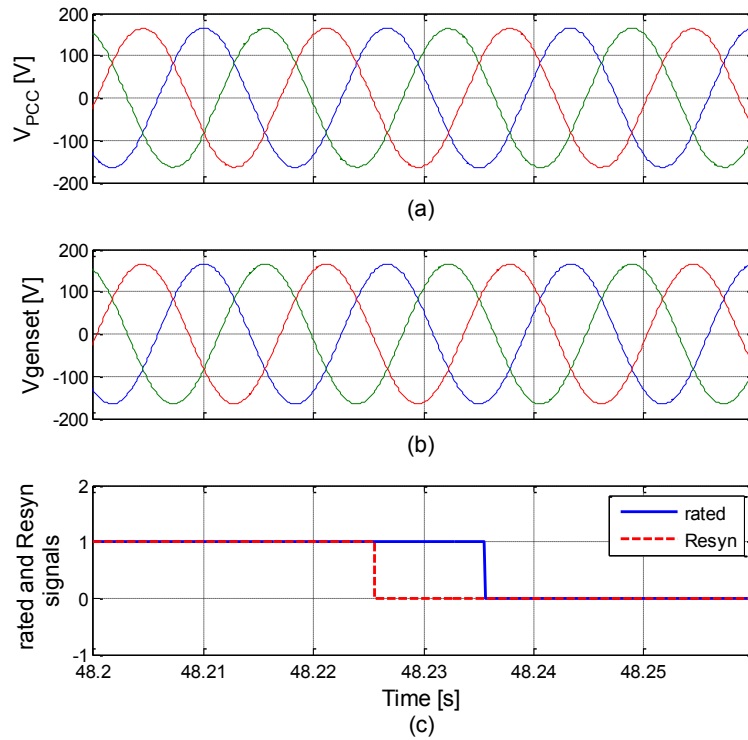
Fig. 3.15. BESS *genset support* to *grid forming* transient step 2: a) voltage at PCC; b) voltage at genset; c) *'rated'* and *'Resyn'* signals.

3.7. BESS *Grid Forming* to *Genset Support* Mode Transition

In order to change the mode of operation from *grid forming* to *genset support*, the MSTS block generates *'gs2f', 'rated', 'Resyn'* and *'mode'* signals to have a smooth transition process. First of all, it generates *'rated'* signal to eliminate, if any, amplitude or frequency differences between the BESS stand-alone grid and the genset output voltage, which is then followed by the *'Resyn'* signal to achieve the synchronization between the genset voltage and the BESS grid. Then the '*mode*' signal changes to 1, to close the genset breaker, and to shift the mode of operation of the BESS from *grid forming* to *genset support*. Finally, genset is loaded by changing *'gs2f'* signal to 0 to get to the normal BESS support operation.

Fig. 3.16(c) shows the beginning of the transition process, where *'rated'* signal starts the process by changing to 1, which eliminates amplitude and frequency differences between the BESS grid and the genset voltage. Then after 0.01 sec, the *'Resyn'* signal changes to 1, by the MSTS block, to start the synchronization process between the BESS grid and the genset. It is clear in Fig. 3.16(d), (e) and (f) that the BESS has synchronized with the genset, after 2.7 sec.

Since the BESS has synchronized with the genset, so now it is safe to connect them together, to be able to change the mode of operation from *grid forming* to *genset support*. Fig. 3.17(a) shows the PCC voltage, which shows the transient when genset is connected to the PCC. A disturbance is observed at 110.035 sec, it is the moment when genset is connected to the PCC. It is to be noted that this disturbance has delayed, after the '*mode*' signal, which directly controls the genset breaker, changes to 1; this delay corresponds to

the closing time of the genset breaker. The Y-connected load configuration during the transition is $Za = Zb = Zc = 44\ \Omega$.

The final operation is to load the genset to return to the normal operating state of the *genset support* mode. Fig. 3.18(a) shows real power curves of the BESS and the load, the difference of which is the genset power; it clearly shows the smooth loading of the genset. The reactive power curve in Fig. 3.18(b) is close to zero since the load is resistive only. The loading process starts when *'gs2f'* signal changes to 0 and finishes after 1.61 sec. Thus, from the presented experimental results, Fig. 3.16, 3.17 and 3.18, it is clear that the MSTS block is capable of performing a smooth transition from *grid forming* to *genset support* mode with the designed critical steps and the proposed control logic. And the implemented control strategy works well during the transition.
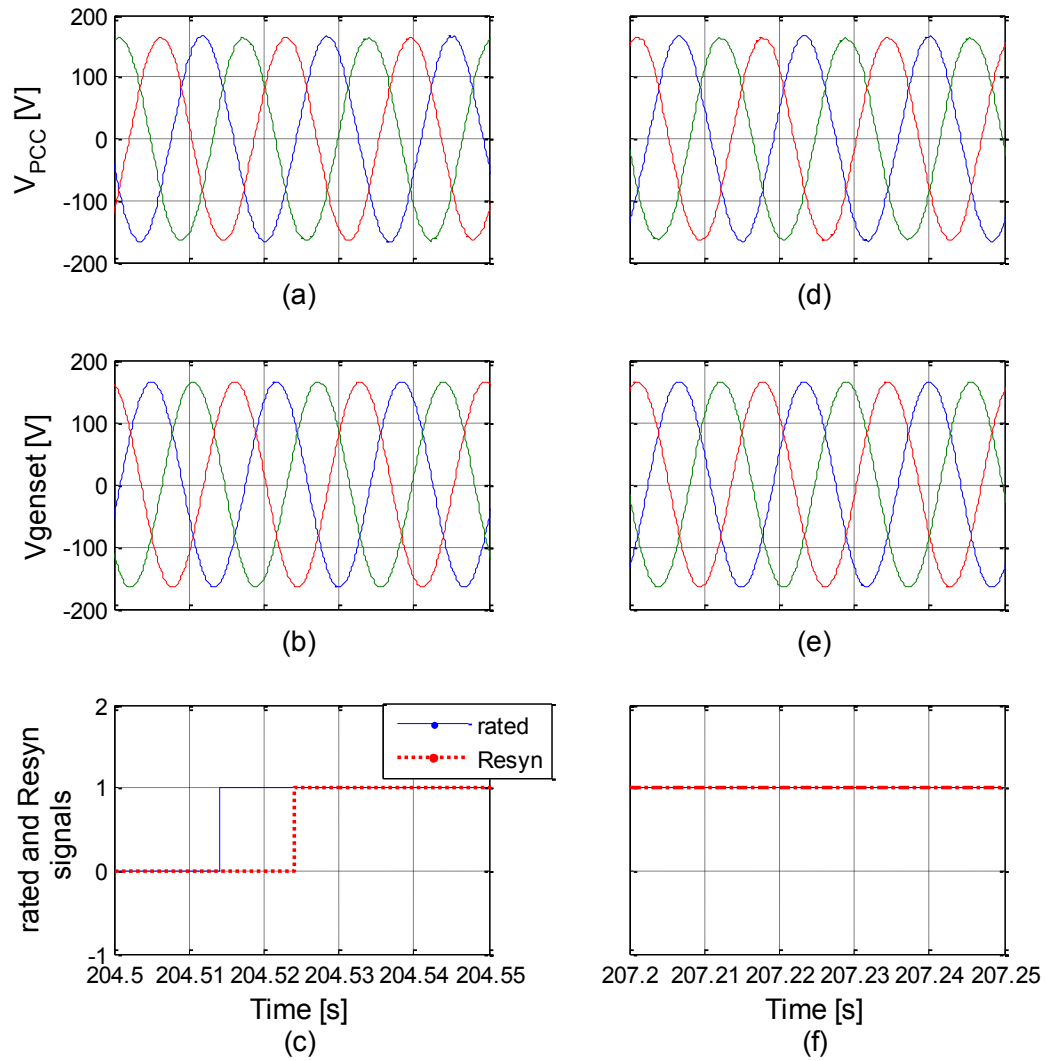
Fig. 3.16. *Grid forming* to *genset support* transient, step 1: (a) and (d) voltages at the PCC; (b) and (e) genset voltages; (c) and (f) *'rated'* and *'Resyn'* signals.
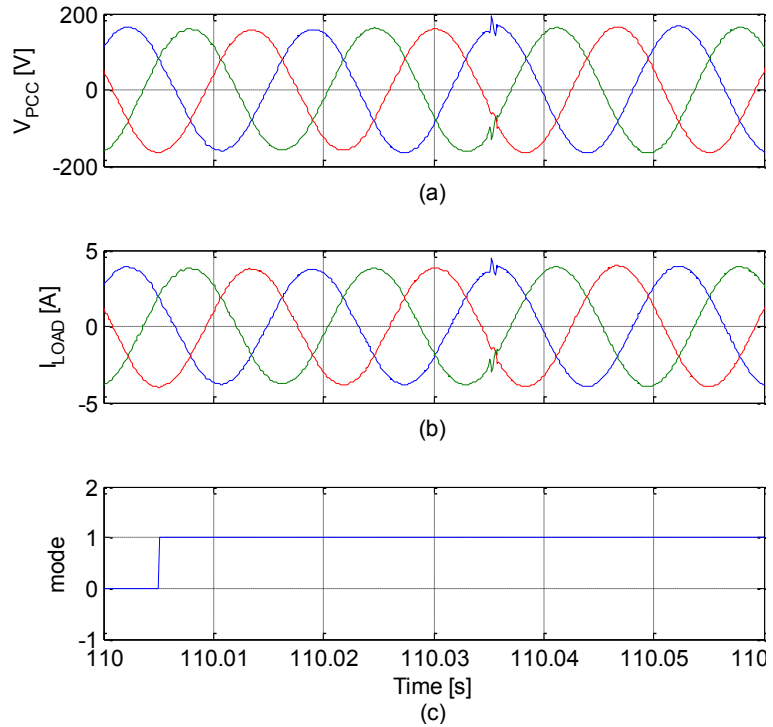
Fig. 3.17. G*rid forming* to *genset support* transient, step 2: a) voltage at PCC; b) load current; c) *'mode'* signal.
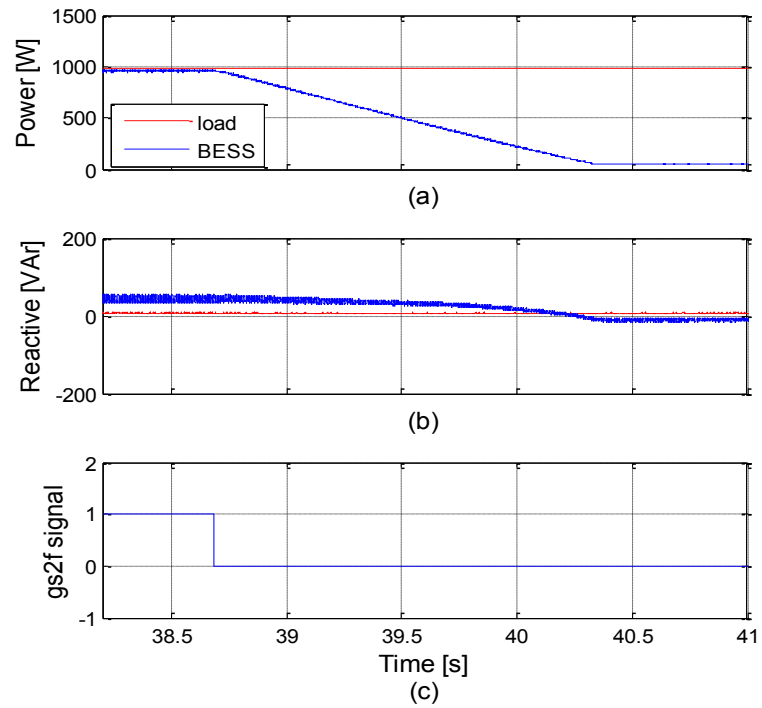
Fig. 3.18. Smooth loading of genset: a) real power curve of the BESS and the load; b) reactive power curve of the BESS and the load; c) *'gs2f'* signal.

3.8. Experimental Verification of BESS in *Grid Forming* Mode

In *grid forming* mode, BESS is expected to form a balanced grid on the highly unbalanced loads. It employs an outer voltage loop for the voltage regulation, which then generates a reference current for the inner current loop. The adopted per-phase dq control strategy is verified in this section, for its capabilities to form a balanced grid on the highly unbalanced loads. For the performance verification, three successive tests were conducted on it, and in the first test, a grid was formed on a balanced Y-connected load ($Za = Zb = Zc = 44\ \Omega$). Fig. 3.19(a) shows the grid voltage formed by the BESS inverter on the balanced load and Fig. 3.19(b) shows the load current. The FFT of this grid voltage is shown in Fig. 3.20, where the THD is found to be 0.94%, which is acceptable according to the IEEE standard 519.
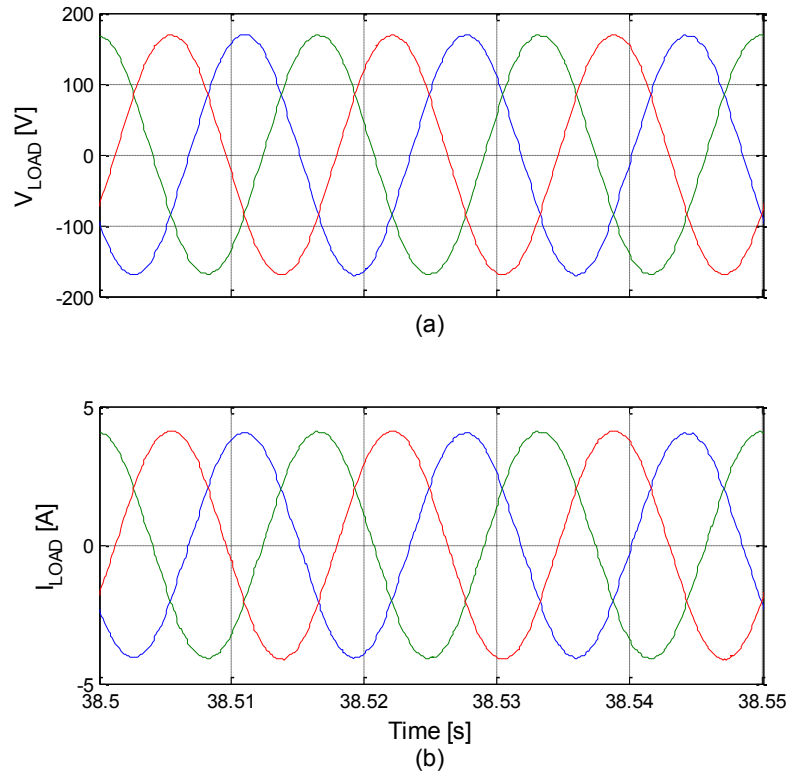
Fig. 3.19. BESS *grid forming* on a balanced load: a) load voltage; b) load current.
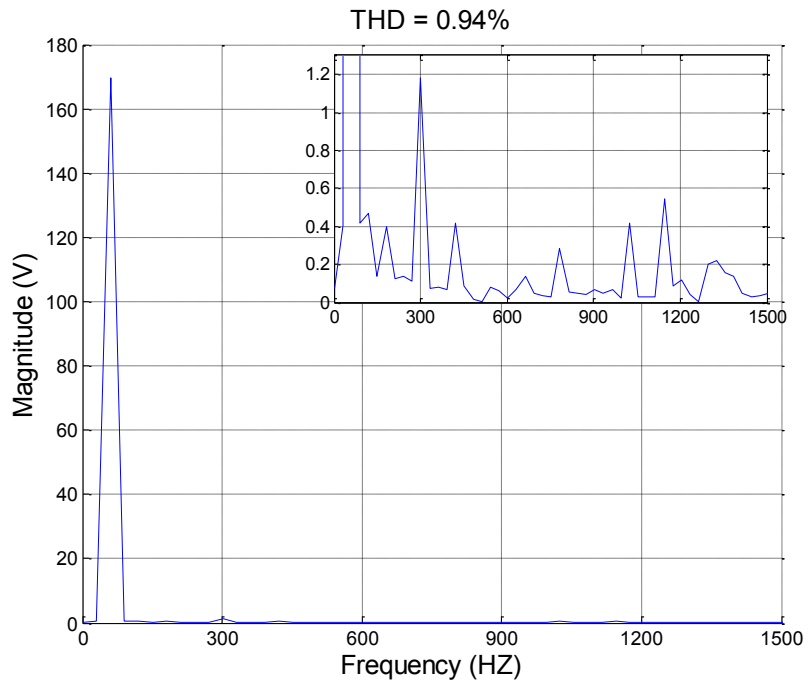
Fig. 3.20. FFT of Fig. 3.19(a); BESS grid forming on a balanced load

86

In the second test, the Y-connected load configuration is made unbalanced and is changed to $Za = Zc = 44\ \Omega$ and $Zb = 22\ \Omega$. The transient response of the BESS grid voltage is presented in Fig. 3.21 and Fig. 3.22, where the PCC voltage and the load currents are shown in terms of their dq waveforms. After a brief transient the load voltage is regulated to the desired value. It should be noted that in the Triphase system due to the limited number of current sensors, the output current feed forward was not adopted in the experimental study which justifies the transient response. Grid voltage reaches steady state at 186.5 sec and the then PCC voltage and load current waveforms are shown in Fig. 3.23(a) and (b). It can be seen in Fig. 3.23(a) and (b) that the load variation has made the system unbalanced and the BESS is capable of maintaining a balanced voltage across the unbalanced loads. The FFT of this grid voltage is shown in Fig. 3.24, and the THD is found to be 1.69%, which is acceptable according to the IEEE std. 519.
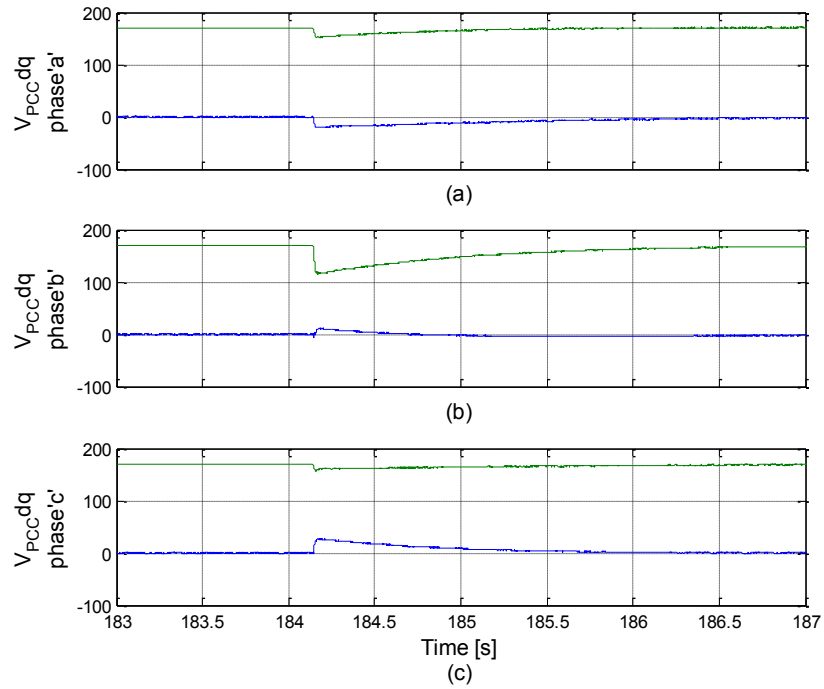
Fig. 3.21. PCC voltages in dq waveforms during a load variation: a) PCC voltage in phase 'a'; b) PCC voltage in phase 'b'; c) PCC voltage in phase 'c'.
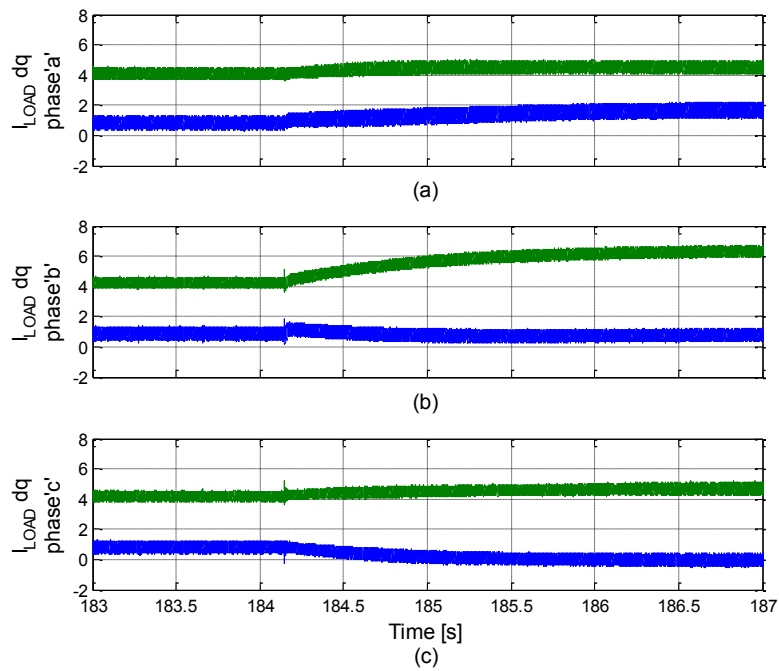
Fig. 3.22. Load currents in dq waveforms during a load variation: a) load current in phase 'a'; b) load current in phase 'b'; c) load current in phase 'c'.

88
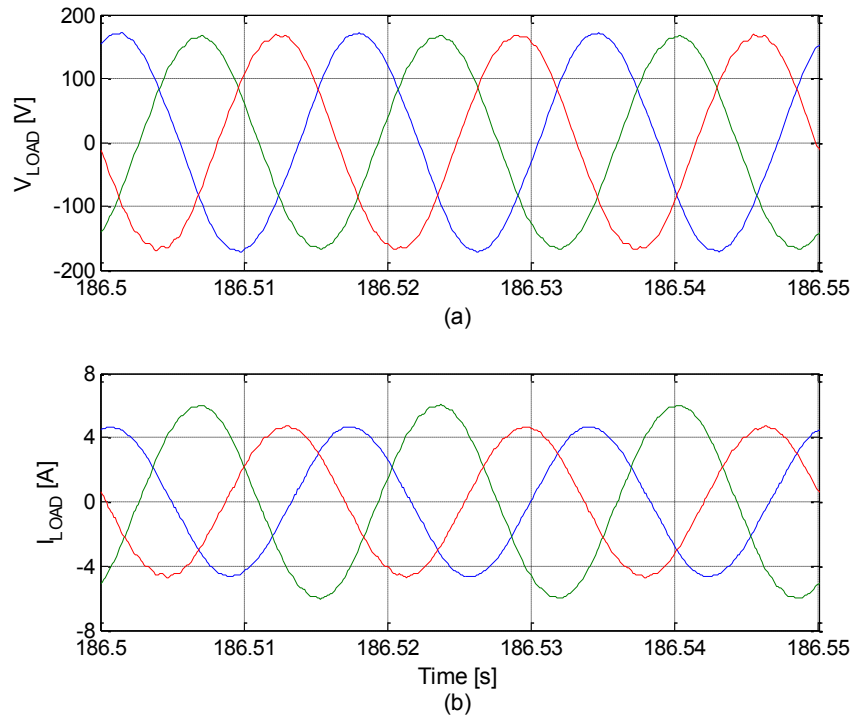
Fig. 3.23. BESS *grid forming* on an unbalanced load in steady states: a) load voltage; b) load current.
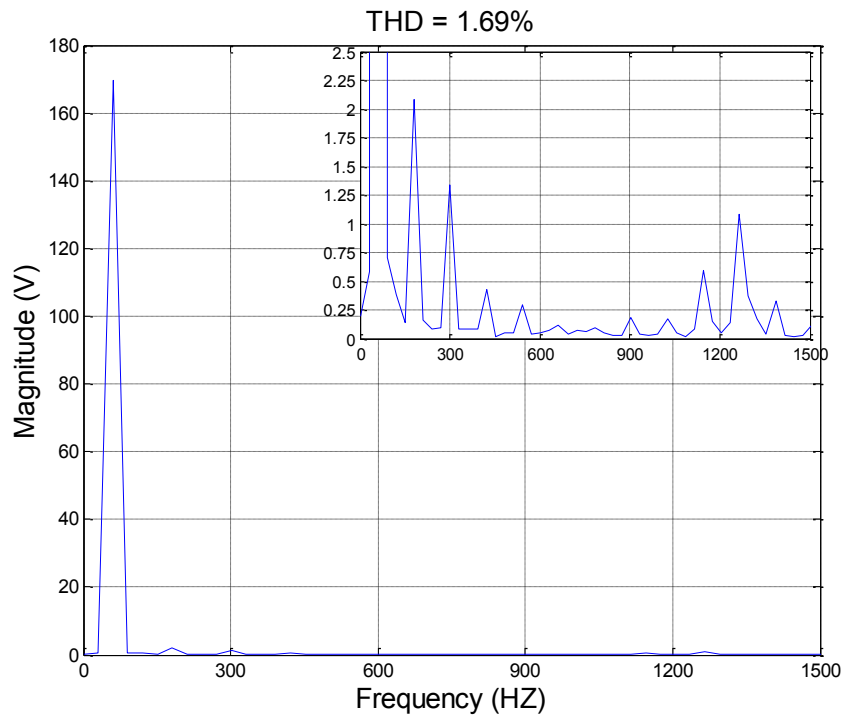
Fig. 3.24. FFT of Fig. 3.23(a); BESS *grid forming* on the unbalanced load.

89

In the third test, the Y-connected load is made highly unbalanced by changing the load configuration to $Za = Zb = 44\ \Omega$ and $Zc = 1000\ \Omega$. This situation is close to the grid forming with one line open, which means that a three phase inverter is supplying a single phase load. For this load configuration, Fig. 3.25(a) shows the balanced grid formed by the BESS inverter and Fig. 3.25(b) shows the highly unbalanced current drawn by loads. The THD of this BESS grid voltage is found to be 2.1%, and its FFT is shown in Fig. 3.26.

Analysis the THD of the grid voltages under the three different load scenarios (tests), it was found that the BESS grid voltage contains least THD of 0.9% when the load is balanced and the highest THD of 2.1% when load is highly unbalanced. The THD of 2.1% (worst case scenario) is acceptable according to the IEEE standard 519, [33], which establishes harmonic limit on voltage as 5 %. From the results presented one can conclude that the adopted per-phase control strategy (implemented BESS) meets the standards of grid forming on the most stringent load conditions.
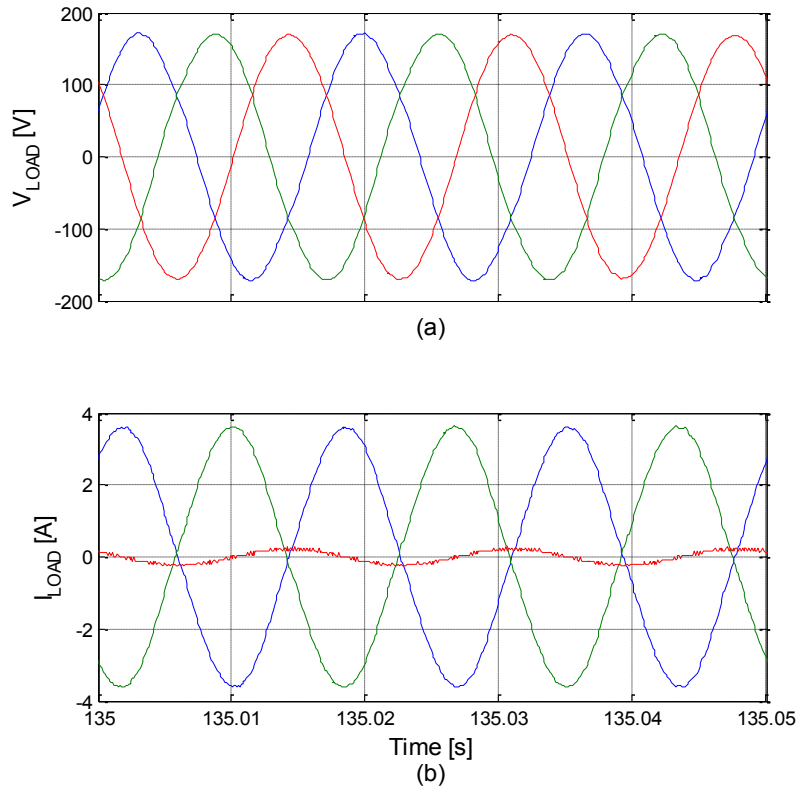
Fig. 3.25. BESS *grid forming* on highly unbalanced load: a) load voltage; b) load current.
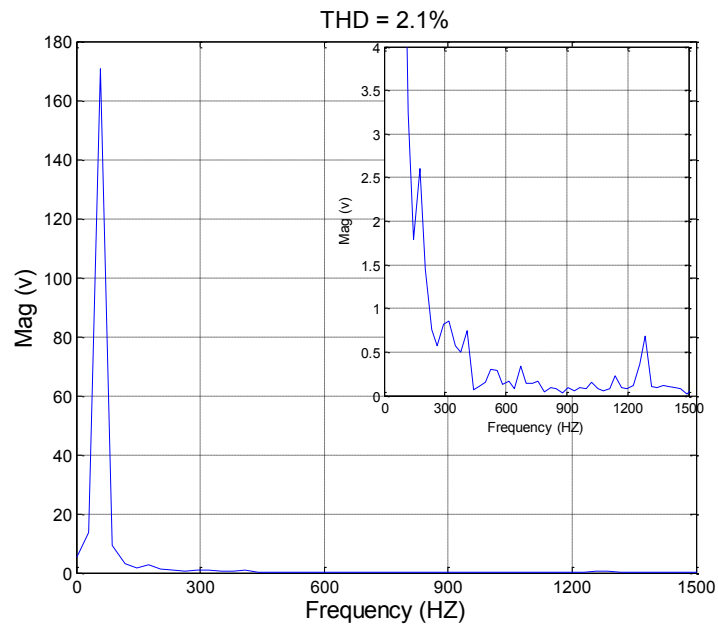
Fig. 3.26. FFT of Fig. 3.25(a); BESS *grid forming* on highly unbalanced load.

3.9. Summary of Chapter 3

This chapter includes the experimental assessment of the control design of the concerned BESS, which was until now assessed with simulation results only. A description of the experimental setup, the employed apparatus and the constructed power circuit, which is used to test the design, is also presented in this chapter. Some changes in the schematic diagram of the Triphase$^{®}$ inverter, to make it suitable for the BESS application have also been shown. In the assessment, the BESS is tested for *genset support mode*, *grid forming mode* and for changing the mode from one to another. From the results presented, throughout this chapter, it is concluded that this BESS control strategy is high effective for *genset support mode*, *grid forming mode* and during the transients. Also the effectiveness of the designed synchronization loop, "2.4 Proposed Per-Phase Synchronizer" to eliminate the need of an intelligent connection agent (ICA) has been proven.

Chapter 4.

Conclusion of Thesis

4.1. Summary of Thesis

The main focus of this M. A. Sc. Thesis was to evaluate experimentally the performance of the BESS control system which was proposed in [1], based on simulation results, for reducing fuel consumption and maintenance cost of diesel-hybrid mini-grids. It is important to mention that the concerned control system was designed to reduce fuel consumption and maintenance cost of diesel-hybrid mini-grids but the actual numerical reduction will however depend on the load profile as well as on the characteristics of the genset. After carefully studying the system and considering the real time challenges of the test bench, some modifications were brought into this system to make it suitable for the voltage unbalance issues, simpler to implement and to enhance its features.

These modifications were: 1) the implementation of the per-phase QSG-PLL [30] to avoid the appearance of the second order harmonic in the PLLs output during the voltage unbalance situation and to eliminate the need of a separate frequency lock loop (FLL) for frequency estimation. It is to be noted that the PLL proposed in [1] was verified by simulation results only, where the system was not subject to any voltage unbalances; 2) the implementation of the proposed per-phase synchronize, a contribution of Thesis, to eliminate the need of an intelligent connecting agent (ICA) for simplification reasons. It is worth mentioning that critical steps were designed to achieve a smooth transition while changing the mode of operation from one to another. The designed control logic of the proposed per-phase synchronizer was tested experimentally and was found to be capable

of replacing the ICA for this application. Its test verification was presented in Chapter 3; 3) the operation of the MSTS block was modified to bring intentional and unintentional change in the mode of operation, additional features. With the intentional feature the power station operator can himself change the mode of operation knowing that the BESS can meet the actual and forecasted load demand, by itself or assisted by a renewable energy sources (RESs), and the unintentional feature will change the mode of operation once the state of charge (SOC) of the battery bank gets full and the load demand is within the capacity of the BESS.

After applying the above said modifications to the BESS system, it was tested in the laboratory to see if it meets the design specifications, where the control was implemented on a programmable inverter called Triphase® inverter system, and a power supply known as Ametek® (California Instruments) was working as a genset. A switchable load was used to test this control system for various load unbalances, considering the various load situations that might occur in the mini-grid distribution system. The battery of the BESS was emulated, a contribution of Thesis, by a diode rectifier connected to Concordia's grid and a controllable bleeding resistor so that the emulated battery can supply and absorb active power to the AC grid.

Based on the experimental evidences, which were presented in Chapters 2 and 3, it is concluded that this BESS system is highly suitable for *genset support* mode, *grid forming* mode and changing the mode from one to another. In the *genset support* mode: 1) it is capable of supplying negative sequence component of the load current into the grid for load balancing, protecting the synchronous generator from overheating and vibrations; 2) It is also capable of supplying load reactive power and maintaining a unity PF, enabling

genset to utilize its full capacity for supplying real power; 3) Finally, it is capable of keeping the genset operating within the high efficiency range (typically in between 40% and 90%), for reducing fuel consumption, maintenance cost and keeping a power reserve for sudden load increase, by itself supplying/ absorbing supplement power, whenever required.

For the mode transients, it is capable of changing the mode of operation from *genset support* to *grid forming* and vice-versa, smoothly, with the proposed transition steps. In the *grid forming* mode, it is capable of forming a well-balanced grid on the possibly highest unbalanced loads to maintain an uninterrupted power supply, while genset undergoes a maintenance operation.

4.2. Suggestions for Future Work

In this thesis, the performance test of the concerned BESS control system was conducted, considering the genset in isochronous mode, so the investigation of its frequency adaptive nature, with the genset operating in the droop-control mode, can be suggested for future work. Besides, some suggestions to advance this BESS would be as follows;

- Capability of providing *genset support* when the latter operates.
- A study of energy management system can be incorporated to this BESS, where the state of charge (SOC) of the battery bank and renewable energy sources (RESs) are taken into consideration for determining, when the genset could be shut down and have the BESS supplying the loads for a reasonable amount of time.

- Incorporating a fault detection function to shift the mode of operation, unintentionally, to the *grid forming* during a sudden break down (or fault) in genset.

- Testing the concerned BESS control system for non-linear loads would further assess its design capabilities and it could be suggested as future work.

- Coordinating the operation of the controllable loads, such as electric water heaters, and water pumps to that of the BESS so as to keep the genset operating in the desired region without stressing the BESS.

BIBLIOGRAPHY

[1]   N. A. Ninad, L.A.C. Lopes, "A BESS control system for reducing fuel-consumption and maintenance costs of diesel-hybrid mini-grids with high penetration of renewables," *IEEE ECCE Asia Down-under (ECCE Asia)*, Australia, pp. 409-415, 3-6 June, 2013.

[2]   F. Katiraei, D. Turcotte, A. Swingler, and J. Ayoub, "Modeling and Dynamic Analysis of a Medium Penetration PV-Diesel Mini-Grid System," *4th European Conference on PV-Hybrid and Mini-Grid*, Greece, 2008.

[3]   R. Pena, R. Cardenas, J. Proboste, J. Clare, and G. Asher, "Wind-Diesel Generation Using Doubly Fed Induction Machines," *IEEE Transactions on Energy Conversion,* vol. 23, no. 1, pp. 202-214, 2008.

[4]   M. W. Davis, R. Broadwater and J. Hambrick, "Modeling and Testing of Unbalanced Loading and Voltage Regulation," Joint Project from DTE Energy Company, Electrical Distribution Design Inc., Virginia Polytechnic Institute and State University, and National Renewable Energy Laboratory (U.S.), 2007.

[5]   Lopes, L. A. C., and M. Dalal-Bachi. "Economic Dispatch and Demand Side Management via Frequency Control in PV-Diesel Hybrid Mini-Grids," *6th European Conference on PV-Hybrid and Mini-Grids,* Chambéry. 2012.

[6]   Kumar, R.S.; Thampathy, K.C.S., "Environmentally constrained optimum economic dispatch," *Energy Management and Power Delivery, 1998. Proceedings of EMPD '98. 1998 International Conference,* vol. 1, no. 1, pp. 265-270, Mar. 1998.

[7]   Arias, D. A.; Mota, A. A.; Mota, L. T M; Castro, C.A., "A bilevel programming approach for power system operation planning considering voltage stability and economic dispatch," *Transmission and Distribution Conference and Exposition: Latin America, 2008 IEEE/PES*, pp. 1-6, Bogota, Aug. 2008.

[8]   Mao Meiqin; Ji Meihong; Dong Wei; Liuchen Chang, "Multi-objective economic dispatch model for a microgrid considering reliability," *Power Electronics for Distributed Generation Systems (PEDG), 2010 2nd IEEE International Symposium*, pp. 993-998, Hefei, China, 16-18 June 2010.

[9]   Whei-Min Lin; Shi-Jaw Chen; Yuh-Sheng Su, "Bid-based demand contingency constrained economic dispatch," *Power System Technology, 2000. Proceedings. PowerCon 2000. International Conference on*, vol. 3, pp. 1647-1652, Perth, WA, 2000.

[10]   Elamari, Khalid Ibrahim. "Using Electric Water Heaters (EWHs) for Power Balancing and Frequency Control in PV-Diesel Hybrid Mini-Grids," *Diss. Concordia University*, 2011.

[11]   Elamari, K.; Lopes, L. A C, "Frequency based control of electric water heaters in small PV-diesel hybrid mini-grids," *Electrical & Computer Engineering (CCECE), 2012 25th IEEE Canadian Conference,* pp. 1-4, April 29- May 2, 2012.

[12]   Wada, K.; Yokoyama, A., "Load frequency control using distributed batteries on the demand side with communication characteristics," *Innovative Smart Grid Technologies (ISGT Europe), 2012 3rd IEEE PES International Conference and Exhibition on*, pp. 1-8, 14-17 Oct. 2012.

[13]   Bellarmine, G.T., "Load management techniques," *Southeastcon 2000. Proceedings of the IEEE*, pp. 139-145, 2000.

[14]   F. Shahnia, R. Majumder, A. Ghosh, G. Ledwich, and F. Zare, "Operation and Control of a Hybrid Microgrid Containing Unbalanced and Nonlinear Loads," *Electric Power Systems Research,* vol. 80, no. 8, pp. 954-965, 2010.

[15]   E. Ortjohann, A. Arias, D. Morton, A. Mohd, N. Hamsic, and O. Omari, "Grid-Forming Three-Phase Inverters for Unbalanced Loads in Hybrid Power Systems," in *Proceeding of IEEE 4th World Conference on Photovoltaic Energy Conversion*, vol. 2, pp. 2396-2399, May, 2006.

[16]   Ninad, N.A.; Lopes, L. A C, "Unbalanced operation of per-phase vector controlled four-leg grid forming inverter for stand-alone hybrid systems," *IECON 2012 - 38th Annual Conference on IEEE Industrial Electronics Society*, pp. 3500-3505, Montreal, QC, 25-28 Oct. 2012.

[17]   Tonkoski, R.; Lopes, L. A C; EL-Fouly, T. H M, "Coordinated Active Power Curtailment of Grid Connected PV Inverters for Overvoltage Prevention," *Sustainable Energy, IEEE Transactions on* , vol. 2, no. 2, pp. 139-147, April 2011.

[18]   Tonkoski, R.; Lopes, L. A C; Turcotte, D., "Active power curtailment of PV inverters in diesel hybrid mini-grids," *Electrical Power & Energy Conference (EPEC), 2009 IEEE*, pp. 1-6, 22-23 Oct. 2009.

[19]   Tonkoski, R.; Lopes, L. A C; EL-Fouly, T. H M, "Droop-based active power curtailment for overvoltage prevention in grid connected PV inverters," *Industrial Electronics (ISIE), 2010 IEEE International Symposium on*, pp. 2388-2393, 4-7 July, 2010.

[20]   Lemkens, K.; Geth, F.; Vingerhoets, P.; Deconinck, G., "Reducing overvoltage problems with active power curtailment —Simulation results," *Innovative Smart Grid Technologies Europe (ISGT EUROPE), 2013 4th IEEE/PES*, pp. 1-5, 6-9 Oct. 2013

[21]   Dolan, M.J.; Davidson, E.M.; Kockar, I.; Ault, G.W.; McArthur, S.D.J., "Reducing Distributed Generator Curtailment Through Active Power Flow Management," *Smart Grid, IEEE Transactions on*, vol. 5, no. 1, pp. 149-157, Jan. 2014.

[22]   Torres, M.; Lopes, L. A C, "Frequency control improvement in an autonomous power system: An application of virtual synchronous machines," *Power Electronics and ECCE Asia (ICPE & ECCE), 2011 IEEE 8th International Conference on*, pp. 2188-2195, May 30- June 3, 2011.

[23]   Torres, M.; Lopes, L. A C, "Inverter-based virtual diesel generator for laboratory-scale applications," *IECON 2010 - 36th Annual Conference on IEEE Industrial Electronics Society*, pp. 532-537, 7-10 Nov. 2010.

[24]   Yan Du; Guerrero, J.M.; Liuchen Chang; Jianhui Su; Meiqin Mao, "Modeling, analysis, and design of a frequency-droop-based virtual synchronous generator for

microgrid applications," *ECCE Asia Downunder (ECCE Asia), 2013 IEEE*, pp. 643-649, 3-6 June 2013.

[25]   Yong Chen; Hesse, R.; Turschner, D.; Beck, H.-P., "Improving the grid power quality using virtual synchronous machines," *Power Engineering, Energy and Electrical Drives (POWERENG), 2011 International Conference on*, pp. 1-6, 11-13 May 2011.

[26]   D'Arco, S.; Suul, J.A., "Equivalence of Virtual Synchronous Machines and Frequency-Droops for Converter-Based MicroGrids," *Smart Grid, IEEE Transactions on*, vol. 5, no. 1, pp. 394-395, Jan. 2014.

[27]   B. Singh, A. Adya, A. P. Mittal, and J. R. P. Gupta, "Application of Battery Energy Operated System to Isolated Power Distribution Systems," in *Proceeding of 7th IEEE International Conference on Power Electronics and Drive Systems (PEDS '07)*, pp. 526-532, 27-30 Nov., 2007.

[28]   Ninad, N.A.; Lopes, L. A C, "Per-phase vector (dq) controlled three-phase grid-forming inverter for stand-alone systems," *Industrial Electronics (ISIE), 2011 IEEE International Symposium on*, pp. 1626-1631, 27-30 June 2011.

[29]   Ninad, N.A.; Lopes, L. A C, "Per-phase DQ control of a three-phase battery inverter in a diesel hybrid mini-grid supplying single-phase loads," *Industrial Technology (ICIT), 2011 IEEE International Conference on*, pp. 204-209, 14-16 March 2011.

[30]   Zong, Q; Hornik, T. "Conventional Synchronisation Techniques", *Control of Power Inverters in Renewable Energy and Smart Grid Integration, John Wiley & Sons*, First Ed., pp. 367-369, 2013.

[31]   Rocabert, J.; Azevedo, G.M.S.; Luna, A.; Guerrero, J.M.; Candela, J.I.; Rodríguez, P., "Intelligent Connection Agent for Three-Phase Grid-Connected Microgrids," *IEEE Transactions on Power Electronics*, vol. 26, no. 10, pp. 2993-3005, Oct. 2011.

[32]   R. E. Fehr, "A Novel Approach for Understanding Symmetrical Components and Sequence Networks of Three-Phase Power Systems", TE-2006000213.

[33]   Halpin, S.M., "Revisions to IEEE Standard 519-1992," *Transmission and Distribution Conference and Exhibition, 2005/2006 IEEE PES*, pp. 1149-1151, 21-24 May 2006.